MARIA S. MERIAN-BERICHTE

SUGAR Site
Gas hydrates as a new energy source
Reconnaissance of a pilot location for the SUGAR project

Cruise No. MSM34

December 6, 2013 – January 16, 2014
Varna, Bulgaria – Varna, Bulgaria

J. Bialas, I. Klaucke, M. Haeckel

Editorial Assistance:

DFG-Senatskommission für Ozeanographie
MARUM – Zentrum für Marine Umweltwissenschaften der Universität Bremen

2014

The MARIA S. MERIAN-Berichte are published at irregular intervals. They are working papers for people who are occupied with the respective expedition and are intended as reports for the funding institutions. The opinions expressed in the MARIA S. MERIAN-Berichte are only those of the authors.

The MARIA S. MERIAN expeditions are funded by the *Deutsche Forschungsgemeinschaft (DFG)* and the *Bundesministerium für Bildung und Forschung (BMBF)*.

Editor:
DFG-Senatskommission für Ozeanographie
c/o MARUM – Zentrum für Marine Umweltwissenschaften
Universität Bremen
Leobener Strasse
28359 Bremen

Author:

Dr. Jörg Bialas
GEOMAR Helmholtz-Zentrum
für Ozeanforschung
Wischhofstraße 1-3,
24148 Kiel
Telefon: +49 431 600-2335
Telefax: +49 431 600-2922
e-mail: jbialas@geomar.de

Dr. Ingo Klaucke
GEOMAR Helmholtz-Zentrum
für Ozeanforschung
Wischhofstraße 1-3,
24148 Kiel
Telefon:+49 431 600-2334
Telefax: +49 431 600-2922
e-mail: iklaucke@geomar.de

Dr. Matthias Haeckel
GEOMAR Helmholtz-Zentrum
für Ozeanforschung
Wischhofstraße 1-3,
24148 Kiel
Telefon: +49 431 600-2123
Telefax: +49 431 600-2928
e-mail: mhaeckel@geomar.de

Citation: J. Bialas, I. Klaucke, M. Haeckel (2014) SUGAR Site Gas Hydrates as a new energy source Reconnaissance of a pilot location for the SUGAR project - Cruise MSM34 – December 06, 2013 – January 16, 2014 – Varna (Bulgaria) – Varna (Bulgaria). MARIA S. MERIAN-Berichte, MSM34, 68 pp., DFG-Senatskommission für Ozeanographie, DOI:10.2312/cr_msm34

ISSN 2195-8483

Table of Contents

1 Summary

Cruise MSM34 of R/V MARIA S. MERIAN aimed to investigate a possible test site location for the German SUGAR project. The well sealed gas hydrate deposit should be accessible by the mobile drilling device MeBo 200.

During the two legs of cruise MSM34 of R/V MARIA S. MERIAN regional 2D seismic surveying, high resolution 2D and 3D seismic imaging, geo-chemical sampling, heatflow measurements and long-term piezometer installations were undertaken.

A grid of 28 2D seismic profiles was collected across the palaeo Danube delta. A number of inactive and partly buried channel systems could be mapped. Most of them were underlain by one or more bottom simulation reflectors (BSR) indicating the existence of gas hydrates. Based on the seismic brute stack images and the limits of the MeBo drilling device a prospective channel system with indications for possible gas hydrate formation at shallow depth (BSR, inverted strong amplitudes) could be identified in about 1500 m water depth. High resolution 2D seismic and 3D P-Cable seismic were used together with OBS deployments in order to allow structural mapping and physical description of the channel infill. Heatflow measurements and geochemical analyses of gravity and multi corer samples accompany these investigations. Neither the multibeam water column images nor Parasound records show any evidence of flares (gas bubbles in the water column) in this working area suggesting a well sealed hydrate reservoir.

Active gas expulsion from the seafloor was observed at about 200 m water depth circling around a slump area. The base plane of the failed sediment volume builds the current seafloor at about 600 m to 700 m water depth. On regional 2D seismic profiles a BSR has been mapped underneath the slope failure with unexpectedly strong upward bending. High resolution 2D and 3D P-Cable seismic investigations with complementary OBS deployment will allow imaging the BSR outline. Moreover velocity analyses, heatflow measurements and geo-chemical samples will be available for a detailed description of hydrate distribution and sediment parameters.

In a third working area high resolution 2D seismic reflection profiles were acquired across a fully buried channel system. Together with the regional seismic lines slope failure of the channel fill material can be studied across the slope extension of the system.

In summary cruise MSM34 achieved all proposed aims. Based on new regional seismic acquisition two working areas were selected for 3D high resolution studies. Investigations of a promising location for a SUGAR pilot site will be supported by a test location for slope stability and analyses of fluid migration pathways in a buried canyon site.

1.1 Zusammenfassung

Die Reise MSM34 des FS MARIA S. MERIAN zielte darauf ab eine mögliche Testlokation für das deutsche SUGAR Projekt zu untersuchen. Dabei sollte das gut bedeckte Gashydratvorkommen in Reichweite des mobilen Bohrgerätes MeBo 200 liegen.

Auf den beiden Fahrtabschnitten MSM34 des FS MARIA S. MERIAN wurden regionale 2D seismische Profile, hoch auflösende 2D und 3D seismische Vermessungen, geochemische Probenahme, Wärmestrommessungen und Installationen von langzeit Piezometern vorgenommen.

Mit einem Netz von 28 regionalen seismischen 2D Profilen konnten zahlreiche inaktive und zum Teil vergrabene Canyonsysteme kartiert werden. Die meisten sind von einem BSR unterlegt, welcher die Existenz von Gashydraten anzeigt. Basierend auf den „Brute-Stacks“ und den Grenzwerten der MeBo Bohranlage wurde in 1500 m Wassertiefe eine mögliche Einsatzstelle mit Indikationen für Gashydrate (BSR, invertierte Amplituden) gefunden. Hochauflösende 2D und 3D P-Cable Vermessungen wurden zusammen mit OBS Auslagen vorgenommen, um eine strukturelle Kartierung und Beschreibung der physikalischen Parameter der Canyonfüllung vornehmen zu können. Wärmestrommessungen und geochemische Analysen von Schwereloten und Multicorern ergänzen diese Messungen. Da weder im Parasound noch im Multibeam Gasfahnen in der Wassersäule beobachtet wurden, kann von einem gut abgeschlossenen Hydratvorkommen ausgegangen werden.

Aktive Gasaustritte wurden in ca. 200 m Wassertiefe entlang der Abrisskante einer Rutschung gefunden. Die Basis der Rutschungsfläche bildet in 600 m bis 700 m Wassertiefe den neuen Meeresboden. Auf den regionalen 2D seismischen Linien wurde ein BSR kartiert, der unter der Rutschung außergewöhnlich stark nach oben biegt. Hochauflösende 2D und 3D seismische Vermessungen werden gemeinsam mit den OBS aufnahmen eine Kartierung des BSR Verlaufs ermöglichen. Darüber hinaus sind Geschwindigkeitsanalysen, Wärmestrommessungen und geochemische Proben verfügbar um eine detaillierte Beschreibung der Hydratverteilung und Sedimentparameter zu erlauben.

In einem dritten Arbeitsgebiet wurden hochauflösende 2D seismische Profile über ein vergrabenes Canyonsystem aufgenommen. Gemeinsam mit den regionalen Linien können Rutschungen des Füllmaterials entlang der Hangausdehnung untersucht werden.

Insgesamt hat die Ausfahrt MSM34 alle gesteckten Ziele erreicht. Anhand neuer regionaler seismischer Profile konnten 2 Arbeitsgebiete für hochauflösende 3D seismische Studien gefunden werden. Die Untersuchungen eines vielversprechenden Standortes für eine SUGAR Feldstudie werden ergänzt durch eine Teststudie zu Hangstabilitäten und Fluidmigrationswegen entlang vergrabener Canyonsysteme.

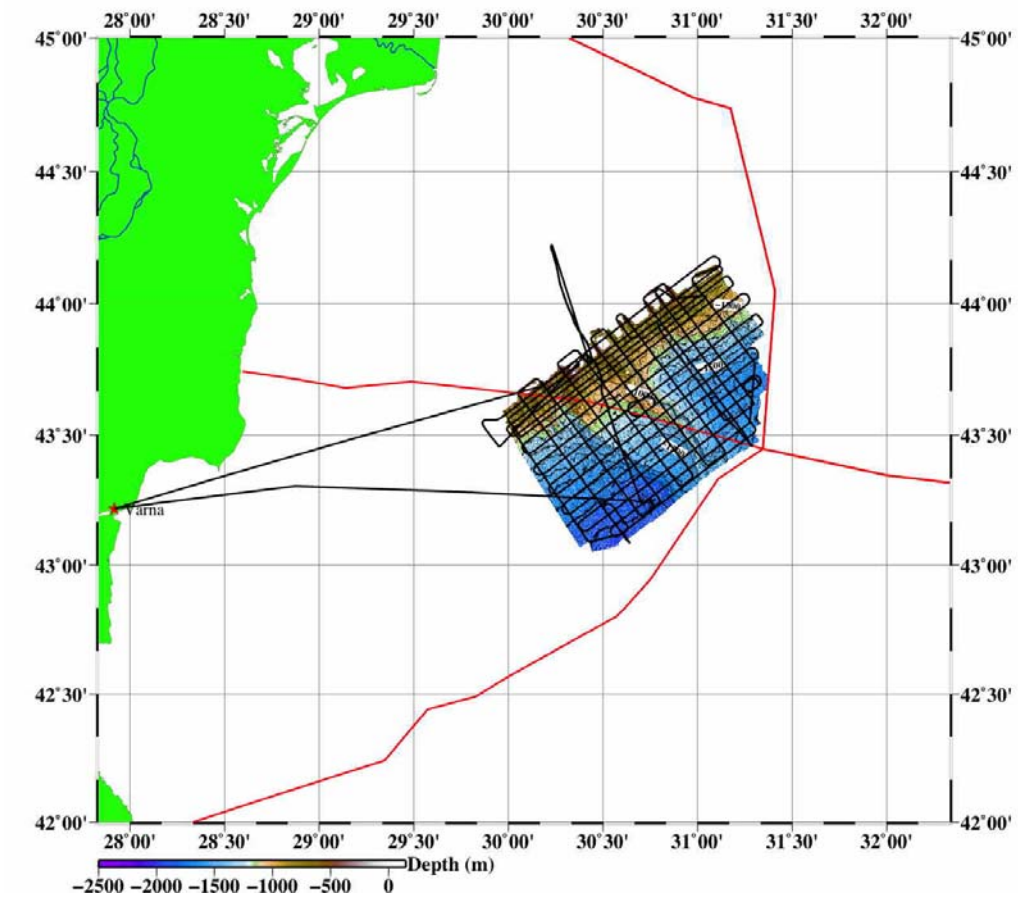

Fig. 1.1 Trackplot of cruise MSM-34 leg-1 - Gridded black lines indicate regional 2D seismic profiles

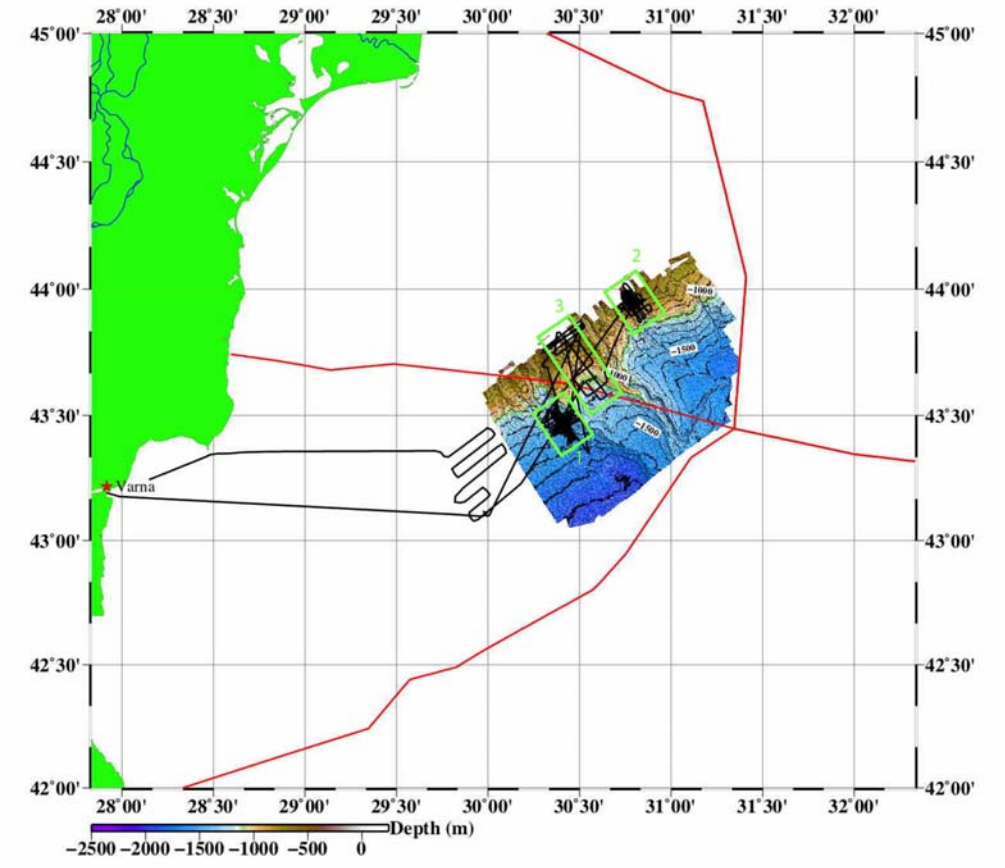

Fig 1.2 Trackplot of cruise MSM-34 leg-2
Green boxes 1, 2 and 3 indicate working areas for high resolution seismic

2 Participants

2.1 Scientists of cruise MSM34/1

Name	Discipline	Institution
Klaucke, Ingo, Dr.	Chief scientist	GEOMAR
Hoffmann, Jasper	Bathymetry	GEOMAR
Schroeder, Henning	Parasound	GEOMAR
Zander, Timo	Seismic Interpretation	GEOMAR
Ferrrant, Anthony	Geotechnics	IFREMER
Roudaut, Mickael	Geotechnics	IFREMER
Bayol, Efe	Seismic	IMST-Seislab
Barin, Burcu	Seismic	IMST-Seislab
Duymaz, Sermet	Seismic	IMST-Seislab
Dondurur, Derman	Seismic	IMST-Seislab
Cifci, Günay	Seismic	IMST-Seislab
Atgin, Orhan	Seismic	IMST-Seislab
Nasif, Aslihan	Seismic	IMST-Seislab
Kücük, Hilmi Mert	Seismic	IMST-Seislab
Özel, Özkan	Seismic	IMST-Seislab
Vasilev, Atanas	Seismic / Observer	IO-BAS

2.2 Scientists of cruise MSM34/2

Name	Discipline	Institution
Bialas, Jörg	Chief scientist / seismic	GEOMAR
Dannowski, Anke	OBS	GEOMAR
Koch, Stefanie	Seismic processing	GEOMAR
Sakar, Sudipta	Seismic interpretation	GEOMAR
Zander, Timo	Seismic interpretation	GEOMAR
Wetzel, Gero	Electronic engineering	GEOMAR
Matthiesen, Torge	Mechanic engineering	GEOMAR
Sauermilch, Isabel	OBS	GEOMAR
Gross, Felix	Parasound/Multibeam	GEOMAR
Schroeder, Henning	Seismic / OBS	GEOMAR
Schroller, Dirk	Geochemistry	GEOMAR
Haeckel, Matthias	Geochemistry	GEOMAR
Dibbern, Meike	Geochemistry	GEOMAR
Bigalke, Nikolaus	Geochemistry	GEOMAR
Pape, Thomas	Geochemistry	MARUM
Atgin, Orhan	Seismic	IMST-Seislab
Kücük, Hilmi Mert	Seismic	IMST-Seislab
Özel, Özkan	Seismic	IMST-Seislab

GEOMAR	Helmholtz-Zentrum für Ozeanforschung Kiel
IFREMER	Institut Français pour la Recherche et l'Exploitation de la Mer, Brest
IMST-Seislab	Institute of Marine Science and Technology, Dokuz-Eylül University, Izmir
IO-BAS	Institute of Oceanography, Bulgarian Academy of Science, Varna
MARUM	Centre for Marine Environmental Sciences, Bremen

3 Research Program

Gas hydrates have been the focus of scientific and economic interest for the past 15-20 years, mainly because the amount of carbon stored in gas hydrates is much greater than in other carbon reservoirs. Several countries including Japan, Korea and India have launched vast research programmes dedicated to the exploration for gas hydrate resources and ultimately the exploitation of the gas hydrates for methane. The German SUGAR project that is financed by the Ministry of Education and Research (BMBF) and the Ministry of Economics (BMWi) aims at developing technology to exploit gas hydrate resources by injecting and storing CO_2 instead of methane in the hydrates. This approach includes techniques to locate and quantify hydrate reservoirs, drill into the reservoir, extract methane from the hydrates by replacing it with CO_2, and monitor the thus formed CO_2-hydrate reservoir. Numerical modelling has shown that any exploitation of the gas hydrates can only be successful, if sufficient hydrate resources are present within permeable reservoirs such as sandy or gravelly deposits.

The ultimate goal of the SUGAR project being a field test of the technology developed within the project, knowledge of a suitable test site becomes crucial. Within European waters only the Norwegian margin and the Danube deep-sea fan show clear geophysical evidence for large gas hydrate accumulations, but only the Danube deep-sea fan most likely contains gas hydrates within sandy deposits. Therefore cruise MSM34 aims to investigate the Danube deep-sea fan for a suitable hydrate deposit. Co-operating with the party of cruise MSM35 a multi disciplinary approach of seismic imaging, geochemical and heatflow sampling and marine electromagnetic investigations should lay the base of a comprehensive database required for the preparation of a future hydrate production test site.

Prior to cruise MSM34 limited information about the Danube delta was available, only. Preparation was mainly based on three sources. Publications by Lericolais et al. (2009), Popescu et al. (2007), Popescu et al. (2006), a Diploma thesis by Baristeas (2006) and reports on the EU projects ASSEMBLAGE and BLASON.

The work of Baristeas (2006) was based on a selection of seismic profiles from a 3D survey undertaken by TOTAL in 1994 and 2001. This data set was not available for the cruise MSM34. Baristeas (2006) mapped two areas of BSR distribution north and south of the Viteaz canyon and interpreted irregular and increased amplitudes underneath channel axes as indications for free gas. Similar patches were interpreted underneath the levees. Baristeas (2006) speculates that microbial gas migrates along the coarse grained high permeable sediment-fill of the channel axis upwards towards the hydrate stability zone. Vertical migration is limited or inhibited by fine grained sediments. Formation of hydrates provides a seal indicated by the BSR. Further distribution of gas will be guided horizontal into the permeable levee system. Baristeas (2006) observed patches of a double BSR in the northern area. Discussions of models for the formation of a multiple BSR were not concluded. Nevertheless in his summary Baristeas (2006) assumes that upward migration of thermogenic

gas may have contributed increased amounts of higher carbon gases, which may have caused secondary BSRs due to modified stability boundaries.

Popescu et al. (2006, 2007) used data provided from the BLASON cruise undertaken by IFREMER and GeoEcoMar in 1998 and 2002. Selected data sets were provided by IFREMER. Popescu et al. (2006) interpreted multiple BSRs in the Danube fan area closely connected to channel-levee systems. They conclude that the uppermost BSR marks the current equilibrium depth of the base of the gas hydrate stability zone (BGHSZ) for gas compositions of more than 99% methane. This BSR1 has been mapped within three areas of the Danube fan. Chaotic reflection patterns underneath the BSR1 were found underneath the channel axis indicating the accumulation of free gas. The levees are partially underlain by stacks of up to four additional BSRs. Indications of free gas are provided by amplitude reversals of the reflection events where they cross the BSRs. Successive steps of climate warming are thought to be the cause of the additional BSRs. Free gas resulting from destabilization through the climate changes is expected to migrate within the strata. Mineral reaction may have taken place locally and provide a seal for fluid migration, which is imaged as paleo-BSR (Popescu et al., 2006).

Seismic data from EU projects ASSEMBLAGE and BLASON were made available by IFREMER, but did not provide a reasonable data coverage of the working area. Industry data used by Baristeas (2006) were not available. Therefore cruise MSM34 set out to establish the bathymetric and seismic database to prepare the selection of further high resolution seismic study areas.

Leg 1 of cruise MSM34 applied a 1 km long multichannel seismic streamer to acquire the necessary regional grid of 2D seismic profiles for an overview of the hydrate distribution along the various channel-levee systems. Brute stacks of the data were analysed on board in order to map the BSR as primary indicator for the gas hydrate distribution. In addition the crew deployed two long-term piezometers operated by IFREMER. Based on the acquired 2D seismic data two target areas were selected for further detailed seismic and geologic sampling during leg 2. 3D high resolution seismic imaging within the two survey areas was accompanied by Ocean-Bottom Seismometers (OBS) deployments. Wide angle observations from the OBS will be used to develop a velocity depth model for the migration of the 3D volume. Amplitude variations of the OBS records and converted shear waves will allow to provide physical parameters of the sediments and contribute to the estimate of hydrate volume. Heatflow measurements should support the calculation of the thermal gradient and provide hints for possible natural leakage of fluids. Gravity cores and multi corer were used to analyse the geochemical parameters of the pore fluids. Gas compositions and isotope distributions will provide further details on hydrate formation and gas sources.

Both 3D volumes could be acquired. Due to unexpectedly favourable weather conditions additional high resolution 2D seismic profiles could be acquired.

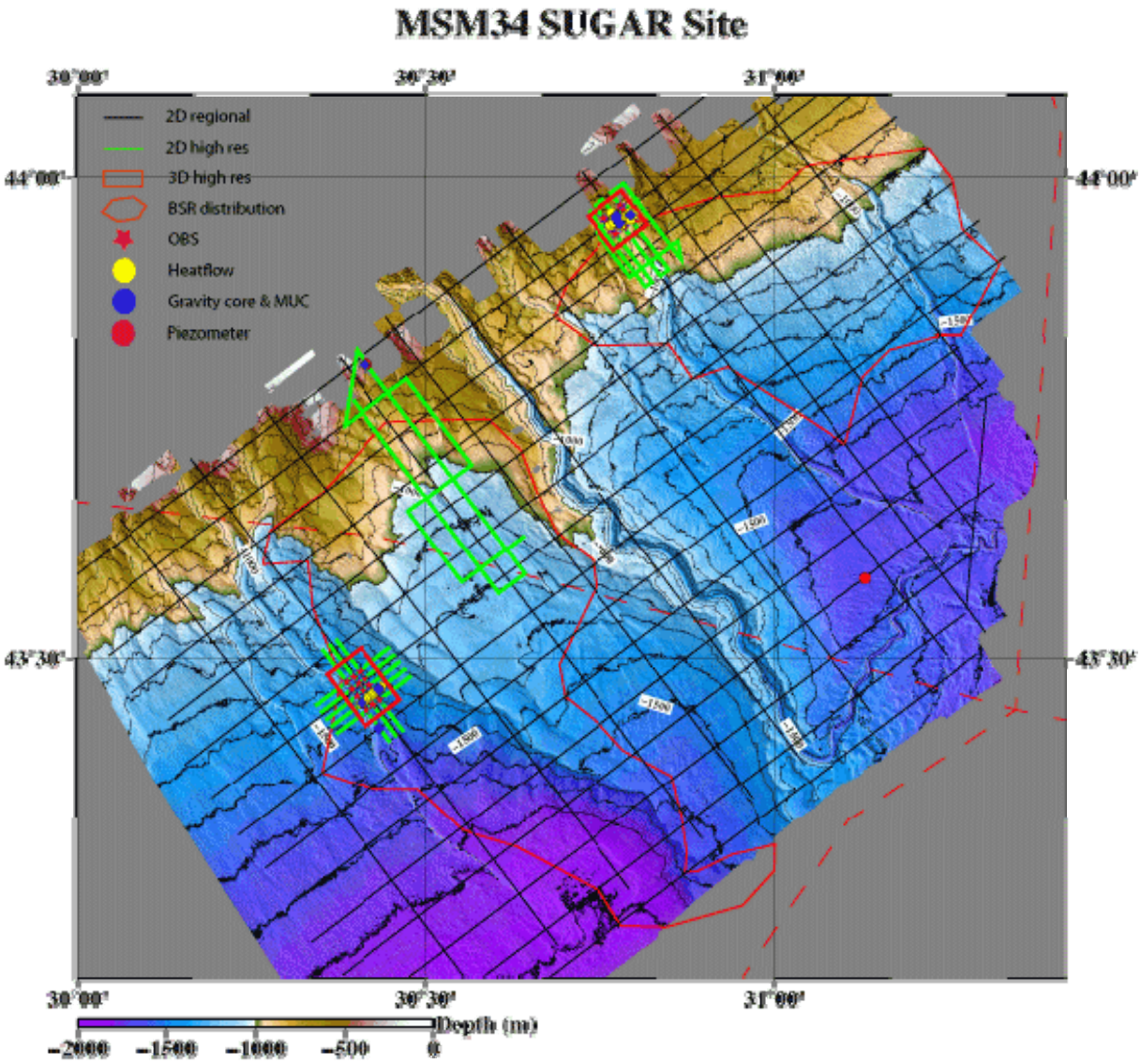

Fig. 3.1 Overview map with outline of the working areas and deployments of cruise MSM34-1 & 2

4 Narrative of the cruise

4.1 Cruise narrative MSM34-1

The first leg of RV MARIA S. MERIAN cruise MSM34 started on December 5, 2013 when a first group of six scientists from Germany and France arrived in Varna, Bulgaria. Cruise MSM34 is dedicated to investigations of marine gas hydrate deposits offshore Bulgaria and Romania in general and the Danube deep-sea fan in particular. During the first leg we intend to acquire 2D-seismic, bathymetry and Parasound data together with in-situ pore pressure measurements while the second leg will acquire 3D seismic and OBS data together with heat-flow measurements and sediment cores for geochemical analysis. All the necessary equipment for both legs was already sent for the very beginning of the MSM34 campaign.

On December 6, 2013 RV MARIA S. MERIAN arrived in the port of Varna and berthed at the container pier for unloading of the equipment from the previous cruise. While waiting for the authorisation to disembark the containers, the equipment of cruise MSM34 arriving by two trucks from Kiel and one truck from Brest, France was already loaded on board. In the

afternoon, RV MARIA S. MERIAN changed berth to the passenger terminal that is just a few hundreds of meters away. The following day, a delayed truck with further equipment from Izmir, Turkey finally arrived and the seismic streamer winch and all the necessary electronics were put onto the vast after-deck of RV MARIA S. MERIAN. In the meantime our colleagues from Brest began installing the piezometer underneath the A-frame and the work stations for the seismic interpretation were mounted in the lab. On December 8 the seven scientists from Germany, France and Bulgaria that already had reached Varna boarded RV MARIA S. MERIAN while waiting for nine colleagues from Turkey. They had missed a connecting flight in Istanbul and only arrived in the afternoon at 16:00 after a very long journey. However, soon after their arrival they started setting up the seismic equipment in the deck's lab.

December 9 started with a safety instruction and a familiarization tour of the vessel at 08:00 o'clock. Departure was scheduled for that morning, but had to be delayed because of strange noises and lack of power of one of the pod propulsions. After many different checks and consultation with the manufacturer, the problem was finally overcome by a renewed complete reboot of the system and RV MARIA S. MERIAN finally sailed out of the port of Varna at 18:00 for an 11 hours transit to our first station. At 05:00 on December 10, 2013 we reached the station and deployed a sound velocity probe in order to obtain a sound velocity profile for the EM122 multibeam system. The subsequent multibeam and Parasound profile towards the locations of the first piezometer deployment had to be stopped at mid-way due to deteriorating weather conditions. Average winds of force 7-8 with gusts of force 9 did not allow collecting useful data and all operations were stopped at 08:10.

By the early morning of December 11 the weather conditions had improved and following a safety and abandon ship drill at 10:30, a first attempt to deploy the piezometer at was carried out at mid-day. This test run intended to determine the possible length of the piezometer was successful and the actual piezometer pipe equipped with sensors was installed on the deployment frame. By 19:30 the first piezometer of the cruise was deployed and RV MARIA S. MERIAN headed towards the starting point of our first seismic profile. At 22:00 the 1050-m long streamer of our Turkish colleagues was deployed and at 01:00 on December 12 we started recording our first seismic profile. Unfortunately, the EM122 multibeam system stopped working properly in the early morning hours of December 12 and it took until the evening before the problem could be fixed. Seismic recording continued smoothly until 12:00 on December 16, when a strange signal on the hydrophone of the airgun urged us to bring the airgun back on deck for verification. After replacement of the airgun umbilical, seismic recording resumed at 16:30 and continued until December 18 at 14:30 when the airgun showed signs of leakage. In order to save time, the airgun was replaced with a spare GI-gun and seismic data acquisition resumed at 17:30.

On December 20 the seismic gear was recovered at 12:45 the seismic gear was recovered for a change of batteries of the bird system. The afternoon and early evening was then used to deploy the second piezometer station that was installed in a location where gas hydrates are expected to be close to the seafloor. By 23:30 the piezometer station was successfully completed and we started a short bathymetry survey to allow the CGG Symphony to move away from our survey area.

At 12:30 on December 21 we redeployed the seismic equipment under perfect weather conditions for seismic acquisition. A loose connection in the acquisition electronics slightly delayed the beginning of the next profile so that we eventually came quite close to the CGG Symphony the next morning. Luckily, although interferences became very strong, they could still be filtered out. By December 24, 12:00 we had completed our preliminary lines and could add several additional lines that appeared to be necessary after initial inspection of the seismic data. With seismic data acquisition still going on, we all celebrated Christmas Eve with a nice special evening program prepared by the crew with a little help of the scientific party. Seismic acquisition was finished on December 26 at 08:00 after 2200 line kilometres of high-resolution and high-quality seismic profiling. By 9:30 the seismic gear was back on deck and we finished our scientific program with a couple of bathymetry and Parasound profiles dedicated at filling some remaining gaps in the bathymetry grid. At 22:00 we had to leave the study area and arrived in time to meet the pilot at 08:00 on December 27 at the entrance to the port of Varna. By 09:00 RV MARIA S. MERIAN had berthed at the pier and by 12:00 the equipment of our colleagues from IFREMER, Brest and SeisLab, Izmir had been loaded onto two trucks waiting at the pier. That was the end of the first leg of cruise MSM34, which was extremely successful, as all goals have been fully achieved.

Fig. 4.1 Group photograph of cruise participants of leg MSM34-1

4.1.1 Cruise narratives of MSM34/Leg 2

On Friday 27.12.13 R/V MARIA S. MERIAN returned from cruise MSM34/ Leg 1 to the port of Varna. PIs of Leg 2, Dr. Bialas and Dr. Haeckel, joined with the PI of Leg1 Dr. Klaucke on board the vessel to discuss the results of the cruise. Seismic 2D profiling on Leg 1 was dedicated to provide a regional overview for the search of buried channel levee systems within the hydrate stability zone of the ancient Danube fan. On a first glance only one promising channel levee system, which seems to be accessible for a future drilling campaign with the mobile drilling device MeBo, could be identified. The outline of the BSR distribution across the 2D seismic grid shows substantial differences to those published previously. Along seismic 2D line 15 the BSR could be mapped upwards the slope until it coincides almost with the seafloor. This area was chosen of second most interest. A third target area was the

possible slump distribution within the vicinity of the shallow piezometer deployment site at the shelf break.

In the evening of 27.12.13 the remaining 11 scientific crew members arrived at the port of Varna. Together with 5 crew members of Leg 1 a total of 18 scientists joined for geophysical and geochemical investigations during cruise MSM34/ Leg 2 on board. To avoid delays caused by season holidays all equipment was already shipped with two trucks for the port call of leg 1.

A safety familiarization was undertaken in the afternoon of the 29.12.13 with all scientists. After two days of preparation major set up of equipment was completed on deck and in the laboratories when R/V MERIAN left the port of Varna on 29.12.13 at 19:00 hrs. Weather conditions were calm with less than 4 Bft. wind and wave heights less than 1.5 m. Weather conditions were stable through the following days.

During transit to the working area two short PARASOUND profiles were recorded across a possible vent site that was observed by our colleagues from NIOZ in early 2013. At this time no flare was observed in the water column. In the morning of 30.12.13 safety instruction training was undertaken with all crew on board. At 10:30 hrs. scientific investigations of MSM34 Leg 2 began with multicore, gravity core and heatflow sampling next to the shallow piezometer site of Leg 1. At 15:30 the acoustic releases of the OBS were tested at 1400 m water depth. A calibration of the heatflow probe and a sound velocity profile were taken as well. Next 15 OBS were deployed within the foreseen area of the 3D seismic cube.

On the 31.12.13 at 01:20 deployment of 15 OBS was completed. After some bathymetric profiles a gravity core was taken at the southern limits of the 3D area before deployment of the P-Cable system. Due to water penetration in the wet end termination of the P-Cable umbilical a 2D seismic survey was run to serve airgun shots for the OBS array. At 18:30 a 45 / 45 cinch GI airgun and 5 streamer sections were deployed. Q/C tests for shot gathers did show interfering signals from M/V CGG SYMPHONY, a seismic 3D industry vessel operating in the Han Asparuh block. Due to far offsets and orthogonal survey outline the signals disappeared in filtered and stacked section display.

At 13:30 on 01.01.14 the 2D seismic survey was completed. Deployment of the P-Cable was completed at 18:30 with 14 nodes. Nodes 5 to 8 were equipped with doubled streamer sections. Airgun shots were fired at 5 sec. interval. Q/C tests did not show any remaining interferences caused by the M/V CGG SYMPHONIY operations.

P-Cable operation was continued until 13:00 hrs. on 04.01.14. In the afternoon two multicorer stations were sampled. At 18:30 hrs. the heatflow probe was deployed. 11 stations were sampled until 01:30 of the 05.01.14. The night hours were used to recover the 15 OBS.

On the 05.01.14 at 10:00 hrs. sampling of two gravity cores at the western and eastern end of the heatflow profile followed. Next the seismic survey was continued after deployment of the P-Cable at 16:30 hrs.

On the 06.01.14 at 10:00 hrs. the injector of the airgun failed and the gun was replaced. Some time later the data connection to the P-Cable streamers was lost. It turned out that the data umbilical between vessel and P-Cable needed to be changed. The repair time was used to deploy a Mini-Corer at 17:30 hrs. At 22:00 hrs. the P-Cable survey was continued.

At 03:00 hrs. on 07.01.14 streamer section 6 delivered incomplete data. Node four of the P-Cable was taken out of the configuration scheme of the recording software and the survey was continued without recovery of the P-Cable.

The remaining 3D survey could be completed without system failure. Acquisition was stopped on 09.01.14 at 10:00 hrs. After a short transit R/V MARIA S. MERIAN arrived in the second work area. At 13:00 hrs. research work continued with acquisition of gravity corer, Multi-Corer samples and a third heatflow profile. Starting at 20:00 hrs. 12 OBS were deployed until 23:00 hrs.

At 01:30 on 09.01.14 hrs. acquisition of the second 3D seismic data volume started. The survey area covered parts of a slump area and the neighbouring canyon system.

The survey was completed without interruption on 13.01.14 at 13:00 hrs. Gravity coring, Multi-Corer and heatflow profiling was undertaken in the afternoon and night hours.

At 14.01.14 at 02:00 hrs. 2D seismic profiling began to extend the survey area beyond the limits of the 3D cube. At 23:00 hrs. recovery of 12 OBS took place until 03:30.

On 15.01.14 heatflow profiling began in order to connect measures from the slump area into the depression of the canyon system. Due to anomalous temperatures measured at the base of the canyon additional temperature and heatflow measurements were taken to better estimate the limits of the anomaly. For ground truthing a gravity core was taken on short notice prior to transit for the third working area. At 14:00 hrs. a final 2D seismic survey began across a buried slump volume.

On 16.01.14 seismic data acquisition was terminated at 08:15 hrs. Following a short transit a last multibeam and Parasound survey investigated the so-called NIOZ bubble site with water column imaging. Scientific work of cruise MSM34 was terminated at 24:00 hrs. when R/V MARIA S MERIAN set course towards the port of Varna.

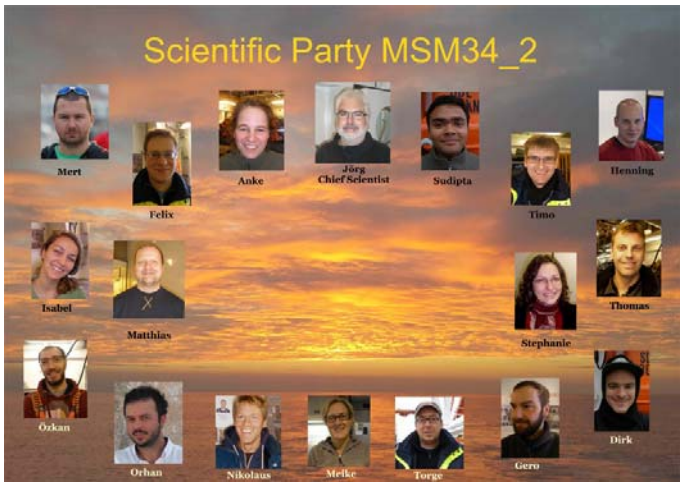

Fig. 4.2 Cruise participants of leg MSM34-2

5 Preliminary results

During leg 1 a grid of regional 2D seismic profiles has been acquired (Fig. 5.1) and has been the basis for choosing three detailed working areas for leg 2. Figures 5.2 to 5.4 summarize the high resolution seismic profiles and station work, first results of which are described below.

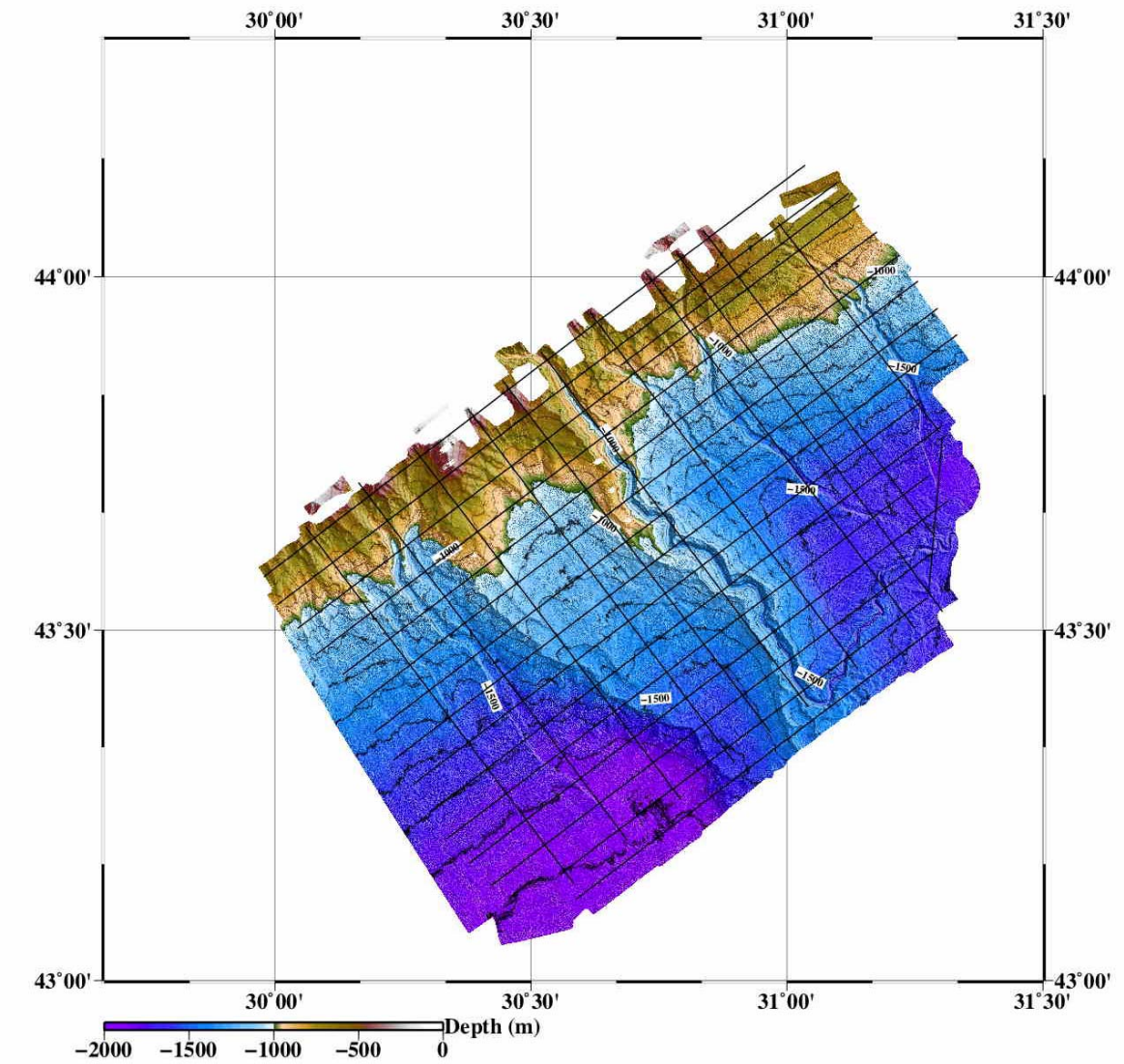

Fig. 5.1 Bathymetric map of the MSM34 working area with the grid of 2D seismic profiles acquired during leg-1 of cruise MSM34 using the one kilometre long streamer of SeisLab

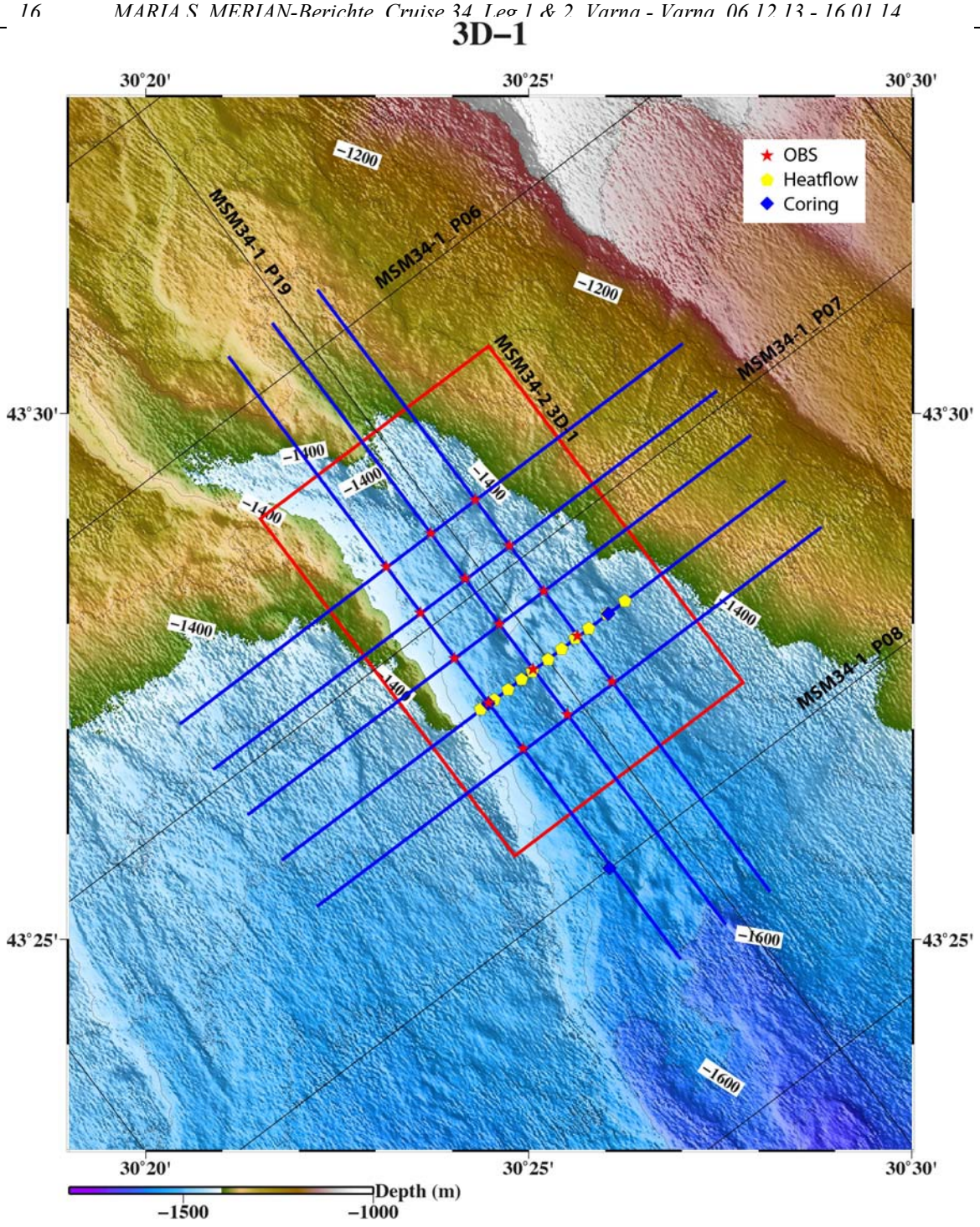

Fig. 5.2 Overview map of working area 1 indicating seismic profiles and sampling stations

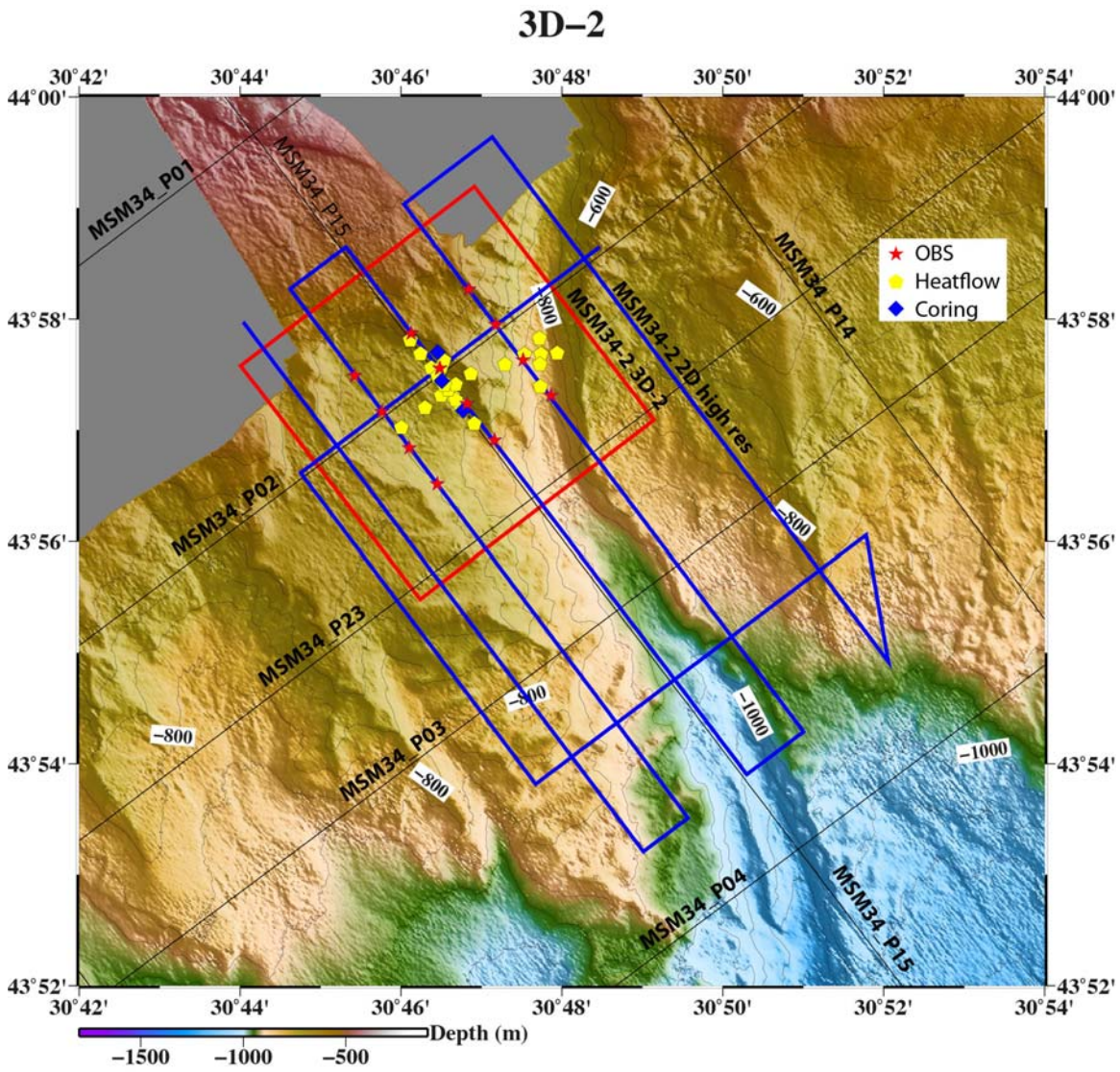

Fig. 5.3 Overview map of working area 2 indicating seismic profiles and sampling stations

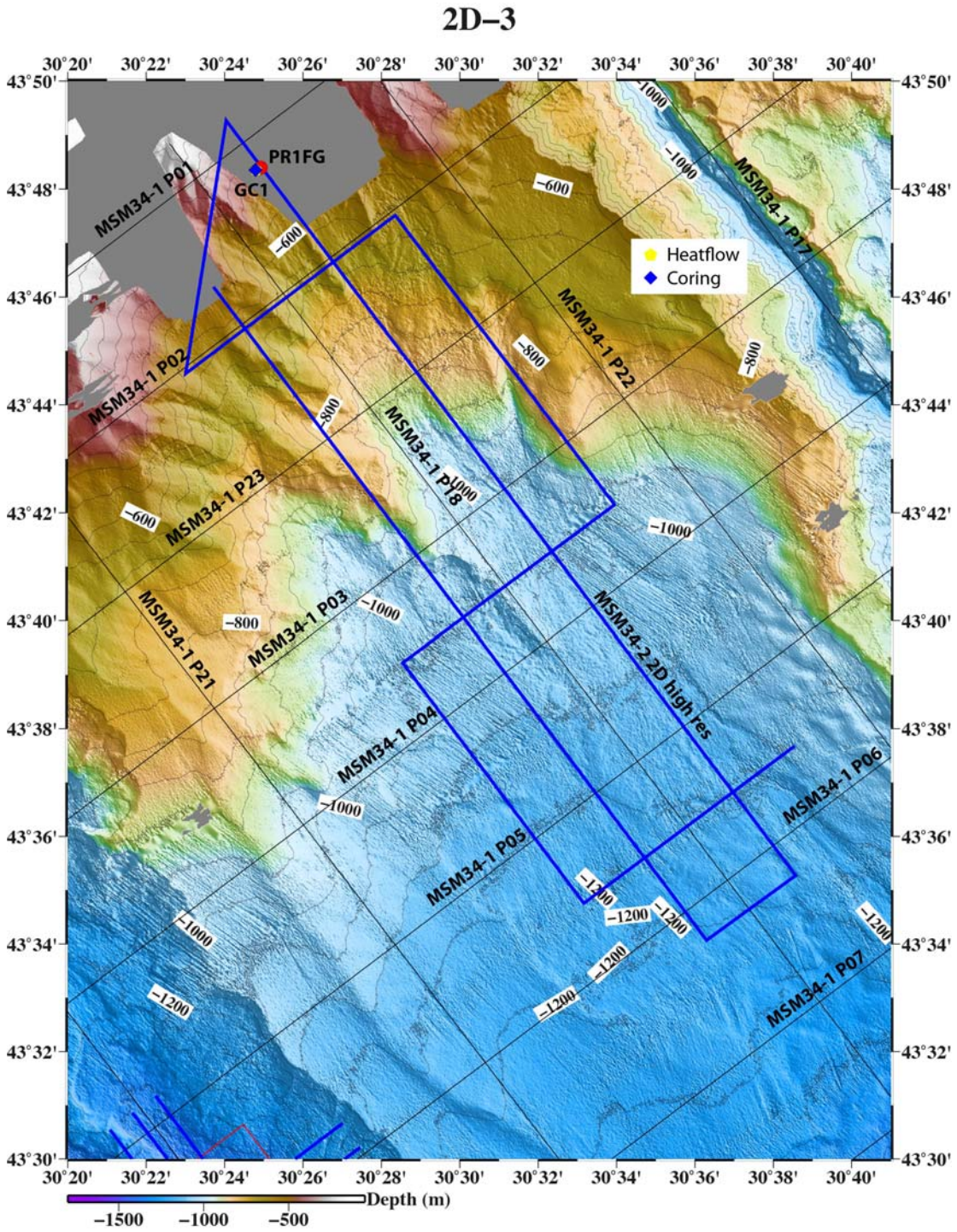

Fig. 5.4 Overview map of working area 3 indicating seismic profiles and sampling stations

5.1 Sound Velocity Profiles (SVPs)

(Felix Gross, Jasper Hoffmann)

Three SVPs were acquired during MSM34 (Fig. 5.1.1). The data was acquired with an AML Oceanographic Plus X probe and were needed for multibeam calibration. The probe measures the sound velocity every meter in depth up to 5000 dBar. The SVP stations are located in the studied area at highest possible water depth (up to 1840 m) for a continuous profile. Data was extracted from the Probe using Seacast software and immediately loaded into the multibeam control software SIS for correct ray tracing through the water column.

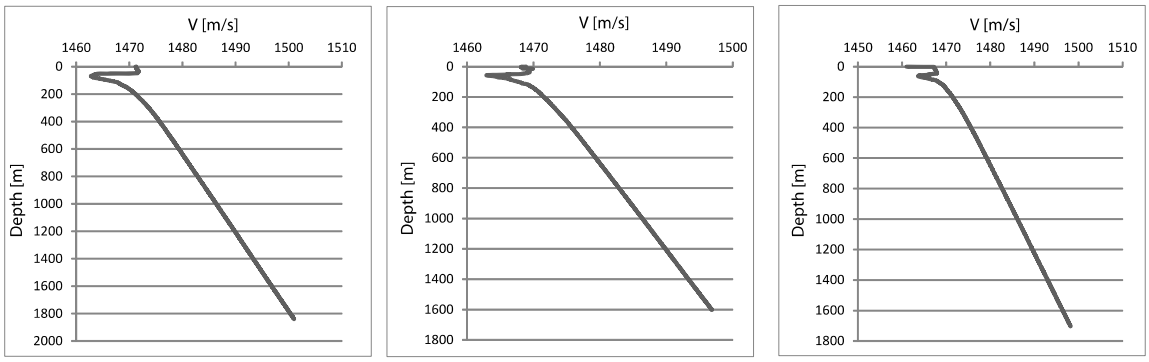

Fig. 5.1.1 From left to right: SVP1 (MSM34-1) SVP2 (MSM34-1) SVP3 (MSM34-2)

5.2 Bathymetry and sediment sounding

5.2.1 Bathymetry

(Jasper Hoffmann, Timo Zander, Henning Schröder, Felix Gross)

Bathymetric data were recorded with the EM122 during the complete cruises MSM34 1 and 2. During the acquisition of the 2D seismic lines it was possible to achieve a sufficient overlapping of the outer beams between adjacent profiles. Thus, it was possible to generate a very detailed 25 m by 25 m bathymetry grid of the main study area (Fig 5.2.1.1). During the second leg of the cruise, additional bathymetry data could be retrieved only on the first and last days of the cruise during the observation of the NIOZ bubble site at the southwestern part of the study area.

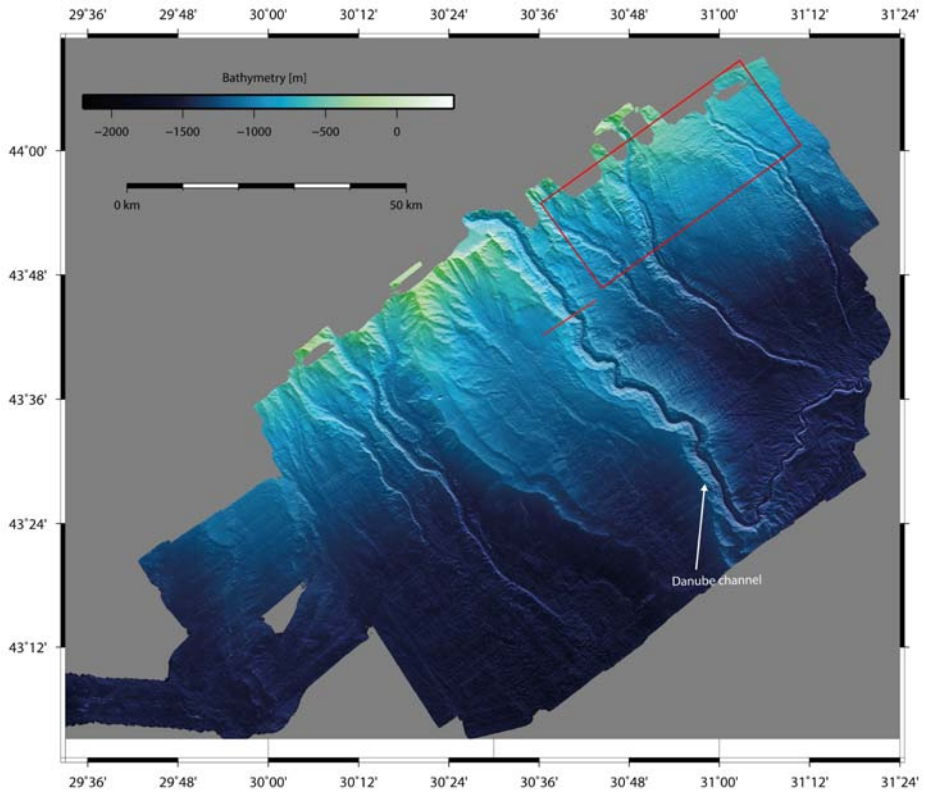

Fig. 5.2.1.1 Bathymetric map of the Danube delta acquired during cruises MSM34-1 & 2
Line in red indicates location of cross section displayed in figure 5.2.1.2
Box in red indicates zoom area displayed in figure 5.2.1.3

The multibeam bathymetry collected in the work area shows several paleo-channels of the Danube river, but only one channel was active at a time Popescu et al. (2006), controlled by sea-level. The most recent channel-levee system that was active during the last sea-level lowstand is the Danube channel in the centre of the study area. The Danube channel cuts deeply into the sediments as shown in the surface profile (Fig. 5.2.1.2)

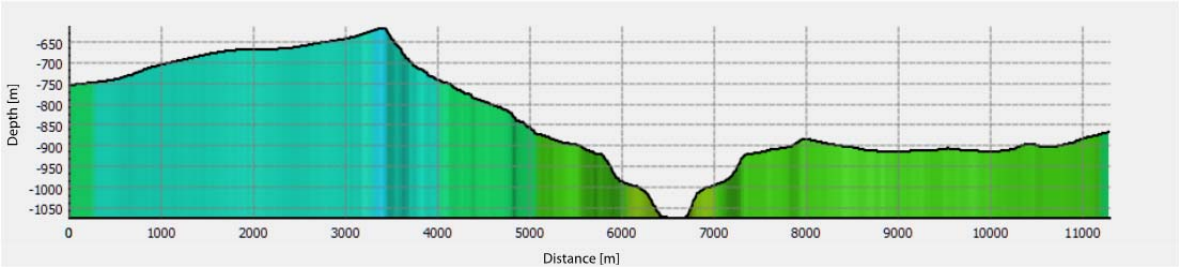

Fig. 5.2.1.2 Bathymetry cross-section through the Danube channel
Location of cross section is indicated in figure 5.2.1.1

The area towards the east of the Danube channel shows a rough surface structure with several blocks (Fig.5.2.1.3), while the area towards the west shows a flat surface in comparison.

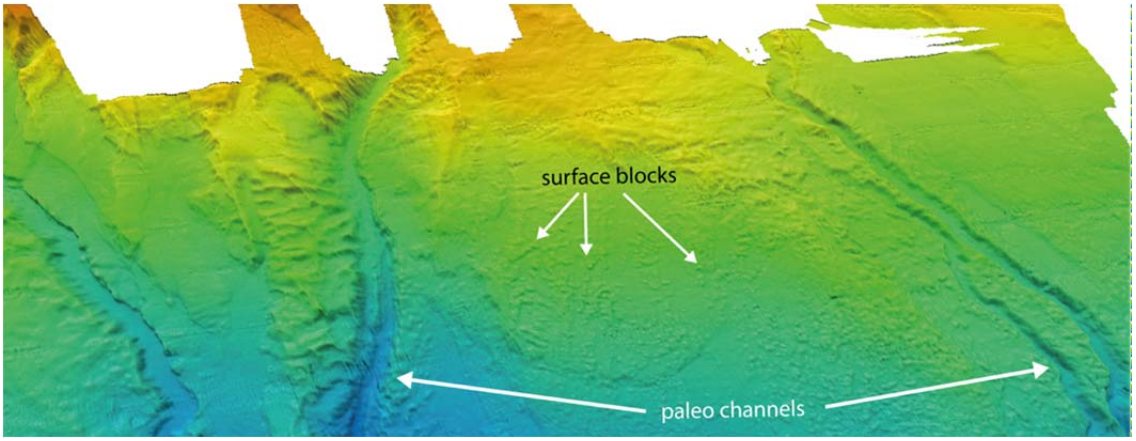

Fig. 5.2.1.3 Perspective view of the eastern part of the work area
Location of zoom area is indicated by red rectangle in figure 5.2.1.1

5.2.2 Parasound

(Felix Gross, Jasper Hoffmann, Timo Zander, Henning Schröder)

The PARASOUND System was operated in a 24/7 mode during the entire cruise and a significant amount of echo-sounder data were collected. As the PARASOUND PS70 is able to resolve sedimentary structures at the cm scale, this system is very helpful for detailed sedimentary studies and the combination with sediment core data.

The general heterogenic geology of the working area is also visible in the PARASOUND data.

Fig. 5.2.2.1a presents a representative PARASOUND profile from the western part of the working area. It features a high penetration of up to 175 ms two-way traveltime (TWT) and exhibits finely laminated sediment packages in the west and a chaotic/transparent facies

overlying well-stratified deposits further East. These chaotic/transparent units are typical for mass transport deposits in PARASOUND data and in particular for debris flow deposits.

Fig. 5.2.2.1b presents a representative PARASOUND Profile from the eastern part of the working area. In comparison to the western area, this area can be characterized by less penetration and therefore indicates a significant change in lithology. Less penetration indicates a high absorption of energy in the upper strata, which generally points towards a higher proportion of coarse-grained deposits.

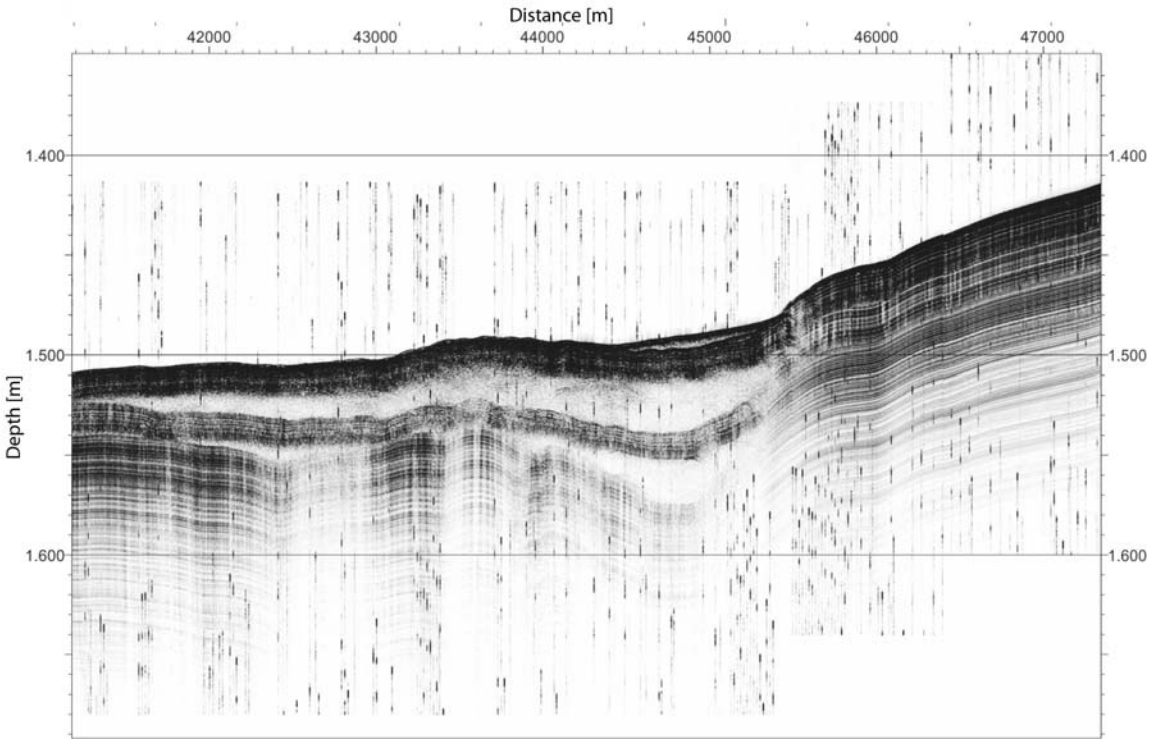

Fig. 5.2.2.1a PARASOUND Profile MSM34-2-06 in the western part of the working area with high penetration.

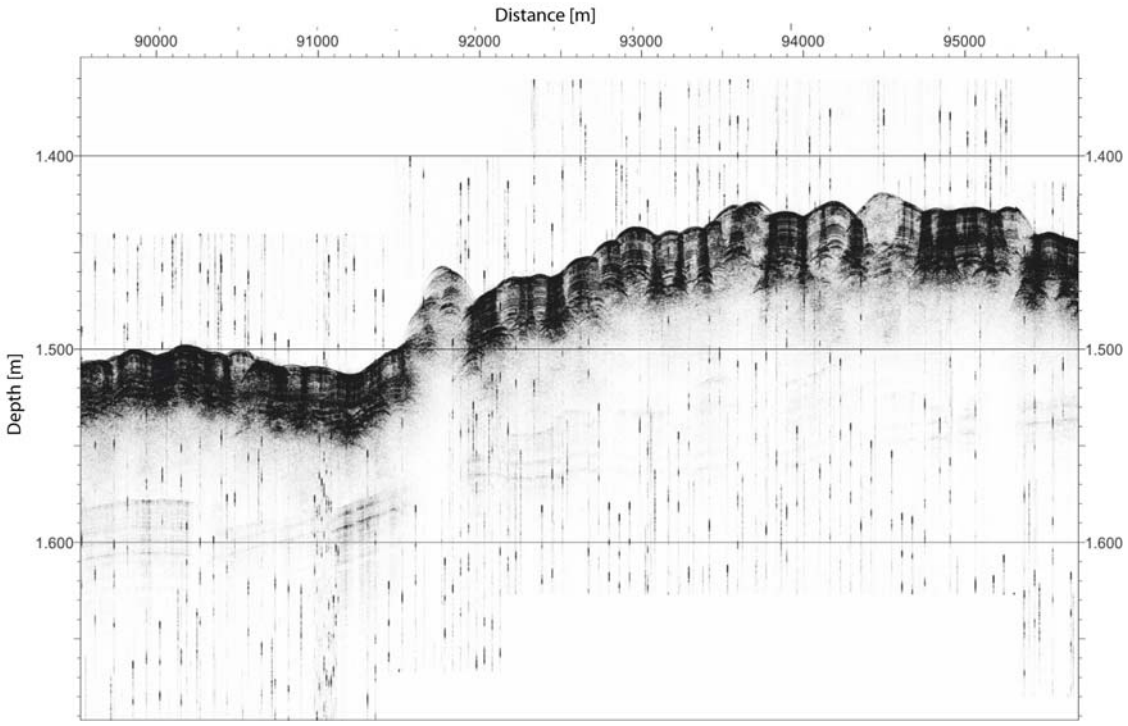

Fig. 5.2.2.1b PARASOUND Profile in the eastern part of the working area with low penetration.

5.2.3 Flare imaging

(Felix Gross)

During MSM 34/2 the Primary High Frequency (PHF) of the PARASOUND P70 was used for flare imaging. The high frequency of 18.8 kHz enables this echo sounder system for water column imaging and images horizontal, as well as vertical structures. This capability makes the PARASOUND P70 feasible for high resolution 2D gas flare imaging within the water column. For less interference and signal distortion in the water column, the PARASOUND was operated in single pulse mode during flare imaging. In addition to the PARASOUND P70, the Kongsberg EM 122 was used for water-column imaging (WCI). The water column was recorded during the second P-Cable survey site. During acquisition, the system showed vertical features in the water column. The data was not processed on board due to missing software.

Beside the gas flares, observed in shallow water depths of ca. 200 m, a special target for flare imaging was the second P-Cable survey area. In this area an unusual upward bended BSR is a possible indicator for gas emissions at the seafloor.

Several gas flares could be imaged within the water column at the second 3D survey area. Their origin at the seafloor lies in water depths between ca. 580 m – 750 m and is clearly associated with prominent morphological expressions at the seafloor (Fig. 5.2.3.1). The abundance of these flares can be traced in the entire second P-Cable survey. The gas emissions seemed to be constant during the survey, as some of the flares were imaged several times by the cruise track. The flares are not influenced by any currents in the water column, as they rise vertically without any bending towards the water surface.

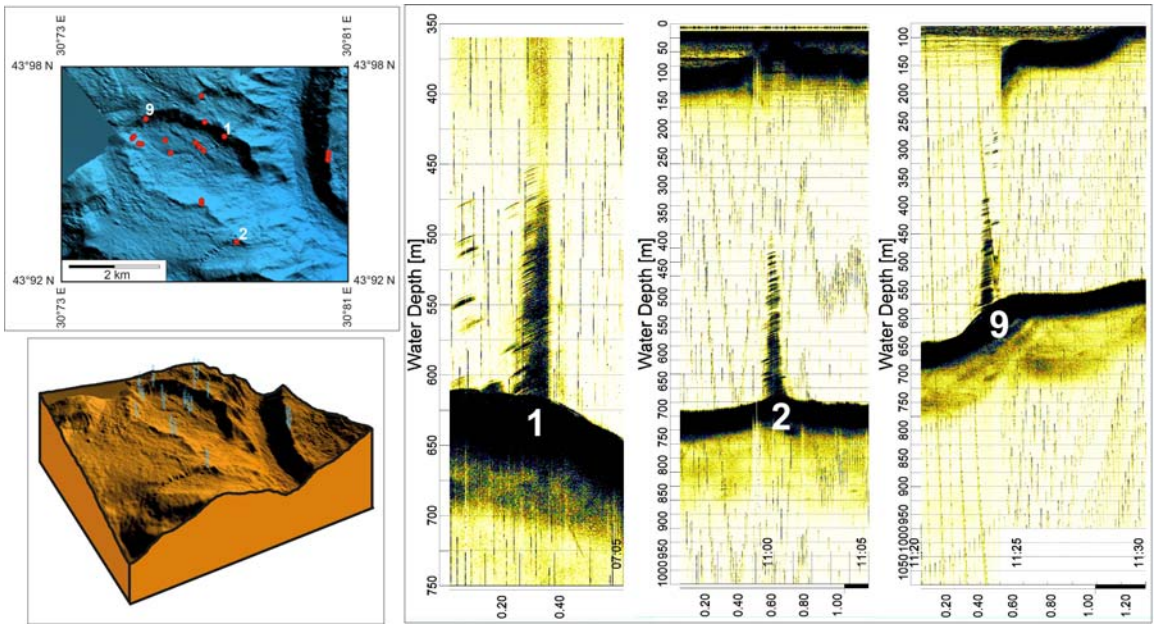

Fig. 5.2.3.1 Top left: Overview map on the second 3D survey area. Several flares were imaged in water depths ranging between 580 m and 750 m.
Bottom left: 3D perspective view on the flare sites (limits as in map above). Gas emissions are indicated by gas bubbles.
Right: Examples of flares, observed in the working area. Their location is marked in the overview map to the top left (nos. 1, 2 & 9).

5.3 Seismic

5.3.1 Regional 2D Seismic

(Orhan Atkin, Burcu Barin, Efe Bayol, Gunay Cifci, Derman Dondurur, Sermet Duymaz, Ingo Klaucke, Mert Kücük, Aslihan Nasif, Özkan Özel, Timo Zander)

A total of 28 regional 2D seismic profiles have been acquired during leg 1. Despite the presence of an industry seismic ship (CGG Symphony) in the vicinity of the working area, the interferences from this vessel could be filtered out (Fig. 5.3.1.1) and a set of high quality seismic profiles has been obtained.

Brute stacks of the 2D seismic acquisition of leg 1 (fig. 5.3.1.2-4) were prepared in a KingDom project for inspection prior to the beginning of leg 2. The main goal of cruise MSM34 was to identify gas hydrate bearing locations, which were favourable for a possible SUGAR test site. Boundary conditions for a test site are given by the request for a reasonable permeability to enable a productive gas flow. To enable application of the MeBo drilling device the hydrates need to be available as shallow as about 100 m below seafloor. It is the assumption of the MSM34 proposal that reasonable permeability is most likely to be expected within the centre and the levees of buried canyon systems. With this in mind the 2D seismic data of leg 1 were discussed between the party chiefs of cruise MSM34 leg 1 and leg 2 prior to start of leg 2 in the port of Varna.

Among the large number of buried channel levee systems only one was found, which seems to fulfil the requirements of the SUGAR project. The system further named work area 1 was identified along profile MSM34-1_19 between the crossing with profile MSM34_07 (Fig. 5.3.1.2) and MSM34-1_08. It is underlain by a continuous BSR indicating availability of free gas. Within the old channel centre at about 1500 m water depth a significant reflector of

inverted polarity was identified within a depth of about 100 m below seafloor. It is assumed that above this horizon hydrate formation has taken place in porous sediment suitable for a test production site.

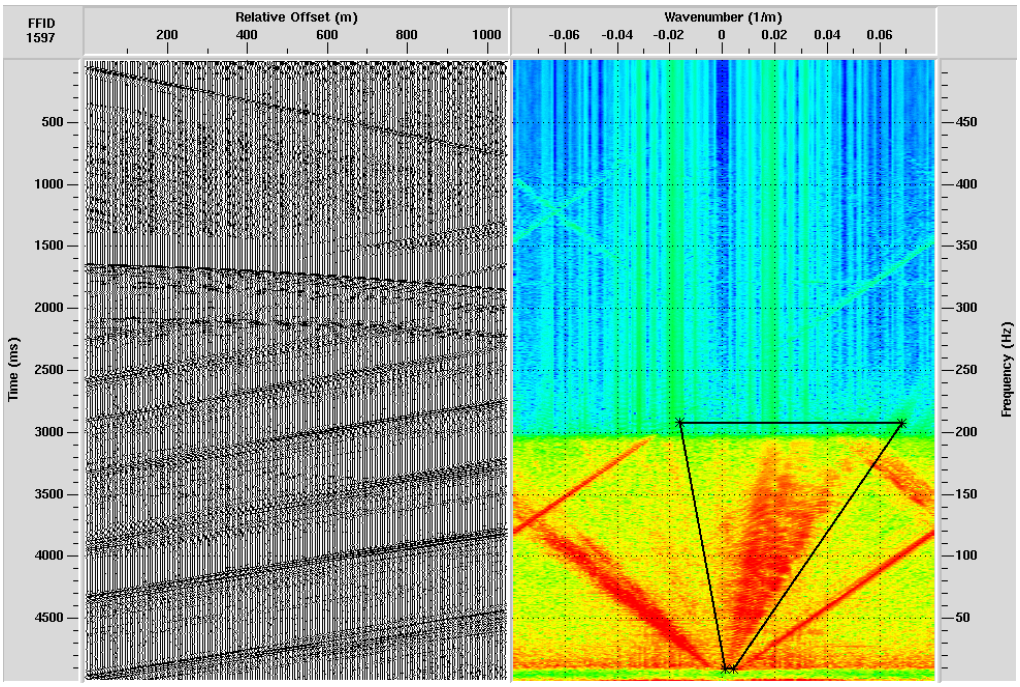

Fig. 5.3.1.1 Seismic interference from far to near end and its FK spectrum related to of symphony (CGG) ship.

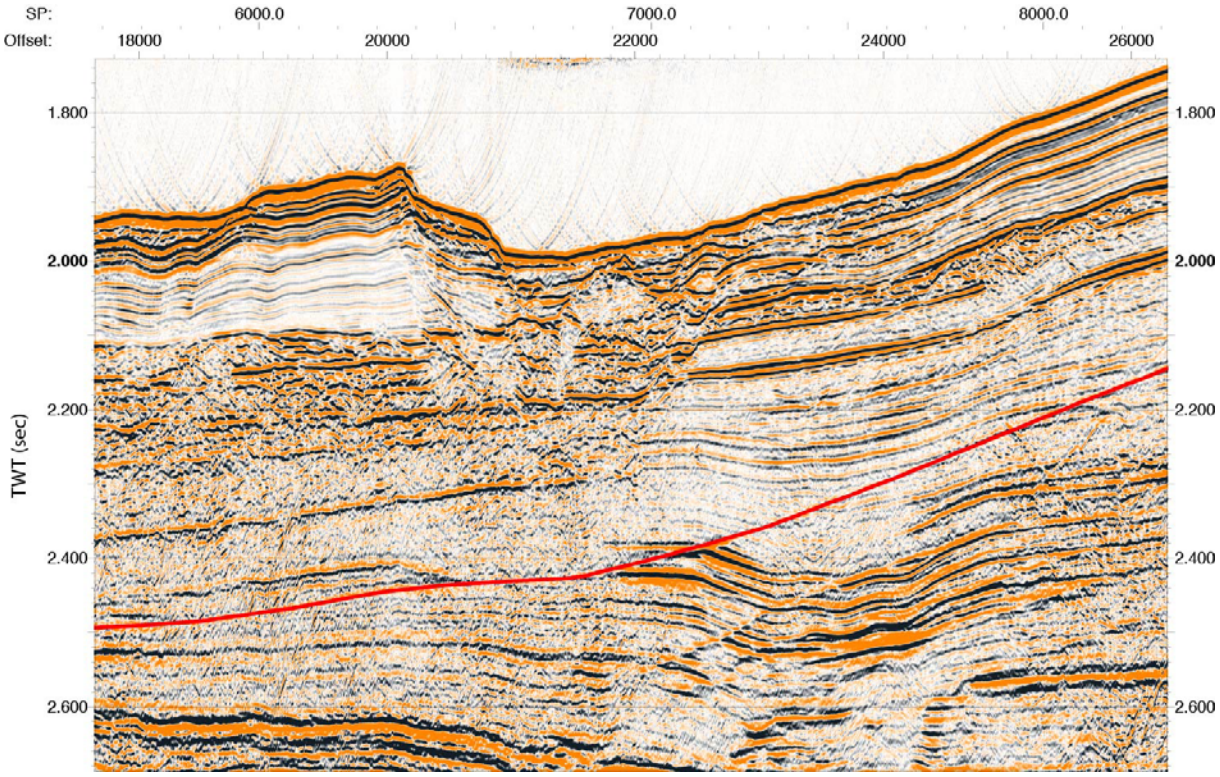

Fig. 5.3.1.2 Zoom of seismic profile MSM34-1_07. The selected window shows the buried channel system chosen for the first 3D acquisition (offset 20000 to 24000). The main BSR is marked in red. Additional BSRs are visible between offset 22000 to 24000 at about 2.4 s TWT and 2.5 s TWT.

A second target of investigation was identified in water depth of about 700 m along profile MSM34-1_15 (Fig. 5.3.1.3) at the cross points with profiles MSM34-1_23 and MSMS34-1_28. At the cross point of profiles 15 and 23 the bathymetric depression of a channel system deviates from its NW-SE trend to north-south heading. Underneath an adjacent oval shaped area of slope failure the seismic section shows a significant upward bending of the BSR. The projected intersection of the BSR with the seafloor would be in roughly 700 m water depth. It is assumed that variations in the subsurface temperature regime are responsible for the anomaly in the hydrate stability.

Two buried channel levee systems were chosen as a potential third target for the investigations of leg-2. At the cross points of profiles MSM34-1_18 and MSM34-1_02 well layered sediment horizons are interrupted by a sequence of chaotic reflection patterns. The base of these structures extend over 6 km on line MSM34-1_02 (Fig. 5.3.1.4). Downslope the reflection pattern could be followed towards the cross point of profiles MSM34-1_18 and MSM34-1_07, where the width of the chaotic pattern reduces to about 4 km.

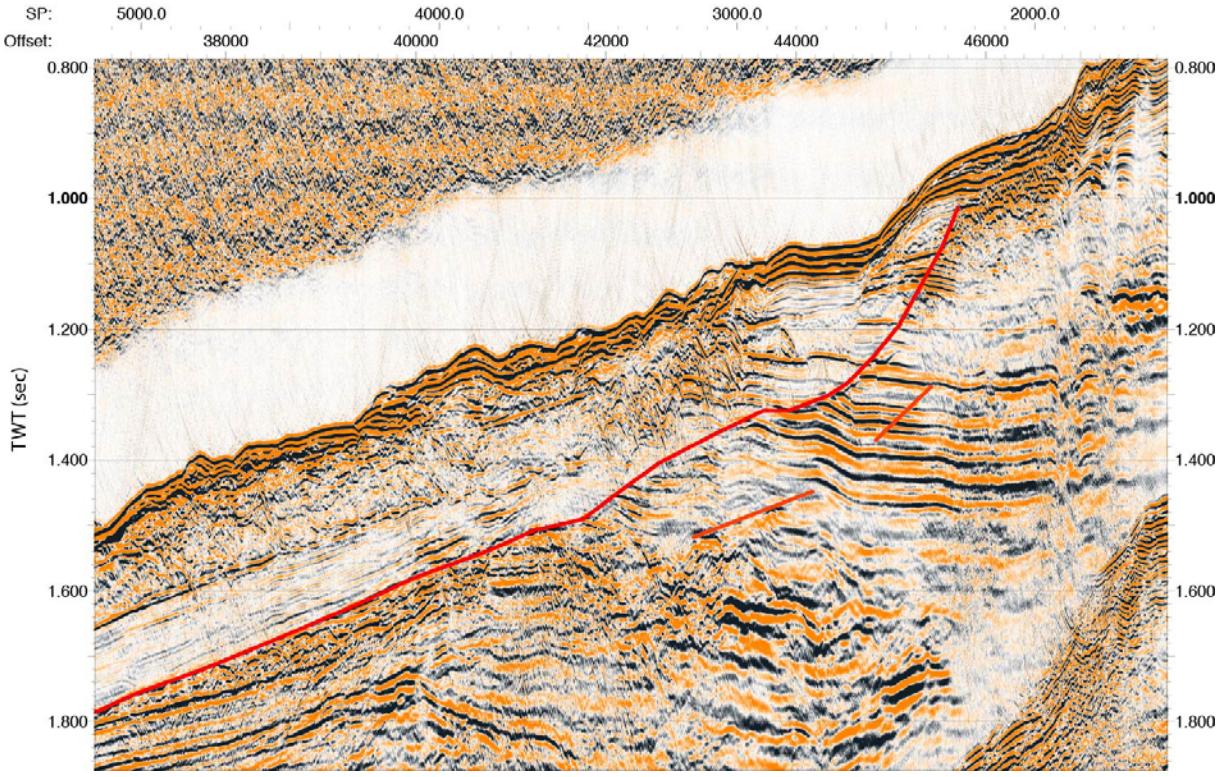

Fig. 5.3.1.3 Zoom of the seismic profile MSM34-1_15. The main BSR is marked continuously (red). An additional BSR could be identified at offsets 44000 and 45000 (red). The remarkably increased upward bending of the BSR indicate a change in the hydrate stability conditions. Therefore this area was chosen as second 3D seismic target.

Based on the 2D seismic grid of MSM34-1 an outline of the BSR extension in the working area was mapped (red polygon in Fig. 5.3.1.5). In the northeast the BSR limits of this investigation are almost coincident with the observations of Baristeas (2006) (yellow polygon in Fig.5.3.1.5). Due to a wider data coverage Popescu et al. (2006) (orange polygon in Fig. 5.3.1.5) continuously mapped the BSR further outside the MSM34 working area. Although the data coverage of this investigation and the work of Baristeas (2006) cover a similar

region, the BSR was mapped to larger water depth in the MSM34-1 data. [*Popescu et al.*, 2006] deviate slightly from the MSM34-1 BSR distribution in water depth greater than 1500 m. While the BSR outline of MSM34-1 and Baristeas (2006) cover a similar area at water depth shallower than 1500 m, the outline by Popescu et al. (2006) extends only half as wide (Fig. 5.3.1.5). Most likely the variations in BSR distribution of the three data sets are caused by different data coverage and data quality.

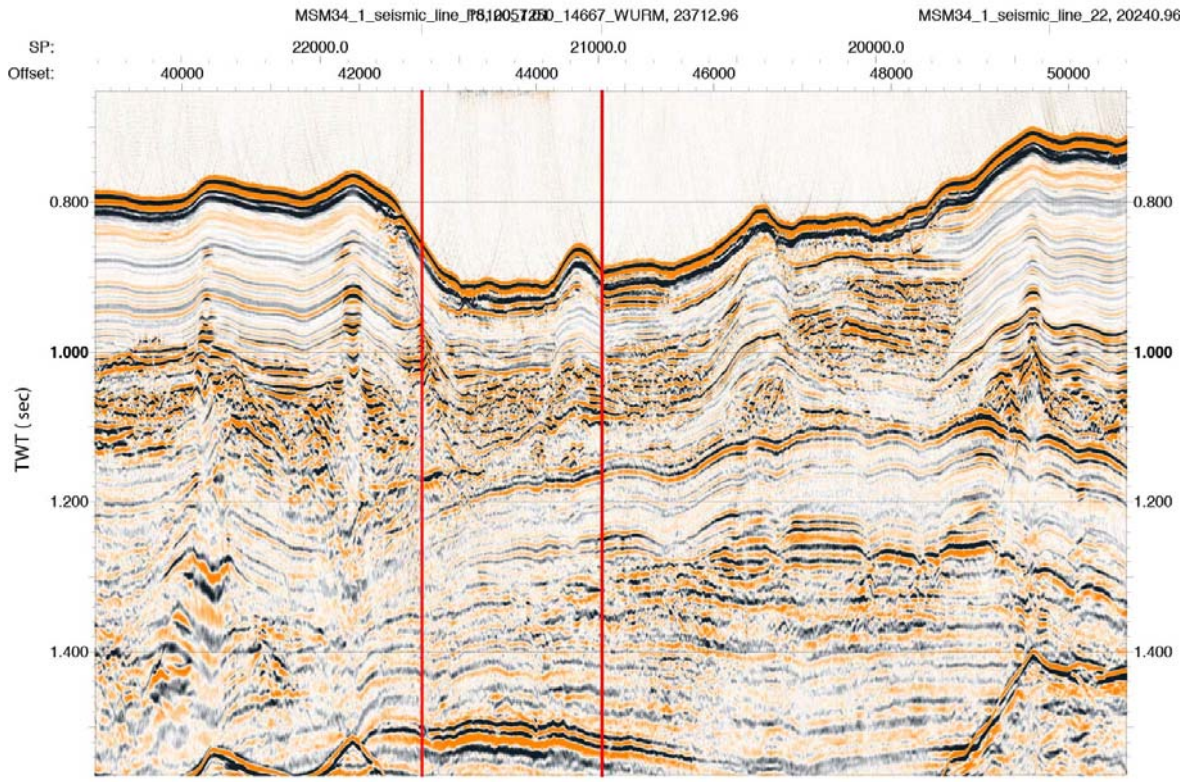

Fig. 5.3.1.4 Zoom of the seismic profile MSM34-1_02. Chaotic reflection pattern between offsets 42000 to 46000 and 47000 to 49000 outline the bottom limits of ancient channel systems.

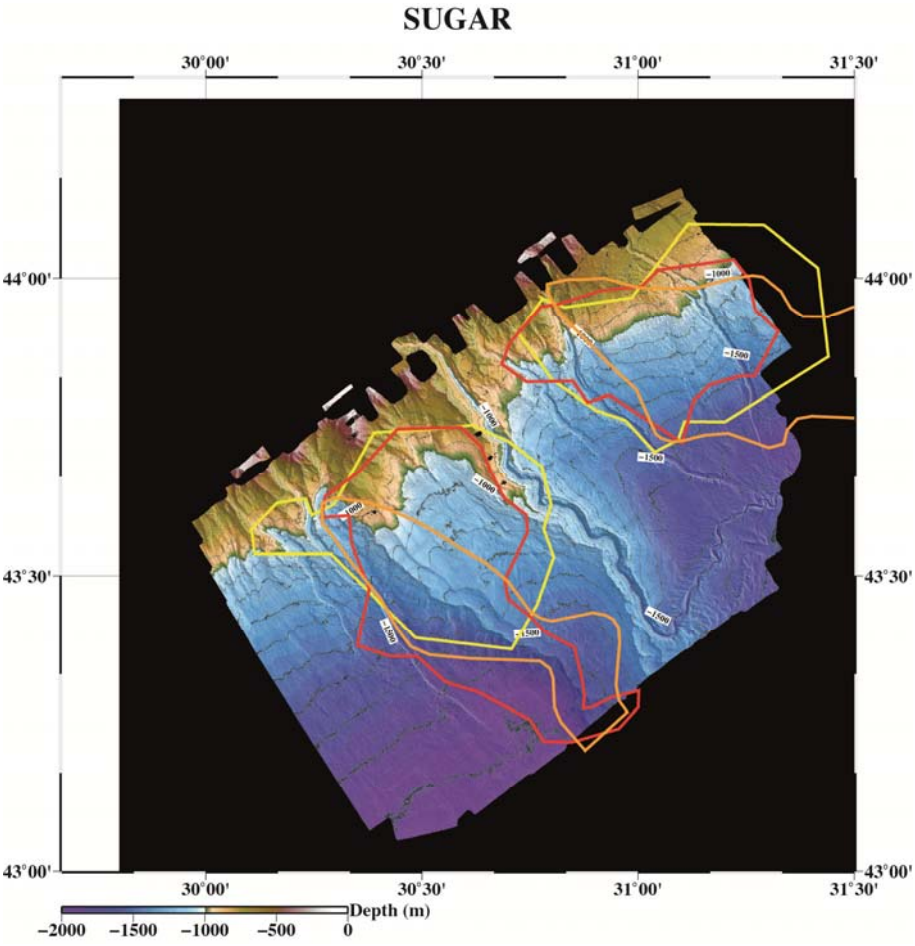

Fig. 5.3.1.5 Bathymetric map of the MSM34 working area. Polygons outline the BSR extend mapped from MSM34 2D seismic data (red), published by Popescu et al. (2006) (orange) and mapped by Baristeas (2006) (yellow).

5.3.1.1 Semblance velocity analysis

(Sudipta Sarkar, Orhan Atkin, Mert Kücük, Özkan Özel)

We used ProMAX™ to carry out semblance velocity analyses and deduce root mean square (RMS) velocities for normal move-out (NMO) correction (fig. 5.3.1.1). For this we made common mid-point (CMP) supergathers using 9 adjacent CMPs and then computed semblance. We picked velocities for which the hyperbolic reflections were best flattened in the CMP-offset display. Once the RMS velocities were computed we used the velocity table to flatten (NMO correction) the reflections.

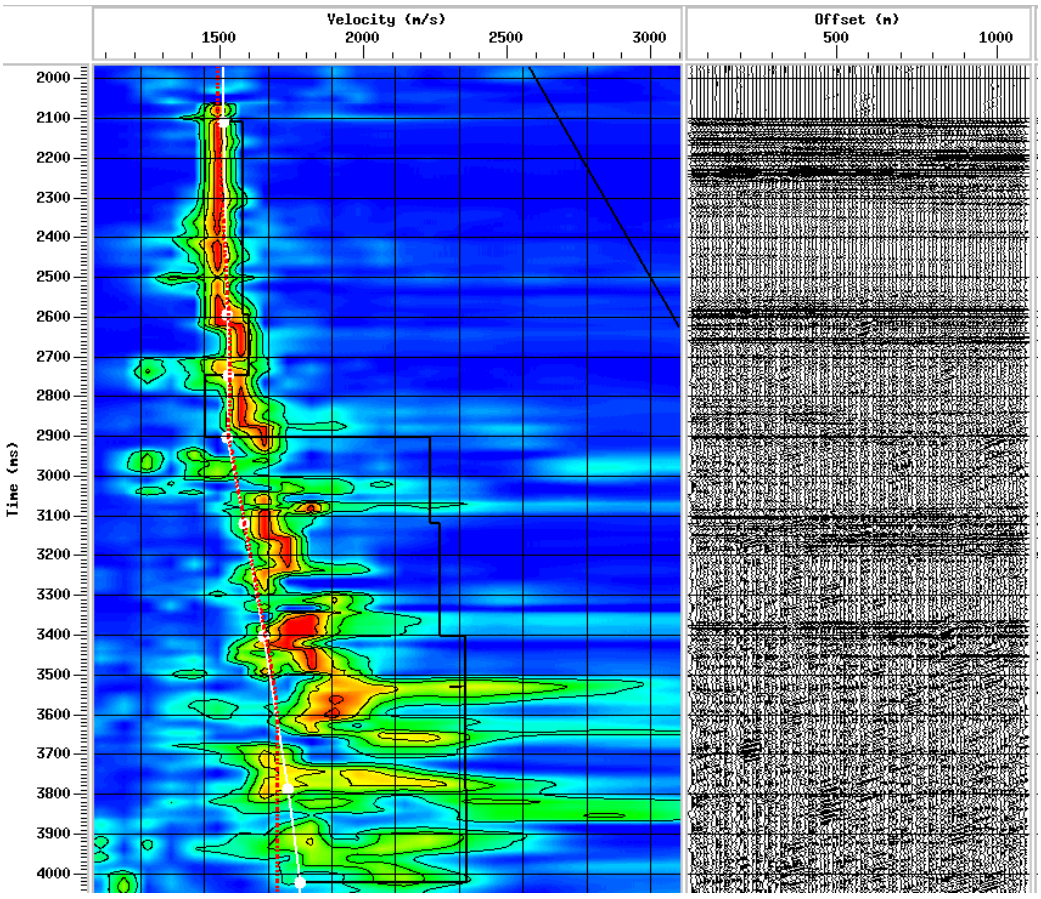

Fig. 5.3.1.1. Semblance velocity panel (left) showing the picks (white points) for which the hyperbolic reflections were best flattened (image on the right). Interval velocity profile (black curve on left image) following Dix's equation was computed from the stacking velocity that was picked on the semblance panel.

5.3.1.2 Stacking and post stack migration

We stacked the NMO corrected CMP gathers and produced a final stacked image. An interval velocity model (Figure 5.3.1.2) was generated from RMS velocities and was finally used to carry out post-stack Stolt migration. An example of a migrated profile is shown in Figure 5.3.1.3. This profile was finally loaded into kingdom for a general comparison with the brute stacked data. The velocity model from this analysis can be further used as an initial input model to prestack time migration processing.

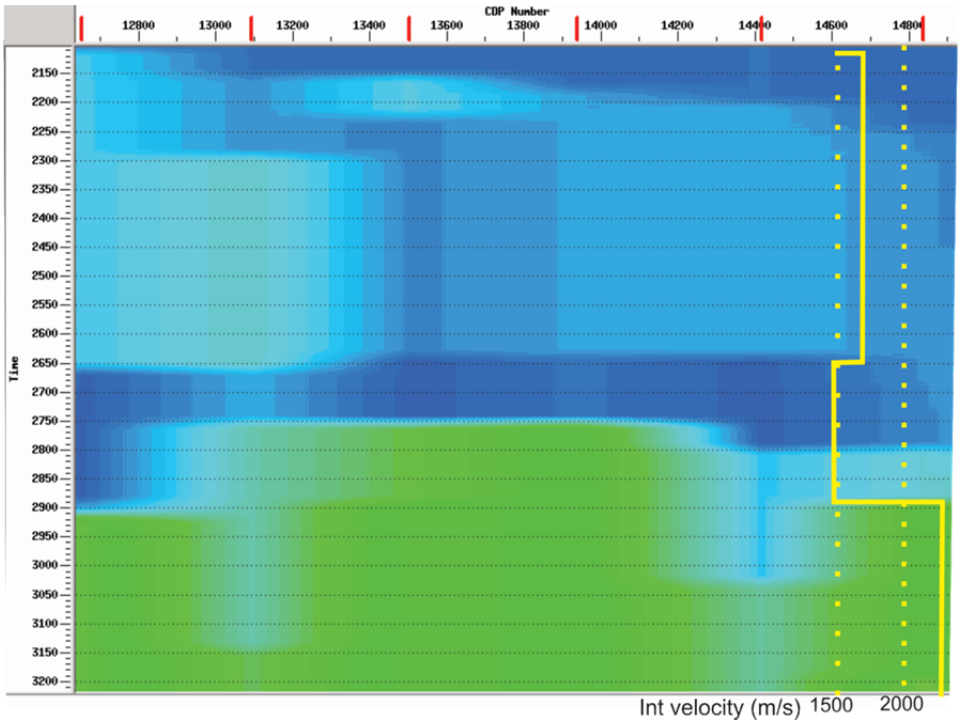

Fig. 5.3.1.2. Interval velocity profile generated from stacking velocities for the seismic section shown in Figure 5.3.1.3.

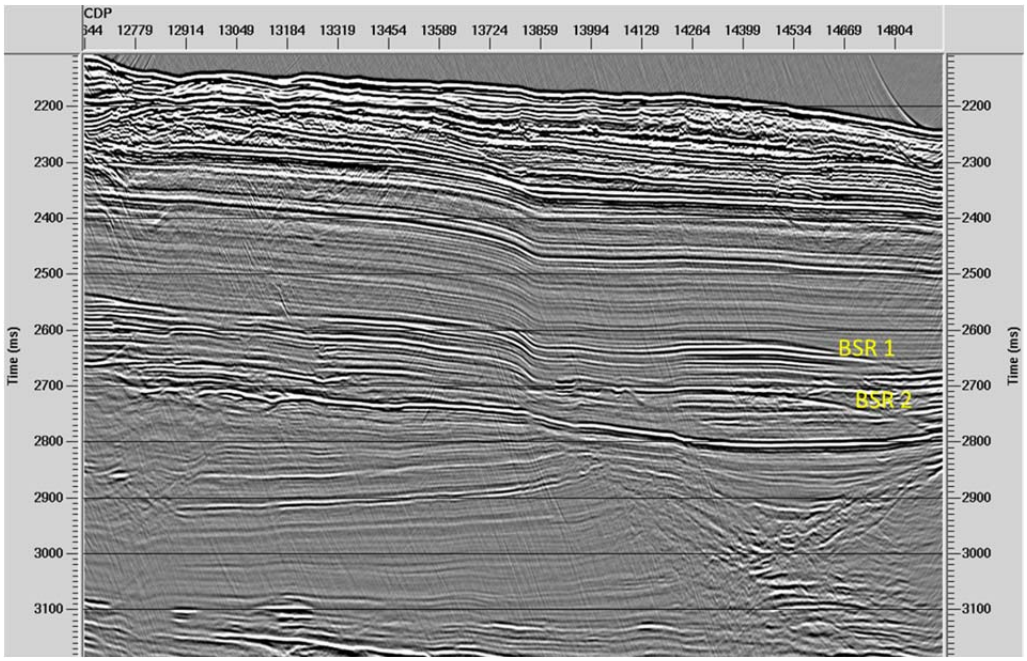

Fig. 5.3.1.3. Post stack Stolt migration result of a seismic profile showing multiple BSRs. The velocity model for this profile is shown in Figure 5.3.1.2.

5.3.2 High resolution 2D seismic

(Timo Zander, Jörg Bialas, Stephanie Koch)

The first set of high resolution 2D seismic lines was acquired across an ancient channel-levee system of the Danube paleo-fan (Fig. 5.1). Seismic line P1107 is shown in fig 5.3.2.1.

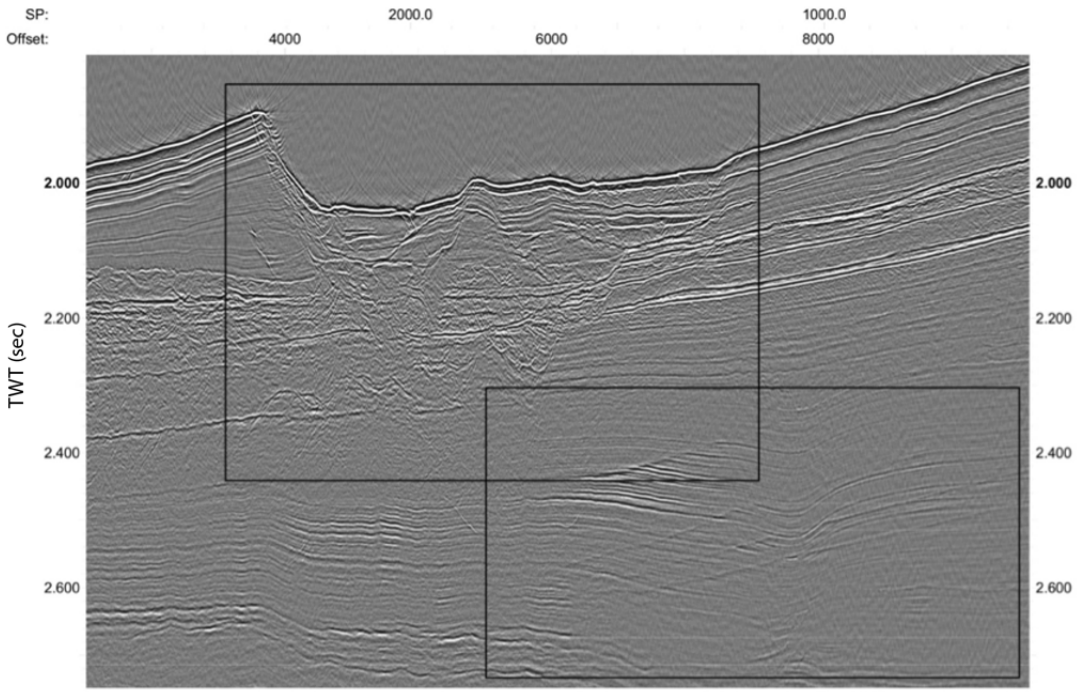

Fig. 5.3.2.1 High resolution 2D seismic profile P1107 across a buried channel levee system in working area 1

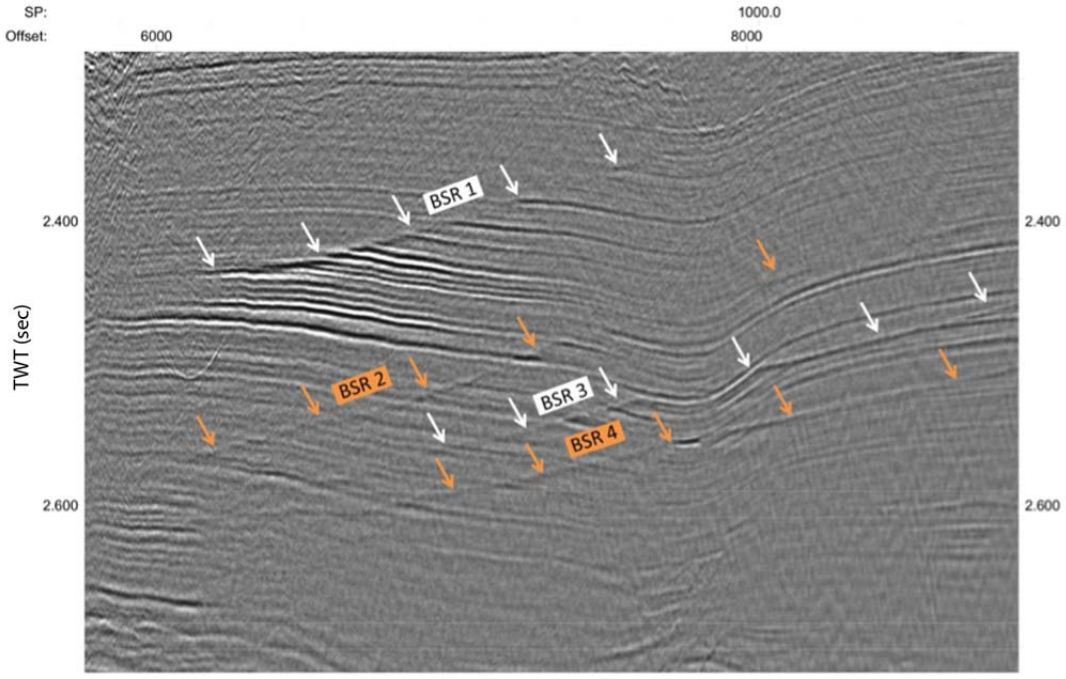

Fig. 5.3.2.2 Zoom of profile P1107 indicating the multiple BSR event in working area 1

In a depth of about 200 ms TWT below the seafloor on the eastern levee of the channel, a distinct BSR can be identified (BSR 1, fig. 5.3.2.2). It shows a reversed polarity, mimics the seafloor and thus crosscuts strata. Towards the axis of the channel, the BSR signature decreases and fades out, but also shows increased amplitudes in the underlying well-stratified sediments indicating a high gas-reservoir potential. The free gas might be trapped below the BGHSZ. Furthermore, up to three additional BSRs could be detected in the seismic data, each with a slightly varying dip (fig. 5.3.2.2). The observation of multiple BSRs agrees with the observations of Popescu et al. (2006).

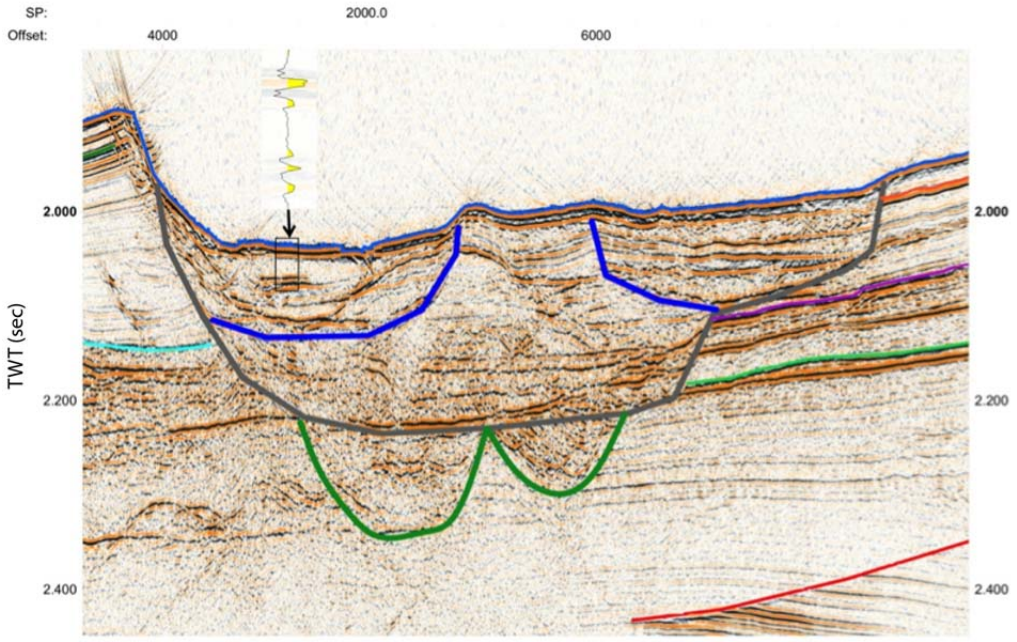

Fig. 5.3.2.3 Zoom of profile P1107 indicating the variability in channel levee systems in working area 1

The seismic line P1107 also reveals the complexity of the channel-levee system (fig. 5.3.2.3). Channel signatures can be identified up to 350 ms subseafloor depth. Only one channel was active at a time, with the most recent active channel in this area on top (west, highlighted dark blue in fig. 5.3.2.3) neighboring and overlying older channel pathways (gray, dark green in fig. 5.3.2.3). The channel sediments are expected to consist of varying coarse grained sand beds depending of the history of channel activity. Several HARs (high amplitude reflections) can be identified in the channel axes, often of reversed polarity as highlighted in (fig. 5.3.2.3).

The levees to both sides of the channel system are well stratified, but show variations in amplitudes. Some strong reflectors (orange, pink, light green, turquoise in fig. 5.3.2.3) are interpreted as facies changes.

BSR 1 is marked red in fig. 5.3.2.3 and is characterized by crosscutting the strata, marking the upper boundary of a package of high amplitude reflections in the well-stratified reflectors below. Therefore, the coarse grained channel sediments in this area are interpreted as a reservoir facies of high gas-hydrate potential.

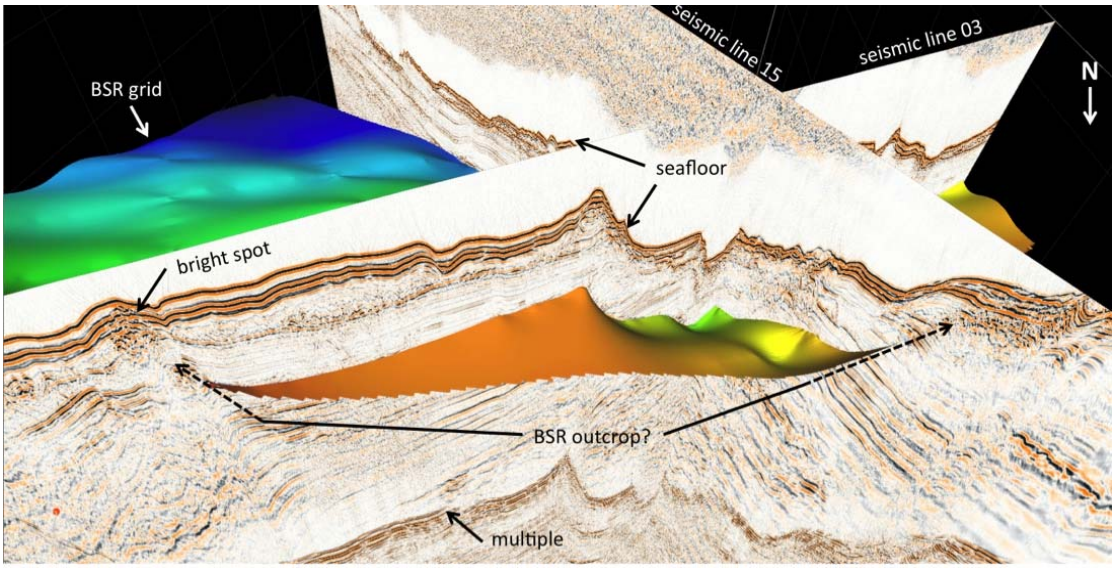

Fig. 5.3.2.4 3D perspective view of BSR1 interpreted from regional seismic 2D profiles

The BSR could be mapped in two areas by picking the BSR horizon on the dense grid of 2D seismic lines which were acquired during MSM34-1. After the picking, two separated BSR areas were identified, and a gridding algorithm interpolated the picks to a 3D horizon (fig. 5.3.2.4).

The eastern area shows a potential outcropping of the BSR from deep towards shallow water depths of about 700 m, which marks the upper boundary of the GHSZ in the Black Sea. Increased amplitudes below the BSR in seismic data as well as disturbed reflections and bright spots close to the seafloor indicate high gas content that migrates along the BSR towards shallower depths. The secondary low frequency SLF PARASOUND data show acoustic blanking in about 30 m depth below the seafloor that might be attributed to shallow gas at the projected BSR outcrop (fig. 5.3.2.5)

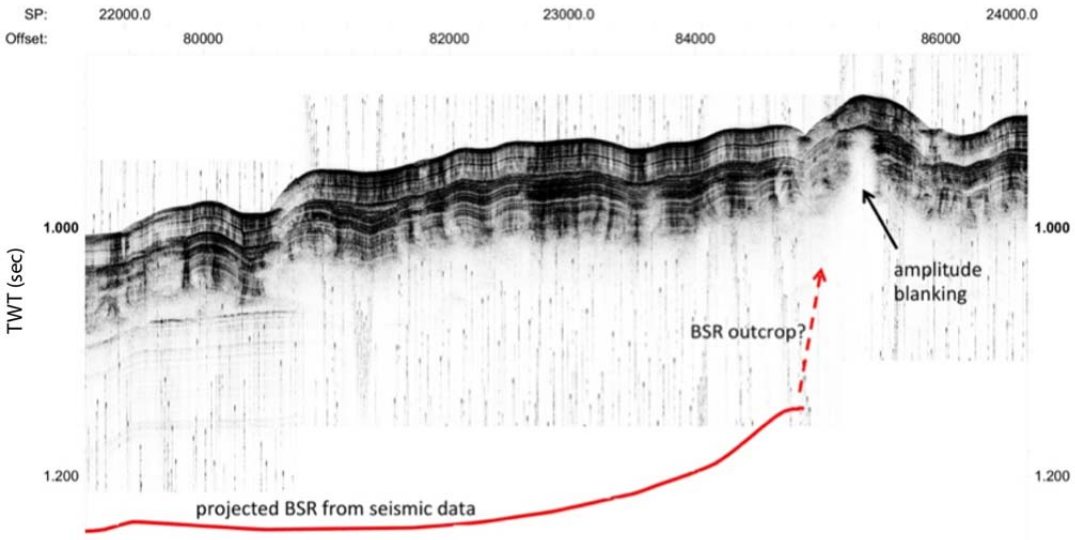

Fig. 5.3.2.5 Parasound image coincident with seismic profile MSM34-1 / 15 indicating a possible gas accumulation above the upward bending and termination of the BSR

A comparison of the seismic line 15 acquired during MSM34-1 with the 1 km SEISLAB streamer section and the seismic line p4103 acquired during MSM34-2 with the 2D P-Cable is shown in fig. 5.3.2.5. Both lines are almost identical in direction with a small parallel offset of about 90 meters. Deeper reflections are much better resolved on long streamer data allowing more channels to be stacked.

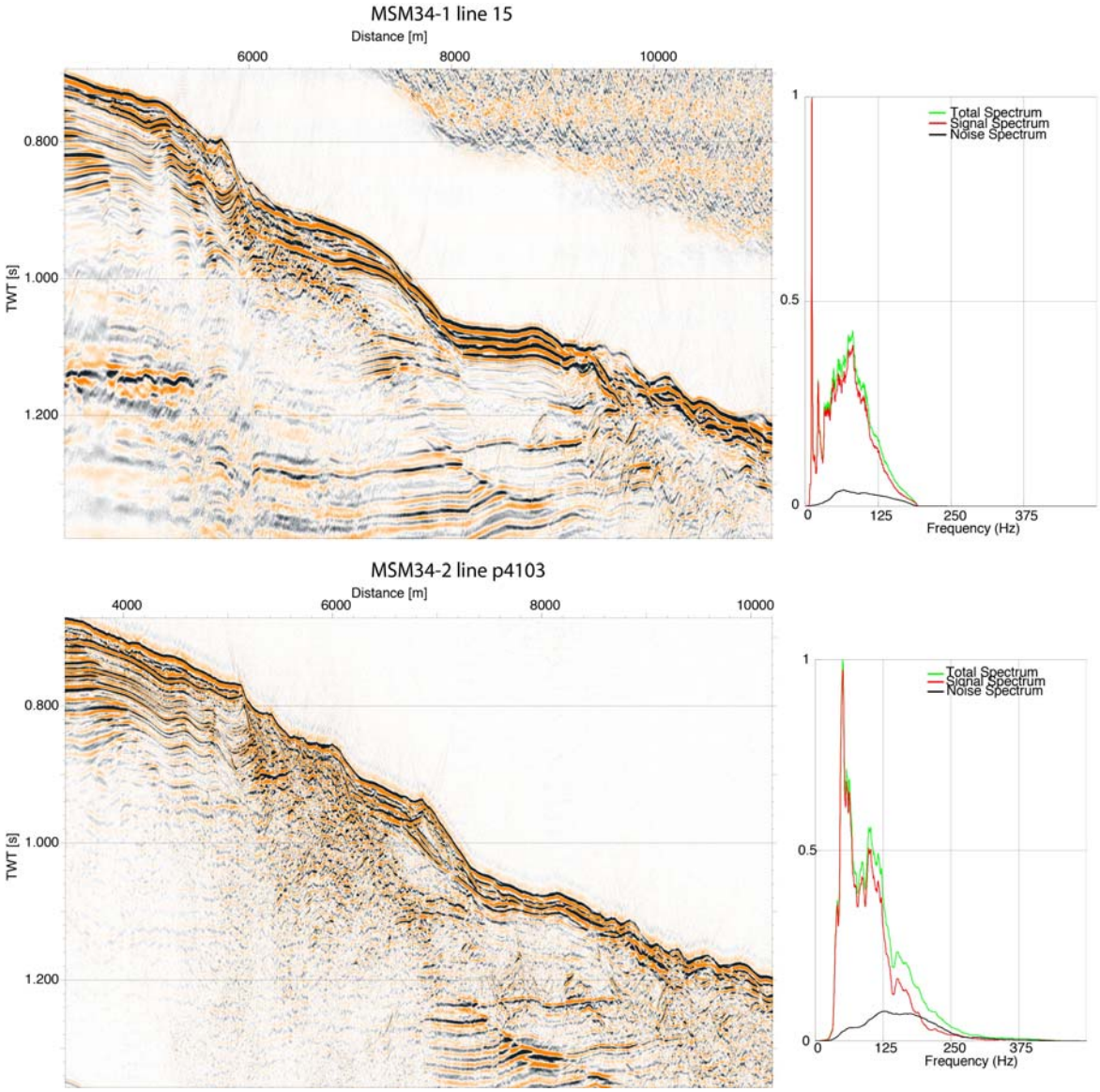

Fig. 5.3.2.6 Comparison of coincident 2D seismic profiles MSM34-1 / 15 and MSM34-2 P4103

5.3.3 3D P-Cable Seismic

(Jörg Bialas, Stephanie Koch, Torge Matthiessen, Gero Wetzel, Orhan Atkin, Felix Gross, Mert Kücük, Sudipta Srakar, Özkan Özel)

5.3.3.1 P-Cable area 1

As outlined in figure 5.1 an area of about 8 km * 6 km was chosen for a first high resolution 3D P-Cable survey.

Restricted to 14 nodes in a first deployment the array could be widened to 15 nodes in the subsequent deployments. Source signals were generated by a 45 cinch / 45 cinch GI airgun at

3 sec shot interval. During three days of profiling 15 OBS were recording the airgun shots as well.

QC test during the time of recording confirmed data quality and navigation information storage for later post processing of the data volume.

5.3.3.2 P-Cable area 2

The second work area for the high resolution 3D seismic studies was chosen above an unusual upward bending of the BSR (chapter 5.3.1). The 4 km * 4 km wide area of the 3D multichannel seismic survey covers a failed part of the slope. Water depth in this area increases from about 600 m to 900 m, including the top of the hydrate stability at about 650 m water depth.

Again the P-Cable array could be deployed with 15 nodes (app. 11.3.3 P3xxx). Source signals were generated by a 45 cinch / 45 cinch GI airgun at 3 sec shot interval. The entire volume was acquired without any interruption. 12 OBS were deployed for a complete record of the 3D airgun shots.

QC test during the time of recording confirmed data quality and navigation information storage for later post processing of the data volume.

5.3.4 OBS data and results

Anke Dannowski, Isabel Sauermilch, Henning Schröder

Ocean Bottom Seismometer (OBS) were deployed in the two main research areas of the cruise MSM34-2. The main target of the deployment was to provide velocity information for 2D and 3D seismic processing and to get a second imaging possibility apart from the streamer and P-Cable seismics. Moreover wide angle OBS observation provide the possibility to apply AVO analyses in order to investigate physical parameters. In case of PS conversion the horizontal components of the OBS can be used for development of a shear wave velocity model.

5.3.4.1 Work area 1

A total of 15 OBS were deployed in three lines with 5 instruments per line (Fig. 5.2). The water depth varied between 1420 m and 1515 m. The instruments were deployed in the evening of December 30th 2013. Afterwards the streamer was deployed and eight profiles (P1101 - P1108) of 2D seismic, crossing the OBS were shot during the following 20 hrs. The shot interval was 5 s with an GI-airgun volume of 45 in^3/ 45 in^3.

After one day the streamer was replaced by the P-Cable system, while the OBS remained on the seafloor. The shot interval was reduced to 3 s the airgun volume remained at 45 in^3/ 45 in^3. During the night from January 4th to 5th 2014 while the P-cable system was on deck for maintenance all OBS were recovered. Thus, the instruments did not record all the shots from the 3D P-cable cube. However shots were recorded from all azimuths around each station. In general the 15 instruments worked continuously well while three geophone components on two different stations failed during recording only. All stations can be used to generate a high resolution velocity model as further input for the 3D and 2D processing and interpretation. A receiver gather example from OBS-1014 along line P1107 is shown in Fig. 5.3.4.1. It represents the overall data quality.

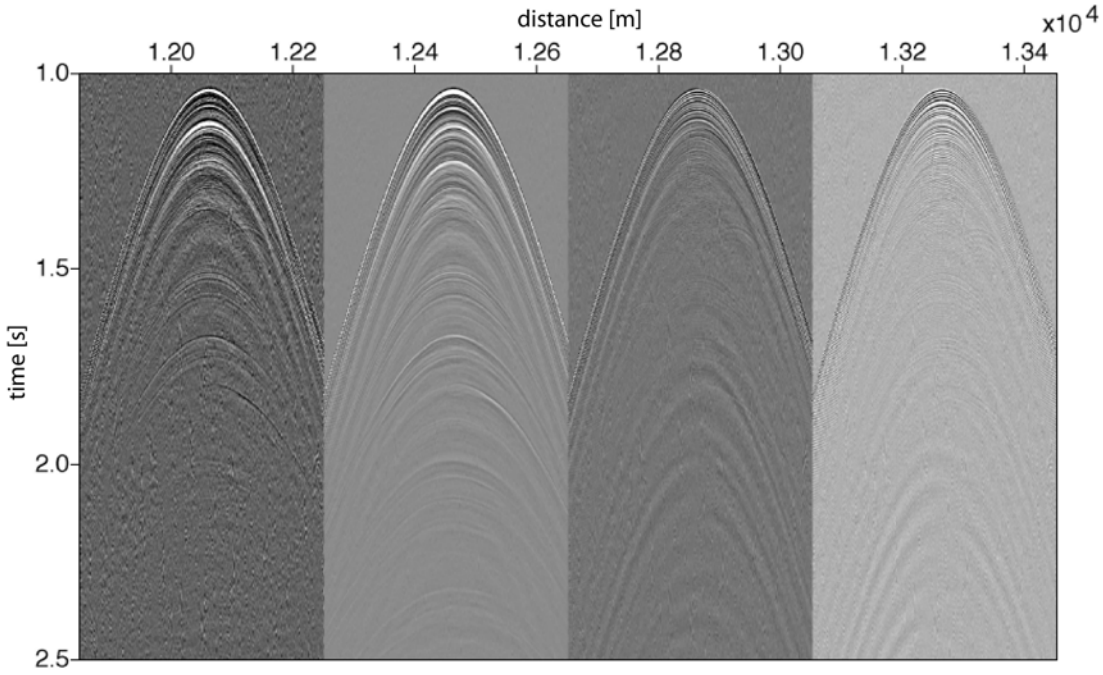

Fig. 5.3.4.1 Receiver gather of OBS-1014 along profile P1107
From left to right: hydrophone, vertical, H1, H2 component

OBS and 2D seismic data can directly be compared which is illustrated in Fig. 5.3.4.2. using OBS-1004 along line P1107. By this method it is easier to follow the horizons from instrument to instrument to pick travel times for the further modelling procedure. A first rough 2D model using apparent velocities (assuming non dipping topography) shows very low seismic P-wave velocities for the uppermost portion of the sedimentary layers. The few first 10th of meters have velocities of about 1600 m/s.

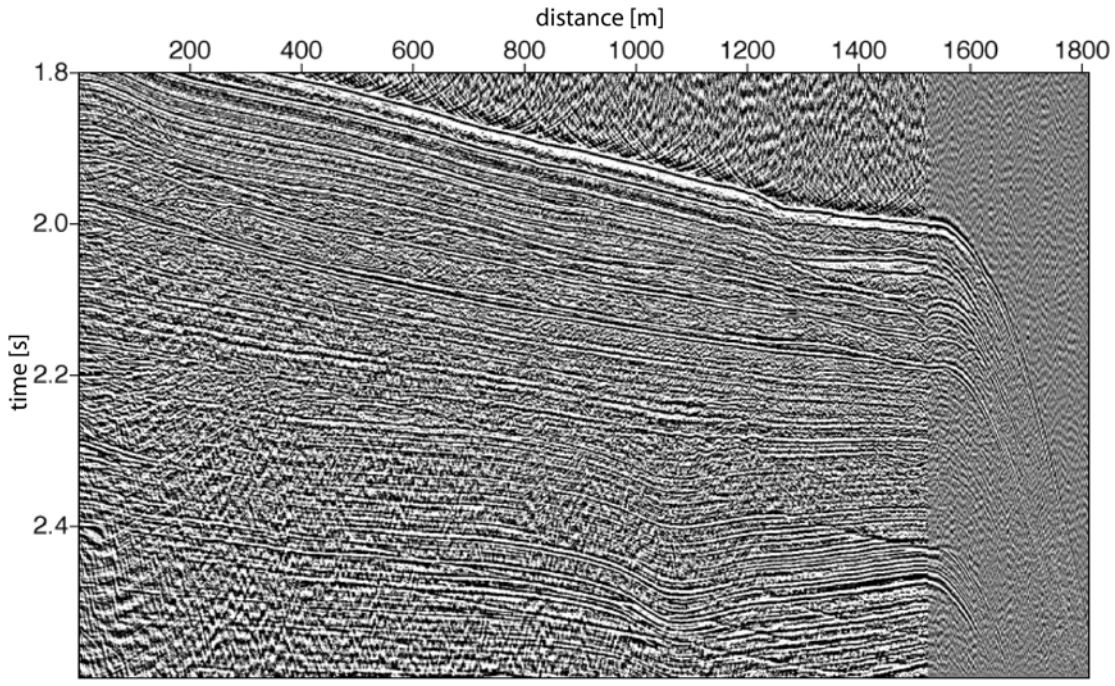

Fig. 5.3.4.2 Simultaneous plot of 2D MCS data of profile P1107 (shots 0 – 1500) and corresponding records of OBS-1004 (shots 1501 – 1800)

Although the seafloor is very muddy and loose, the geophones, separated from the system carrier, provided a good coupling to the seafloor resulting in good quality data. However, a high frequency ringing could be observed with frequencies higher than 150 Hz (fig. 5.3.4.3).

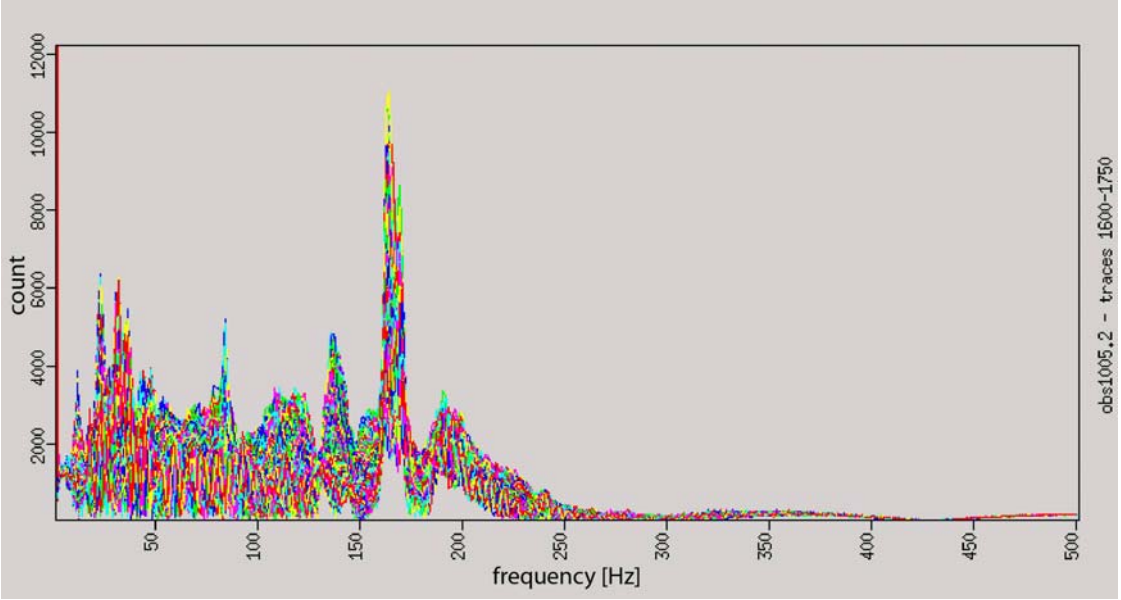

Fig. 5.3.4.3 Frequency spectra of OBS-1005 with a noticeable frequency peak at 160 Hz

Figures 5.3.4.4.a-c display OBS-1005 without filtering and with two different filter settings, respectively. The ringing might be caused due to the soft seafloor in the observation area since it did not appear so strong during deployments with seafloor having higher P-wave velocities.

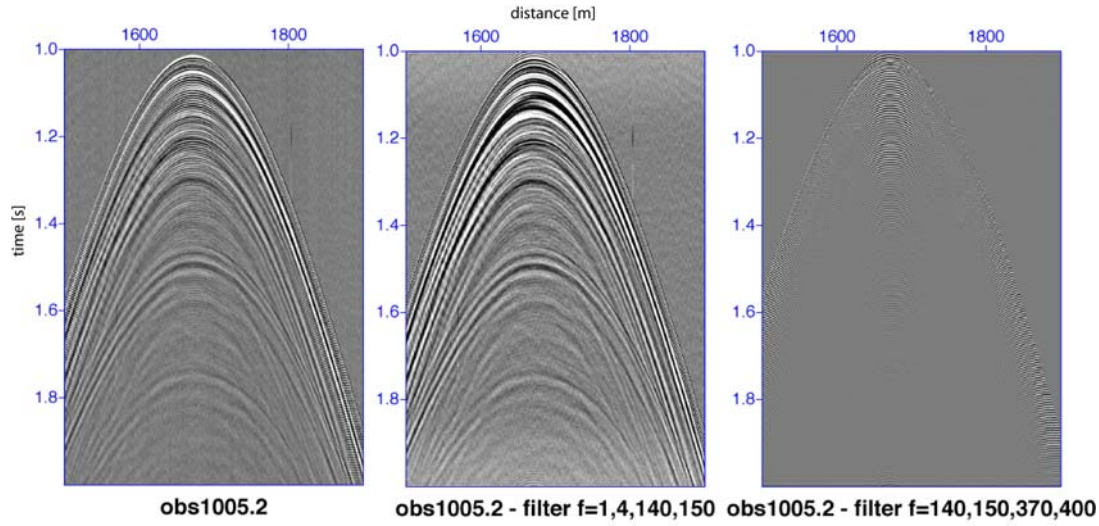

Fig. 5.3.4.4 from left to right vertical component of OBS-3005 a) raw data , b) bandpass filtered excluding the 160 Hz peak, c) remaining high frequency energy

5.3.4.2 Work area 2

In the second working area 12 instruments were again deployed in three lines in the centre of the 3D seismic cube (fig. 5.3). In the evening of January 09 2014 they were deployed and remained on the seafloor until January 14 2014. This area was shallower than area 1. The deployment depth for the OBS ranged between 600 and 860 m. The 12 OBS recorded all the

shots from the second 3D cube of the P-cable acquisition. Additionally, they recorded the airgun shots of the following 2D seismic lines that were acquired in the night from January 13 to 14 2014. Some of the instruments went low on battery and may not record all 2D seismic lines, but still kept their synchronisation. The data quality of the OBS in the second area is again very high and this time each instrument delivered data for every single component without any failure. A shot gather example of OBS-3008 is shown in (fig. 5.3.4.5).

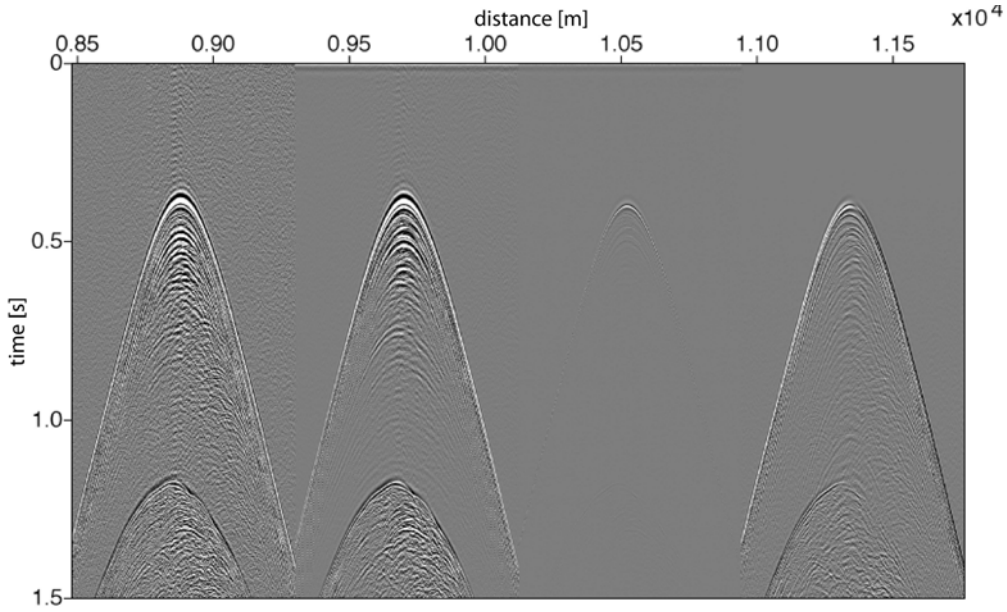

Fig. 5.3.4.5 Receiver gather of OBS-3008
From left to right: hydrophone, vertical, H1, H2 component

Figure 5.3.4.6 displays the OBS receiver gather compensated for direct arrival of station OBS-3001 during relocation processing of the OBS. All stations showed a similar difference between deployment position and recording position, thus, the OBS drifted while sinking to the seafloor in the direction of sea currents.

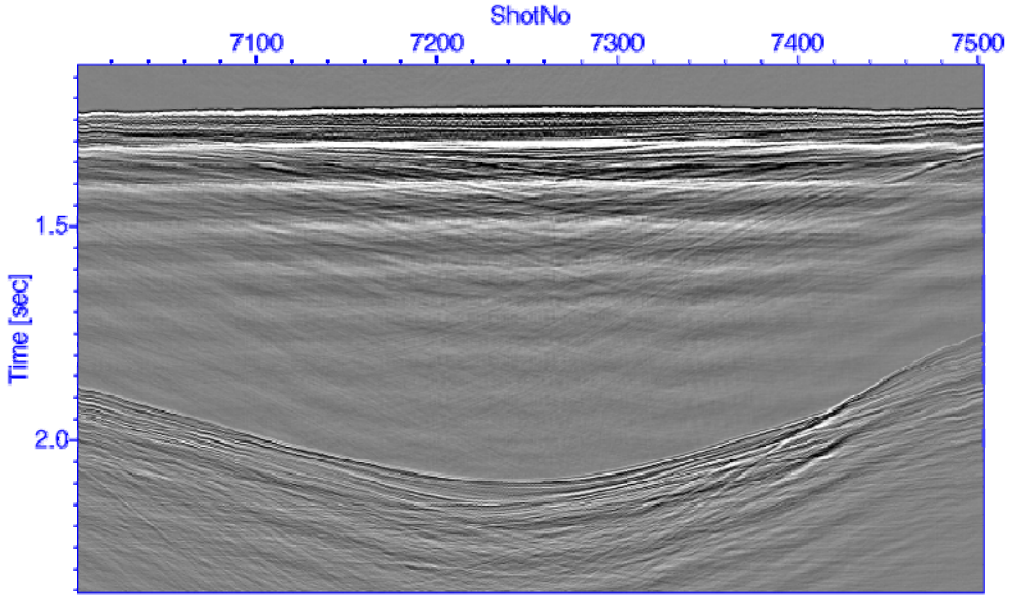

Fig. 5.3.4.6 Receiver gather of OBS-3001 displayed with direct arrival compensation for verification during relocation processing

A comparison of OBS-3005 with the MCS data from line P4103 can be seen in figure 5.3.4.7. Major phases seen in the MCS data can be resolved in both datasets down to the first multiple. This comparison helps to correlate the phases between the OBS, a crucial step for further data interpretation and the generation of a background velocity field for the MCS data and the processing of the 3D P-cable cube.

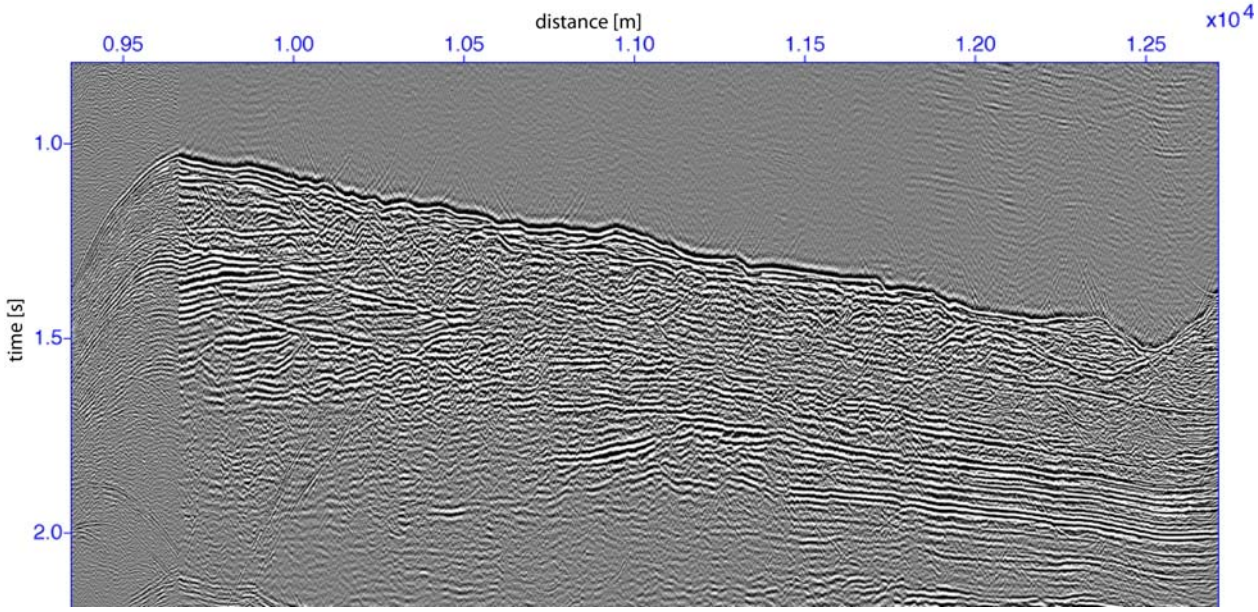

Fig. 5.3.4.7 Simultaneous plot of 2D MCS data of profile P4103 (shots 9800 – 12500) and corresponding records of OBS-3005 (shots 9400 – 9800)

5.4 Geochemistry

(Matthias Haeckel, Thomas Pape, Meike Dibbern, Nikolaus Bigalke, Dirk Schroller)

5.4.1 Introduction

The geochemical analyses of the porewaters and sediments of the Paleo Danube deltas in the Black Sea aim at quantifying methane fluxes and turnover rates of associated biogeochemical processes as well as determining the sources of gases and fluids migrating in the subsurface and forming gas hydrate accumulations in the area. Therefore, a comprehensive geochemical dataset has been collected on this cruise.

On board, the collected samples were analysed for their content of NH4+, PO43-, SiO44-, H2S, total alkalinity, and dissolved methane. In addition, sub-samples were taken for further shore-based analyses: methane δ13C and δD isotope ratios, DIC content and its δ13C isotope ratio, dissolved metal cations, SO42-, Br-, Cl-, and I- concentrations, isotopic ratios of Sr, Cl, Li, H, and O in the porewater as well as porosity, carbonate, POC, PON, and sulfur content of the solid phase (Table 5.4.1).

The sampling locations were chosen, where gas and gas hydrate accumulations in the deeper subsurface are anticipated from the 2-D seismic information collected on the first leg (Fig. 5.1 & 5.2).

5.4.2 Materials and Methods

5.4.2.1 Sediment and porewater sampling

Surface and subsurface sediment samples were retrieved using a mini-corer (MIC) and a gravity corer (GC). The sediments were extruded out of the MIC plastic liners with a piston and cut into 0.5 to 2 cm thick slices, whereas GC cores were cut in half and 3-5 cm thick slices were taken in approximately 20-40 cm intervals. Subsequently, the porewater was extracted in the ship's cold room (4 °C) using a low pressure-squeezer (argon at 3-5 bar, sometimes up to 7 bar). While squeezing, the porewater was filtered through 0.2 µm cellulose acetate Whatman filters and collected in recipient vessels.

About 5 ml of wet sediment of each sediment slice was collected for porosity, carbonate and CNS element analyses at home. Aliquots of the extracted porewater were sub-sampled for various on board and further shore-based analyses (Table 5.4.1). Subsamples for ICP-AES analysis were acidified with 30 µl of conc. suprapure HNO3 per 3 ml of porewater sample (i.e. pH<1) and subsamples (~1.9 ml) for δ13C and DIC were treated with 10 µl of HgCl2 to inhibit further microbial degradation. All samples for home-based analyses were stored refrigerated. In total, 364 samples from 17 cores were collected for porewater analysis (Table 5.4.1).

For analysis of light hydrocarbons dissolved in porewater in MIC and GC cores, 3 ml of wet sediment was subsampled with cut-off syringes and transferred into 20-ml glass vials prefilled with 5 ml of a 1M NaOH solution for on board headspace methane and higher hydrocarbon analyses. The vials were closed with butyl rubber stoppers and capped, thoroughly shaken and stored at 4 °C for at least 12 h before analysing. From the 17 cores retrieved during the cruise a total of 520 sediment samples was collected and analysed during the cruise (Table 5.4.1).

5.4.2.2 Porewater analyses

Analyses for the nutrients NH4+, PO43-, SiO44- as well as H2S were completed onboard using a Hitachi UV/VIS spectrophotometer. The respective chemical analytics followed standard procedures (Grasshoff et al., 1999), i.e. ammonium was measured as indophenol blue, phosphate and silicate as molybdenum blue, and sulfide as methylene blue. Since high sulfide contents (> 1 mM) interfere with the reactions of NH4+, PO43-, and SiO44-, the respective sub-samples were bubbled with argon to strip any H2S prior to the analysis.

The total alkalinity of the porewater was determined by titration with 0.02 N HCl using a mixture of methyl red and methylene blue as indicator. The titration vessel was bubbled with argon to strip any CO2 and H2S produced during the titration. The IAPSO seawater standard was used for calibration.

The analytical precision and accuracy of each method are given in Table 5.4.2.

Table 5.4.2 Analytical methods of onboard geochemical analyses.

Parameter	Method	Detection limit	Analytical precision/accuracy
H_2S	Photometer	3 µmol/l	3 %
NH_4^+	Photometer	5 µmol/l	5 %
PO_4^{3-}	Photometer	1 µmol/l	5 %
SiO_4^{4-}	Photometer	5 µmol/l	2 %
Alkalinity	Titration	0.1 meq/l	2 %
CH_4	Gas chromatograph	0.1 ppmV	2 %

5.4.2.3 Headspace gas analyses

Gases (methane and higher hydrocarbons) dissolved in the porewater were analyzed onboard using an Agilent Technologies 6890N gas chromatograph equipped with a capillary column and a flame ionization detector. Calibrations and performance checks of the analytical system were conducted regularly using commercial pure methane standards and hydrocarbon mixtures. The coefficient of variation determined for the analytical procedure was lower than 2%.

5.4.3 Results

The geological stratigraphy and geochemical processes in Black Sea sediments as well as their associated porewater profiles are well-known from previous cruises, e.g. TTR-15, M72/3, M84/2, SPUX. Observed variations in stratigraphy, geochemical gradients and solid phase compositions reflect the local setting, which may be influenced by turbidites and mass wasting at the slopes and upward migrating methane gas along faults and fractures. Hence, the sediment sequences and porewater profiles observed in cores retrieved during MSM34/2 are discussed against the general Black Sea lithology and geochemistry of the upper few meters below seafloor, which are recapitulated here.

A complete photo documentation of individual cores retrieved with GC and MIC is given in Appendix 11.1.

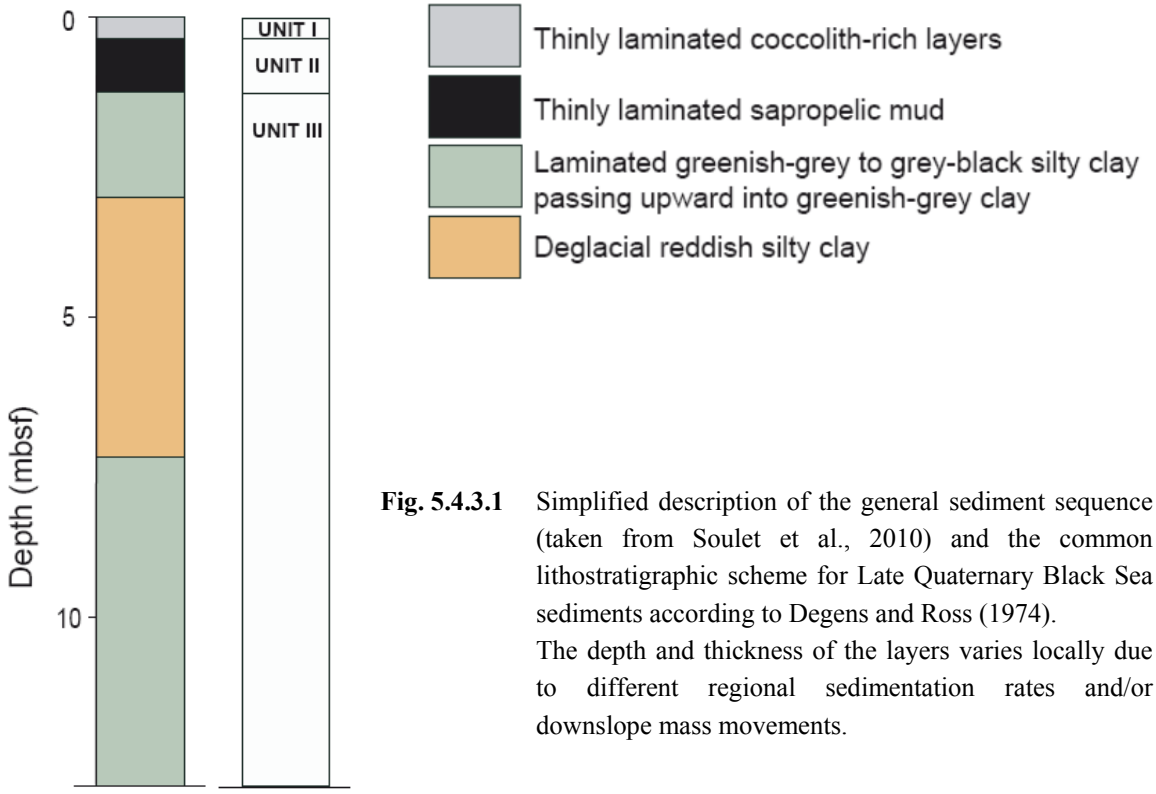

Fig. 5.4.3.1 Simplified description of the general sediment sequence (taken from Soulet et al., 2010) and the common lithostratigraphic scheme for Late Quaternary Black Sea sediments according to Degens and Ross (1974).
The depth and thickness of the layers varies locally due to different regional sedimentation rates and/or downslope mass movements.

5.4.3.1 Late Glacial to Holocene Black Sea Sediment Lithology

Typical Black Sea sediments comprise of finely laminated coccolith ooze (Unit 1; Fig. 5.4.3.1) at the top, followed by a finely laminated sapropel (Unit 2; Fig. 5.4.3.1) with distinct light laminations rich in needle-shaped authigenic aragonite towards the base. Both, Unit 1 and 2, represent the current marine stage of the Black Sea. Further downcore grayish mud of lacustrine origin follows (Fig. 5.4.3.1), representing the limnic stage of the Black Sea during the last glacial. During this time, the global sea level fell below the sill depth of the Bosphorus (~35 m; Bahr et al., 2008), leading to a disconnection of the Black Sea from the Sea of Marmara and the Mediterranean Sea. The reconnection of the Black Sea with the Sea of

Marmara occurred at around 9.4 ka (Major et al.,2006). The inflow of saline marine water caused the formation of the present stratification of the Black Sea water column and the manifestation of anoxic conditions below ~150 m water depth. These anoxic conditions lead to the accumulation of the organic-rich sediments of Units 1 and 2. The base of the sapropel (Unit 2) has been dated to 7.5 ka by Jones and Gagnon (1994), an age that has later been refined to 8.0 ka (Lamy et al., 2006). The first prolonged invasion of coccolithophorides occurred at 2.7 ka (Jones and Gagnon, 1994) marking the base of Unit 1. An often recurring feature of Unit 3 is a distinct blackish-dotted/-banded interval (in 250-350 cm) rich in amorphous Fe-sulfides (Neretin et al., 2004), termed “hydrotroilite” (Limonov et al., 1994). These black horizons are related to the anaerobic oxidation of methane (AOM, see geochemistry further below) that produces hydrogen sulfide as one reaction product and which is subsequently precipitated below the AOM reaction zone. The black color is lost within a few hours if the core is opened, since these Fe-sulfides oxidize rapidly. Seep-influenced cores often show disturbed bedding and a “moussy” consistency due to degassing

during core retrieval (see e.g., 66-2 GC7), making exact assignment of unit boundaries difficult.

5.4.3.2 General Black Sea Sediment Geochemistry

Background sediments in the Black Sea are those not influenced by gas (methane) and/or oil seepage or mud expulsion. Since these sediments are overlain by completely anoxic bottom water – in the Black Sea oxygen and nitrate are typically consumed within the upper ~150 m of the water column – sulfate reduction and methanogenesis are the dominant early diagenetic processes. In fact, the upward diffusing methane typically consumes the dissolved sulfate that is diffusing into the sediment within the upper 250-350 cm of the sediment. This anaerobic oxidation of methane (AOM) leads to an increase in total alkalinity and hydrogen sulfide. The produced hydrogen sulfide then reacts with dissolved iron in the porewater forming FeS that is readily recognized as black spots and layers in the sediment and often builds up a continuous zone of several decimeters to a meter in thickness (see 'hydrotroilite' discussion in the above lithology section). Similarly, dissolved phosphate is consumed by mineral formation with e.g., dissolved iron, roughly 100 cm below the depth of H2S depletion. Dissolved ammonium and phosphate are released during the microbially mediated degradation of organic material in the sediment, which occurs primarily via sulfate reduction and methanogenesis. In contrast to phosphate, ammonium is not involved in any mineral formation or other reactions and hence continuously accumulates in the porewater leading to concentrations of 1-2 mM in the upper 5-6 m of the sediment. Likewise, concentrations of methane, one of the final products of organic carbon degradation, are also increasing below the depth of sulfate penetration. This can be witnessed on deck by a downcore increasing intensity of degassing of the sediment, since methane solubility drops drastically due to pressure reduction during core retrieval.

Table 5.4.1 List of sampled cores and collected sub-samples.

Station Device	Area	Latitude (N)	Longitude (E)	Water depth / m	PW	Poros / CNS	IC	ICP-AES / $^{87/86}Sr$	CH4 / $\delta^{13}C_{CH4}$	DIC / $\delta^{13}C_{DIC}$	Iso	Length of core / cm	No. of PW samples	No. of gas samples
3-2 MIC1	IFREMER Piezometer	43°48.353'	30°24.792'	420	X	X	X	X		X	X	50	29	20
3-3 GC1	IFREMER Piezometer	43°48.354'	30°24.786'	420	X	X	X	X	X	X	X	500	22	24
22-1 GC2	SW channel-levee multiple BSR, seismic 8b	43°25.679'	30°26.055'	1550	X	X	X	X	X	X	X	485	17	28
26-1 MIC2	SW channel-levee multiple BSR, channel	43°27.237'	30°24.470'	1498	X	X	X	X		X	X	51	24	30
27-1 MIC3	SW channel-levee multiple BSR, levee	43°28.099'	30°26.040'	1465	X	X	X	X		X	X	40	21	28
39-1 GC3	SW channel-levee multiple BSR, channel	43°27.245'	30°24.472'	1500	X	X	X	X	X	X	X	485	17	32
40-1 GC4	SW channel-levee multiple BSR, levee	43°28.093'	30°26.036'	1470	X	X	X	X	X	X	X	484	20	35
42-1 MIC4	SW channel-levee multiple BSR, seismic 8b	43°25.675'	30°26.055'	1550	X	X	X	X		X	X	42	21	38
43-1 GC5	NE channel-levee, upbending BSR, slump	43°57.443'	30°46.506'	674	X	X	X	X	X	X	X	484	19	33
43-2 MIC5	NE channel-levee, upbending BSR, slump	43°57.443'	30°46.508'	680	X	X	X	X		X	X	38	20	39
51-1 GC6	NE channel-levee, upbending BSR, slump	43°57.177'	30°46.272'	724	X	X	X	X	X	X	X	448	22	31
65-1 MIC6	NE channel-levee, upbending BSR, slump	43°57.177'	30°46.722'	726	X	X	X	X		X	X	41	22	38
66-1 MIC7	NE channel-levee, upbending BSR, slump	43°57.177'	30°46.530'	638	X	X	X	X		X	X	44	22	40
66-2 GC7	NE channel-levee, upbending BSR, slump	43°57.177'	30°46.529'	635	X	X	X	X	X	X	X*	500	21	30
74-1 MIC8	NE channel-levee, upbending BSR, slump	43°57.439'	30°46.513'	679	X	X	X	X		X	X	42	21	39
74-2 GC8	NE channel-levee, upbending BSR, slump	43°57.440'	30°46.512'	678	X	X	X	X	X	X	X	500	21	35
89-1 GC9	NE channel-levee, upbending BSR, channel	43°57.685'	30°47.750'	827	X	X	X	X	X	X	X	500	25	45

GC = gravity corer; MIC = mini-corer; PW = porewater analyses of TA, H_2S, NH_4, PO_4, SiO_4; IC = ion chromatography (SO_4, Br, Cl, I); ICP-AES = inductively-coupled atomic emission spectroscopy (for various dissolved cations); Iso = Isotope ratios of porewater O, H, Cl, Li; *no Li

Another peculiarity of Black Sea porewaters is the linearly decreasing chloride concentration in the surface sediments. Chloride and other sea salt ions are still diffusing from the overlying, marine and thus, saline, water body into the salt-depleted lacustrine sediments from before 10,000 years ago. Minimum Cl concentrations of 25-30 mM are reached in 20-25 m sediment depth (Manheim and Schug, 1978; Soulet et al., 2010). This circumstance will be used to determine, how much surface sediment was lost during recovery and overpenetration of the GCs. For overpenetrated cores, we, consequently, report sediment depths as 'coring depth', whereas if the sediment surface was recovered, i.e. with the MIC, we report actual sediment depths.

5.4.3.3 IFREMER piezometer site at shallow water depth

A mini-MUC and a GC core (3-2 MIC1 and 3-3 GC1) were retrieved at a shallow water site (~420 m), where the piezometer of IFREMER was deployed on the first leg (see chapter 5.6). The GC overpenetrated a lot and we currently estimate that the top ~150 cm were lost during recovery. The site is characterized by higher POC degradation at larger depth, i.e. below core penetration, as indicated by the NH4 concentrations that increase linearly to almost 2.5 mM at 500 cm sediment depth (Fig. 5.4.3.2). The POC degradation rate is slightly higher than observed in other areas of the Black Sea (see previous cruise reports from TTR15, M72/3, and M84/2). The typical diffusively fueled AOM is observed with a reaction peak at ~75 cm coring depth, as indicated by a maximum total alkalinity (TA) value of ~20 meq/l and linearly decreasing values towards the sediment surface (see also MIC1) and towards the bottom of the core. H2S peaks at a similar coring depth. A strong CH4 concentration gradient occurred between ca. 40 and 150 cm coring depth.

5.4.3.4 SW channel-levee system / multiple BSRs

3 sites were sampled in the southwestern channel-levee system that exhibits multiple BSR reflections at depth and a strong seismic reflector within the shallowest channel-fill (see chapter 5.3). As indicated by TA values of less than 10-12 meq/l and broad peaks (Fig. 5.4.3.3), AOM appears to be less intensive than typical, i.e. lower methane flux from below. In the channel (26-1-MIC2, 39-1 GC3) the upward methane flux and, hence, the AOM activity is slightly higher than at the levee site (27-1 MIC3, 40-1 GC4).

5.4.3.5 NE channel-levee system / upward bending BSR

In total 9 cores were sampled at the northeastern channel-levee system, where the 2-D seismic data (see chapter 5.3) indicated an upward bending BSR. At this site the limit of the gas hydrate stability is approached, i.e. at a water depth of 665 m. Fig. 5.4.3.4 shows the methane–seawater phase diagram for bottom water salinities of 22.3 and porewater salinities of ~3 in relevant sediment depths of 25-300 m and regional geothermal gradients.

3-2 MIC1

3-3 GC1

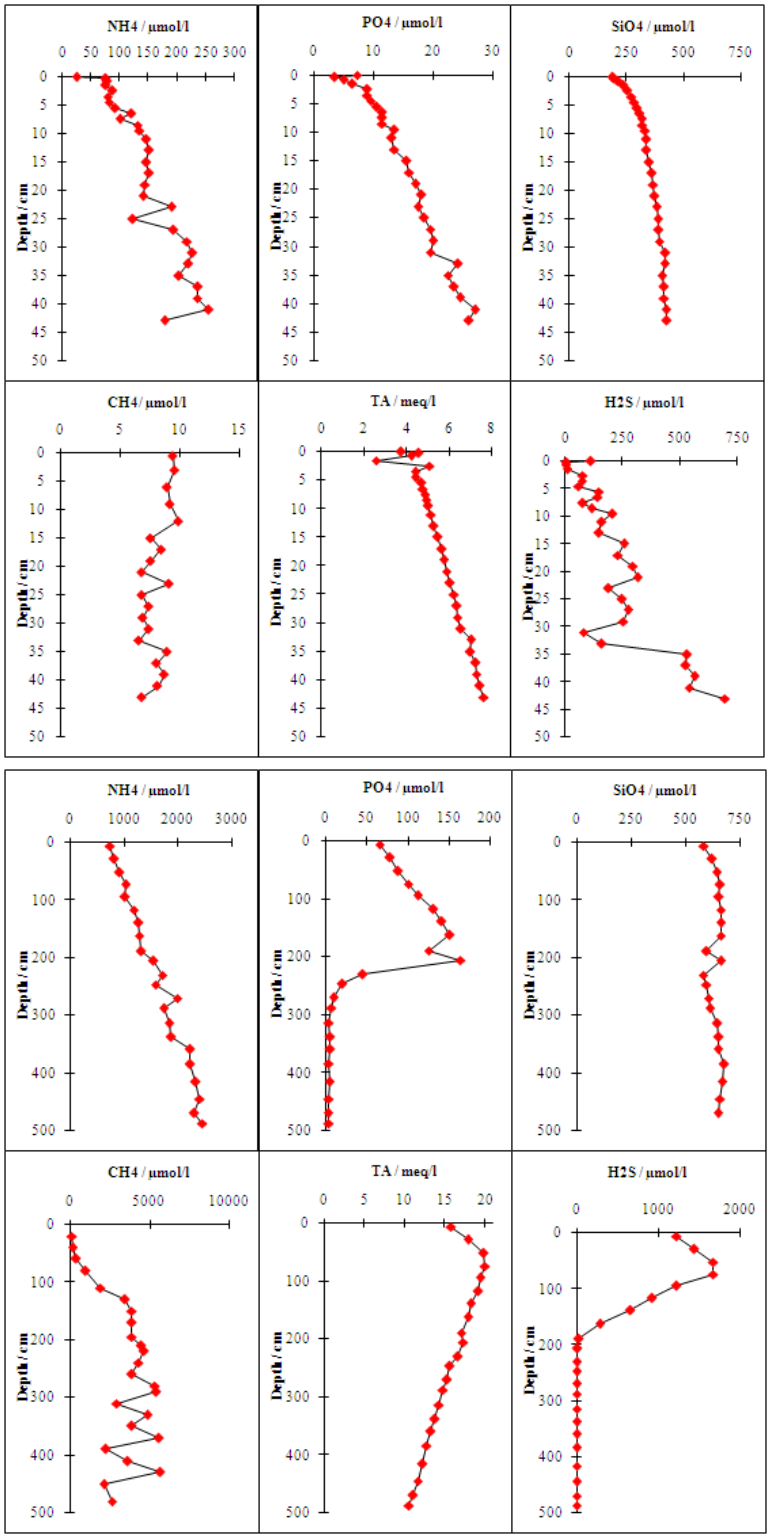

Fig. 5.4.3.2 Measured concentrations of porewater constituents of 3-2 MIC1 (top) and 3-3 GC1 (bottom) at the 420-m piezometer location. Note the different concentration scales for MIC and GC. The sediment gap between MIC and GC is an estimated 150 cm.

39-1 GC3

40-1 GC4

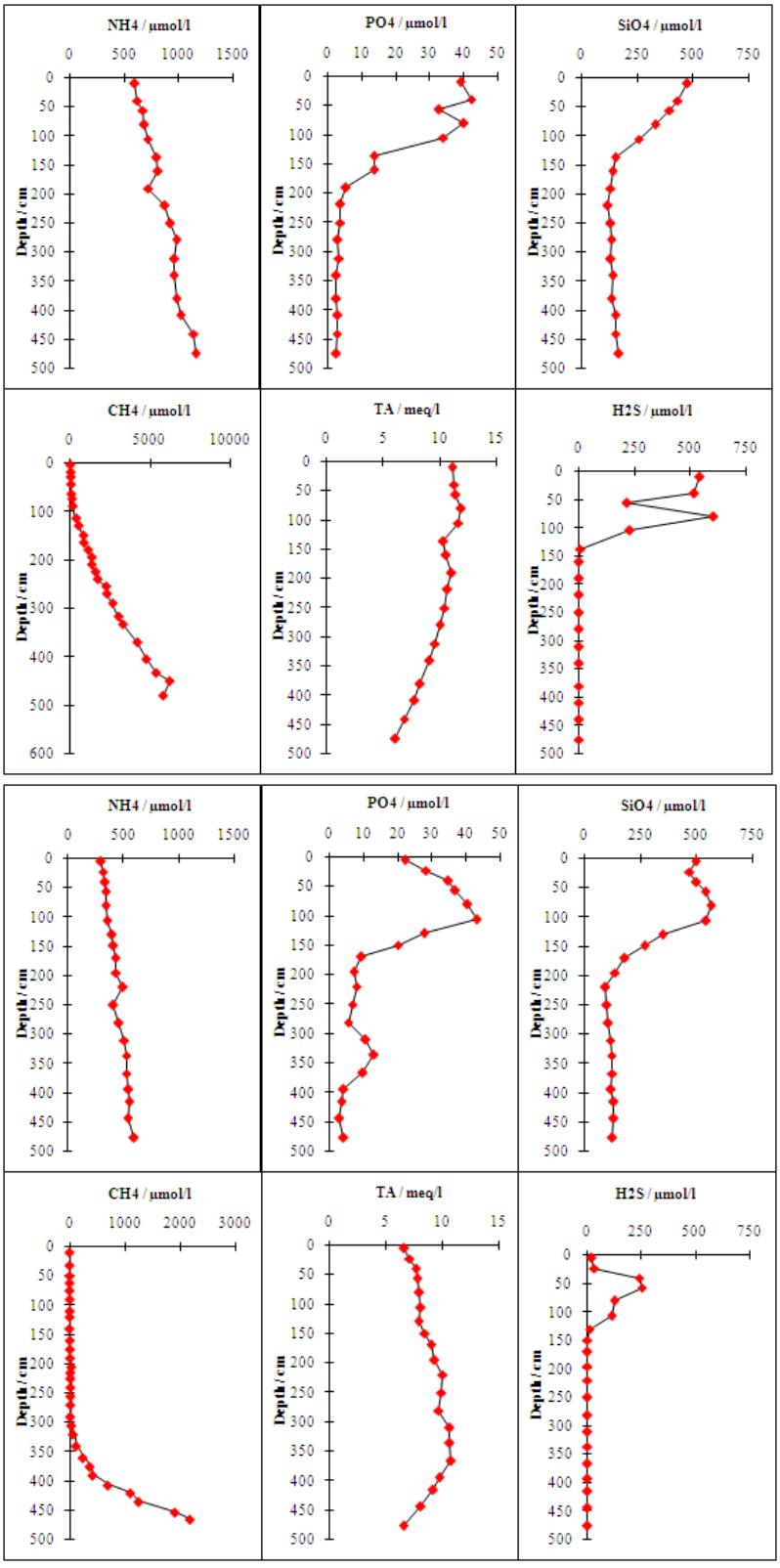

Fig. 5.4.3.3 Measured concentrations of porewater constituents in the channel (39-1 GC3, top) and the levee (40-1 GC4, bottom).

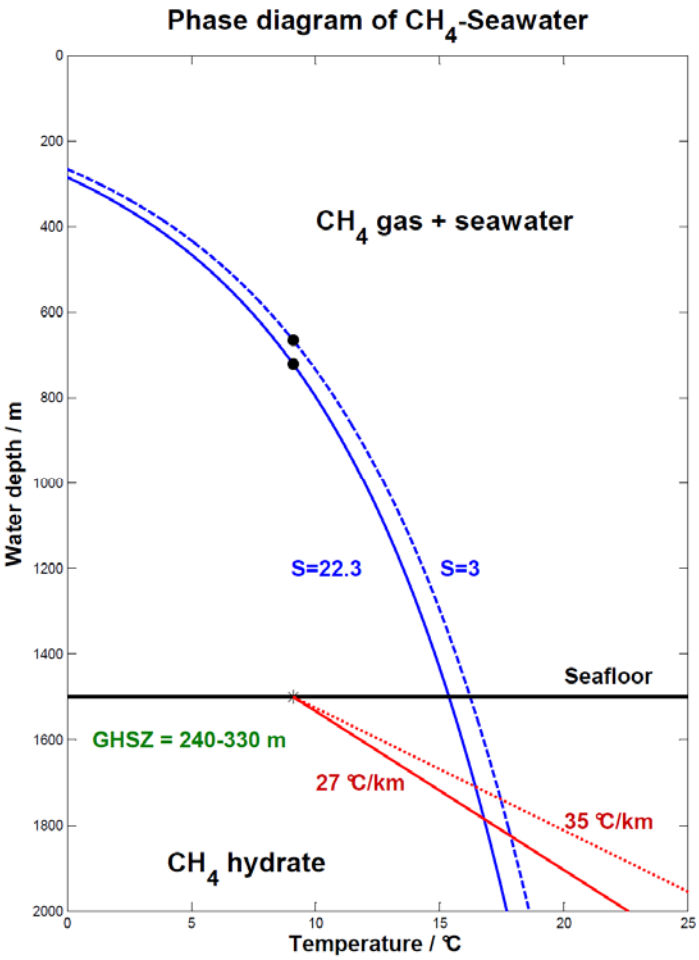

Fig. 5.4.3.4: Gas hydrate stability for pure s-I methane hydrate for porewater (S=3; in 25-300 m sediment depth) and bottom water (S=22.3) salinities.

The minimum water depths, where gas hydrates are stable under ambient bottom water temperatures of 9.1 °C are indicated by black dots: 665 m for S=22.3 and 721 m for S=3.

For the regional observed geothermal gradients of 27-35 °C/km (see chapter 6.4) a gas hydrate stability zone (GHSZ) of 240-330 m (relevant salinity is S=3) results.

The upward bending BSR coincided with a sediment slump at the seafloor, located above the levee west of the channel. We took sediment cores at the eastern flank of the slide and its eastern head wall, where gas seepage was detected with the Parasound system. As expected, the methane flux and respectively the AOM rate are highest at the gas seep (66-1 MIC7; Fig. 5.4.3.5) with maximum TA and H2S values at ~30 cm sediment depth and a strong methane increase in the same depth.

Generally, the methane flux seems to correlate with the observed geothermal gradient (see chapter 5.5), respectively heat flow, i.e. the higher the heat flow, the more intense is the upward methane flux and corresponding AOM. The geothermal gradient and the methane flux appear to be lowest, exactly where the water depth matches the upper limit of the GHSZ (around 670 m). This may potentially indicate that here, gas hydrates are dissociating and thereby cool down the heat flow. The highest heat flow and correspondingly a high methane flux were observed in the channel itself (89-1 GC9; Fig. 5.4.3.5).

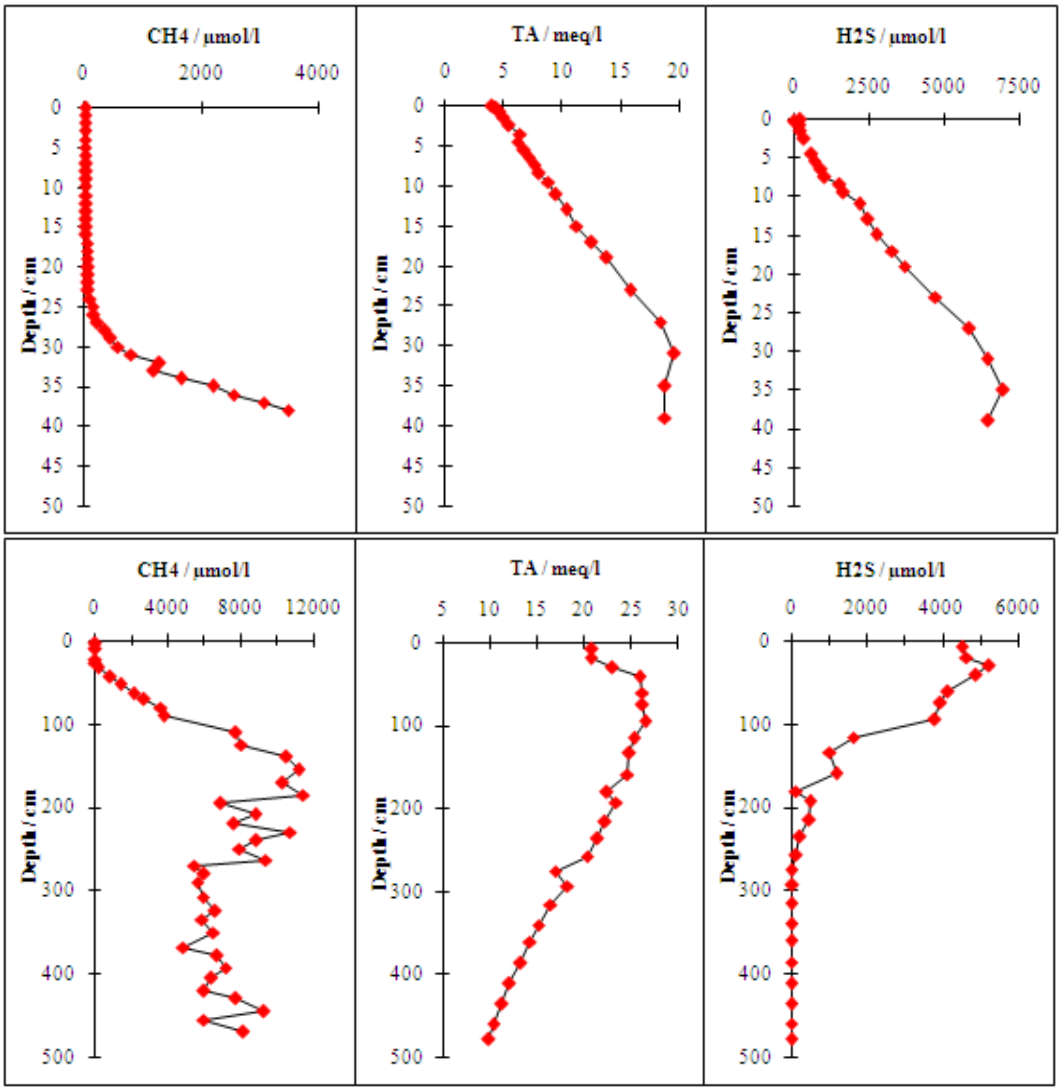

Fig. 5.4.3.5 Measured porewater TA, H_2S, and CH_4 concentrations at the seep site at the slump head wall (66-1 MIC7; top) and in the channel (89-1 GC9; bottom).

5.5 Heatflow measurements

(Jörg Bialas, Gero Wetzel)

Heatflow operations started with a single deployment next to piezometer station PR1FG in 418 m water depth. After decline of the temperature pulse induced from the penetration a heat pulse was released. From the heat pulse decay a temperature conduction coefficient of 1.05 W/m K was calculated. The corresponding temperature gradient was calculated with 26.6 K/m (Table 5.5.1).

A calibration deployment in about 1.500 m water depth was undertaken. A temperature measurement in the water column was used to achieve deviation values for the single temperature sensors of the string.

5.5.1 Working area 1

The second deployment of the heatflow probe was used to achieve a profile across the buried canyon system, which was investigated with the first 3D data set. 11 sampling points were distributed starting at the foot of the western wall of the most recent canyon (Fig. 5.2). On the 2D

seismic image of profile MSM34-1_07 (Fig. 5.3.12 and P1107, fig. 5.3.2.3) two buried canyon systems were identified, which terminate eastwards into well stratified parallel sediment layers. The heatflow profile was terminated with sampling station HF2-11 in this regime (Table 5.5.2).

Table 5.5.1 Seafloor positions of heatflow probe during deployment 1
Deduced from the heat pulse test at station HF1 the temperature gradient was calculated with a conductive coefficient of 1.05 W/m K

Station	No.	Latitude N	Longitude E	Water depth EM122 (m)	Temperature gradient (K/m)	Thermal Conductivity W/m K HP = heat pulse
HF1-1	3-1	43°48.355	30°24.797	418	26.6	1.3 HP

Table 5.5.2 Seafloor positions of heatflow probe during deployment 2

Station	No.	Latitude N	Longitude E	Water depth EM122 (m)	Temperature gradient (K/m)	Thermal Conductivity W/m K HP = heat pulse
HF2-1	28-1	43°28.216	30°26.256	1430	29.2	1.06 HP
HF2-2	29-1	43°28.092	30°26.021	1468	29.5	0.98 HP
HF2-3	30-1	43°27.956	30°25.782	1466	32.2	0.98 HP
HF2-4	31-1	43°27.863	30°25.607	1470	32.0	1.35
HF2-5	32-1	43°27.760	30°25.430	1478	29.1	1.35
HF2-6	33-1	43°27.660	30°25.253	1475	29.8	1.35
HF2-7	34-1	43°27.547	30°25.045	1478	27.3	1.35
HF2-8	35-1	43°27.471	30°24.905	1495	33.0	1.35
HF2-9	36-1	43°27.373	30°24.729	1500	37.3	1.35
HF2-10	37-1	43°27.276	30°24.550		37.1	1.35
HF2-11	38-1	43°27.189	30°24.372	1500	34.4	1.35

5.5.2 Working area 2

Major interest of working area 2 was the observation of an upward bending BSR in the seismic data of profile 15 recorded during leg 1. Seven heatflow locations were planned along profile 15 with a distance of about 300 m between the sample points. Two were located in larger water depth than the BSR projection to the seafloor, one right on top and four in shallower water depth (Fig. 5.3).

At the first deployment site a heat pulse was generated after decline of the penetration temperature signal. From this measurement heat conduction k was calculated to be 0.93 W/m K. The residual of the temperature gradient was found to be 0.038 K/m. From this measurement a value of 1 W/m K has been deduced and used to calculate the temperature gradient of the remaining stations for which the decline of the penetration pulse has been observed only.

Heatflow values were found to be in general in the range of 27 K/km to 36.8 K/km (Table 5.5.3). Increased values were found in the centre of the channel system to the east of the slump area for the stations HF4-18 and following (Table 5.5.3). The Reduced temperature gradients of 27 K/km were calculated for stations HF3-3 and HF3-4 both at a seafloor depth of 670 m. HF3-3 is located at the interpolated cross point location for BSR and seafloor of seismic profile MSM34-15. Moreover the profile is located at the foot of the eastern headwall of a slump area. It is suggested that recent slumping has caused a deviation from steady state conditions for gas hydrates with continuous dissolution and cooling.

A second deployment of the heatflow probe was used for intermediate sampling stations. A small region of reduced temperature gradients clusters around stations HF3-3 and HF3-4. The location of HF3-4 was chosen for a gravity core and a Mini MUC.

In the bathymetric map a small fault is visible, which cuts through the middle of the failed area. Therefore a third heatflow deployment was carried out to provide a regional picture on temperature gradients crossing that fault. With respect to the model of gas migration along the canyon centre further measurements provide a link into the centre of the nearby canyon depression. HF4-18 sampled the canyon floor. Here the probe sunk into the sediment without a clear sign of tension release. At the same time the temperature values increased for all sensors of the device. The deepest sensor recorded about 9.5 °C. Additional measurements indicate that the area of increased temperature is limited by the canyon walls (HF4-20 and HF4-24), while along the trench temperature values remain anomalously high (HF4-20 to HF4-23). Although seismic and Parasound data do not show any anomaly for this area a gravity core was taken at the site.

Table 5.5.3 Seafloor positions of heatflow probe during deployments 3, 4 and 5

Station	No.	Latitude N	Longitude E	Water depth EM122 (m)	Temperature gradient (K/km)	Thermal Conductivity W/m K HP = heat pulse
HF3-1	44-1	43°57.0580	30°46.9120	752	36.8	0.93 HP
HF3-2	45-1	43°57.1860	30°46.7710	726	34.4	1.35
HF3-3	46-1	43°57.3080	30°46.6430	700	27	1.35
HF3-4	47-1	43°57.4400	30°46.5120	670	28	1.35
HF3-5	48-1	43°57.5600	30°46.3770	670	33.6	1.35
HF3-6	49-1	43°57.6850	30°46.2430	650	35.6	1.35
HF3-7	50-1	43°57.8110	30°46.1150	636	32.5	1.35
HF4-1	67-1	43°57.231	30°46.727	713	32	0.91 HP
HF4-2	68-1	43°57.273	30°46.679	703	28.6	0.94 HP
HF4-3	69-1	43°57.313	30°46.498	696	30.5	0.97 HP
HF4-4	70-1	43°57.363	30°46.587	703	33.1	0.89 HP
HF4-5	71-1	43°57.411	30°46.680	696	34.4	0.9 HP
HF4-6	72-2	43°57.406	30°46.538	688	29.8	0.97 HP
HF4-7	73-1	43°57.485	30°46.457	674	28.4	0.98 HP
HF4-12	76-1	43°57.023	30°46.005	700	32.9	0.92 HP
HF4-13	77-1	43°57.201	30°46.299	710	34.5	0.93 HP
HF4-10	78-1	43°57.567	30°46.502	650	27.7	0.96 HP
HF4-Flare1	79-1	43°57.627	30°46.533	620	20	1.33 HP
HF4-15	80-1	43°57.506	30°46.869	630	17.6	0.96 HP
HF4-17	81-1	43°57.591	30°47.293	760	31.7	0.97 HP
HF4-18	82-1	43°57.684	30°47.749	830	53.7	0.68 HP
HF4-19	83-1	43°57.684	30°47.740	830	55.6	1.35
HF4-20	84-1	43°57.682	30°47.535	816	43.8	0.85 HP
HF4-21	85-1	43°57.827	30°47.721	816	50.1	0.79 HP
HF4-22	86-1	43°57.592	30°47.726	832	65.4	0.69 HP
HF4-23	87-1	43°57.393	30°47.733	838	47.3	0.93 HP
HF4-24	88-1	43°57.693	30°47.941	801	36.7	1.35

5.6 Piezometer installation

(Mickael Roudaut, Anthony Ferrant)

During cruise MSM34 Leg-1 two piezometers were assembled and deployed for long-term measurements. Both instruments were left in the ground for recovery during the French GHASS project. The instruments are expected to achieve a minimum of 6 month of observation time and can operate for up to 3 years.

	Latitude	Longitude	Depth	# sensors	Lenght lance
PR1FG	43° 48.396' N	30° 24.92' E	394 m	10	10 m
PR1HS	43° 34.981' N	31° 07.949' E	1645 m	11	10.8 m

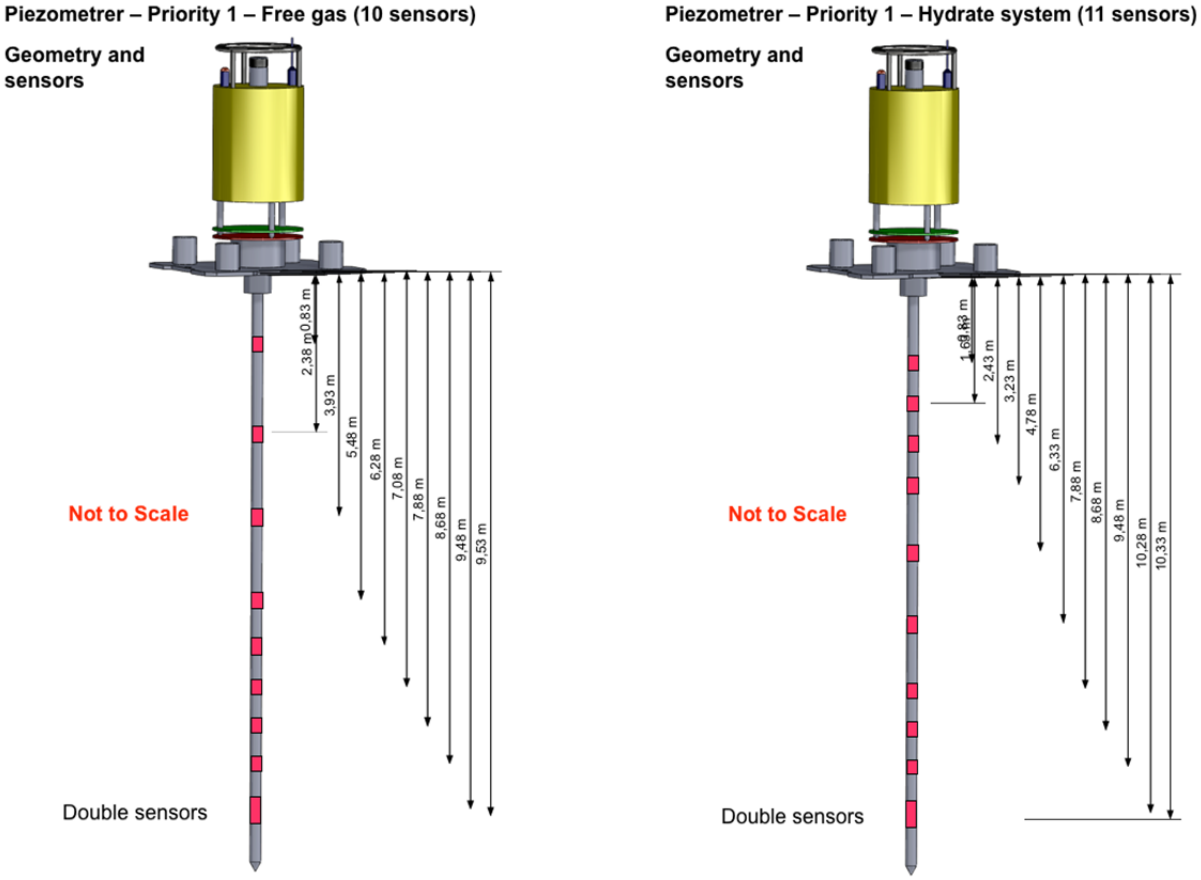

Fig. 5.6.1 Measures of the pressure sensor distribution selected for the two long-term installations.

6 Ship's Metrological Station

n.a.

7 Station List

7.1 Station List MSM34-1

Station No.	Name	Date	Time UTC	Position Lat	Position Lon	Depth [m]	Gear
MSM34/894-1		10.12.2013	03:08	43° 14.76' N	30° 41.89' E	1893.9	Schallprofilsonde
MSM34/895-1		10.12.2013	04:52	43° 14.76' N	30° 41.89' E	1897.8	MB und ParaSound Start
MSM34/895-1		10.12.2013	06:10	43° 21.09' N	30° 38.75' E	1767.3	MB und ParaSound End
MSM34/896-1		11.12.2013	10:09	43° 48.39' N	30° 24.91' E	391.9	Piezometer_Probe
MSM34/896-1		11.12.2013	16:24	43° 48.40' N	30° 24.92' E	397	Piezometer
MSM34/897-1	Profile-01	11.12.2013	22:57	43° 34.24' N	29° 58.16' E	688.8	Seismic reflection profile
MSM34/897-1		12.12.2013	12:00	44° 9.81' N	31° 2.86' E	519.5	Seismic reflection profile
MSM34/897-1	Profile-02	12.12.2013	13:12	44° 7.79' N	31° 5.58' E	620.9	Seismic reflection profile
MSM34/897-1		13.12.2013	02:22	43° 32.53' N	30° 0.92' E	850.5	Seismic reflection profile
MSM34/897-1	Profile-03	13.12.2013	03:24	43° 30.37' N	30° 3.13' E	1028.4	Seismic reflection profile
MSM34/897-1		13.12.2013	16:43	44° 5.65' N	31° 7.77' E	780.1	Seismic reflection profile
MSM34/897-1	Profile-04	13.12.2013	18:13	44° 3.60' N	31° 10.17' E	922.8	Seismic reflection profile
MSM34/897-1		14.12.2013	07:15	43° 28.30' N	30° 5.55' E	1187.1	Seismic reflection profile
MSM34/897-1	Profile-05	14.12.2013	08:24	43° 26.33' N	30° 8.15' E	1275.1	Seismic reflection profile
MSM34/897-1		14.12.2013	21:26	44° 1.57' N	31° 12.71' E	989.9	Seismic reflection profile
MSM34/897-1	Profile-06	14.12.2013	22:34	43° 59.33' N	31° 14.79' E	1146.5	Seismic reflection profile
MSM34/897-1		15.12.2013	11:40	43° 23.63' N	30° 9.81' E	1386.2	Seismic reflection profile
MSM34/897-1	Profile-07	15.12.2013	12:50	43° 21.42' N	30° 11.94' E	1474.2	Seismic reflection profile
MSM34/897-1		16.12.2013	02:00	43° 56.98' N	31° 17.02' E	1170.9	Seismic reflection profile
MSM34/897-1	Profile-08	16.12.2013	02:57	43° 54.86' N	31° 19.46' E	1273.3	Seismic reflection profile
MSM34/897-1		16.12.2013	10:26	43° 34.72' N	30° 42.43' E	1185.2	Seismic reflection profile
MSM34/897-1	Profile-08b	16.12.2013	14:26	43° 36.48' N	30° 45.61' E	990.3	Seismic reflection profile
MSM34/897-1		16.12.2013	20:54	43° 19.23' N	30° 14.49' E	1569.1	Seismic reflection profile
MSM34/897-1	Profile-09	16.12.2013	22:00	43° 17.05' N	30° 16.66' E	1624.5	Seismic reflection profile
MSM34/897-1		17.12.2013	10:09	43° 49.25' N	31° 15.46' E	1612.1	Seismic reflection profile
MSM34/897-1	Profile-10	17.12.2013	11:14	43° 47.14' N	31° 17.72' E	1661.7	Seismic reflection profile
MSM34/897-1		17.12.2013	23:36	43° 14.34' N	30° 18.02' E	1700.1	Seismic reflection profile
MSM34/897-1	Profile-11	18.12.2013	00:39	43° 12.40' N	30° 20.61' E	1778.8	Seismic reflection profile
MSM34/897-1		18.12.2013	12:08	43° 42.83' N	31° 16.07' E	1738.8	Seismic reflection profile
MSM34/897-1	Profile-12	18.12.2013	13:14	43° 40.99' N	31° 18.85' E	1743.8	Seismic reflection profile

Station No.	Name	Date	Time UTC	Position Lat	Position Lon	Depth [m]	Gear
MSM34/897-1		18.12.2013	13:25	43° 40.51' N	31° 17.95' E	1731.6	Seismic reflection profile
MSM34/897-1		18.12.2013	15:32	43° 40.81' N	31° 18.49' E	1730.6	Seismic reflection profile
MSM34/897-1		19.12.2013	02:42	43° 10.41' N	30° 23.38' E	1820.6	Seismic reflection profile
MSM34/897-1	Profile-13	19.12.2013	03:39	43° 8.34' N	30° 25.74' E	1858	Seismic reflection profile
MSM34/897-1		19.12.2013	14:10	43° 36.71' N	31° 17.29' E	1666.1	Seismic reflection profile
MSM34/897-1	Profile-14	19.12.2013	14:30	43° 38.03' N	31° 17.27' E	1673	Seismic reflection profile
MSM34/897-1		19.12.2013	21:45	44° 3.99' N	30° 50.12' E	343.9	Seismic reflection profile
MSM34/897-1		19.12.2013	22:07	44° 4.25' N	30° 48.16' E	254.3	MB und ParaSound Start
MSM34/897-1		19.12.2013	23:03	44° 1.75' N	30° 43.49' E	188.2	MB und ParaSound End
MSM34/897-1	Profile-15	19.12.2013	23:30	44° 0.09' N	30° 43.70' E	337.2	Seismic reflection profile
MSM34/897-1		20.12.2013	05:35	43° 38.18' N	31° 6.64' E	1642.1	Seismic reflection profile
MSM34/897-1	Profile-15b	20.12.2013	08:31	43° 37.85' N	31° 6.98' E	1650.7	Seismic reflection profile
MSM34/897-1		20.12.2013	10:42	43° 30.07' N	31° 15.04' E	1624.1	Seismic reflection profile
MSM34/898-1		20.12.2013	13:19	43° 34.98' N	31° 7.95' E	1648.5	Piezometer_Probe
MSM34/898-1		20.12.2013	20:05	43° 34.98' N	31° 7.95' E	1648.1	Piezometer
MSM34/899-1		20.12.2013	23:54	43° 55.75' N	30° 46.44' E	687.5	MB und ParaSound Start
MSM34/899-1		21.12.2013	10:30	43° 7.23' N	30° 36.50' E	1934.2	MB und ParaSound End
MSM34/900-1	Profile-20	21.12.2013	12:05	43° 8.53' N	30° 34.83' E	1912.9	Seismic reflection profile
MSM34/900-1		21.12.2013	13:14	43° 12.66' N	30° 30.58' E	1848.6	Seismic reflection profile
MSM34/900-1		21.12.2013	15:36	43° 8.64' N	30° 34.71' E	1910.5	Seismic reflection profile
MSM34/900-1		22.12.2013	00:00	43° 38.88' N	30° 3.52' E	529.7	Seismic reflection profile
MSM34/900-1	Profile-19	22.12.2013	01:27	43° 42.08' N	30° 10.32' E	458.3	Seismic reflection profile
MSM34/900-1		22.12.2013	09:49	43° 11.91' N	30° 41.41' E	1891.1	Seismic reflection profile
MSM34/900-1	Profile-21	22.12.2013	11:17	43° 15.77' N	30° 47.36' E	1879.3	Seismic reflection profile
MSM34/900-1		22.12.2013	19:38	43° 45.71' N	30° 16.01' E	379.3	Seismic reflection profile
MSM34/900-1	Profile-18	22.12.2013	21:01	43° 48.55' N	30° 22.87' E	200.4	Seismic reflection profile
MSM34/900-1		23.12.2013	05:11	43° 19.14' N	30° 53.39' E	1611.1	Seismic reflection profile
MSM34/900-1	Profile-22	23.12.2013	06:20	43° 21.49' N	30° 57.88' E	1480.7	Seismic reflection profile
MSM34/900-1		23.12.2013	14:33	43° 50.79' N	30° 27.13' E	551.9	Seismic reflection profile
MSM34/900-1	Profile-17	23.12.2013	15:46	43° 53.28' N	30° 31.52' E	833.8	Seismic reflection profile
MSM34/900-1		24.12.2013	00:05	43° 23.39' N	31° 2.56' E	1369.4	Seismic reflection profile
MSM34/900-1	Profile-16	24.12.2013	01:22	43° 26.96' N	31° 8.06' E	1510.8	Seismic reflection profile
MSM34/900-1		24.12.2013	09:42	43° 57.03' N	30° 36.88' E	409.3	Seismic reflection profile
MSM34/900-1	Profile-23	24.12.2013	11:32	43° 52.63' N	30° 40.79' E	893.7	Seismic reflection profile

Station No.	Name	Date	Time UTC	Position Lat	Position Lon	Depth [m]	Gear
MSM34/900-1		24.12.2013	16:44	44° 6.72' N	31° 6.66' E	701.2	Seismic reflection profile
MSM34/900-1	Profile-24	24.12.2013	18:45	44° 4.31' N	30° 59.19' E	679.4	Seismic reflection profile
MSM34/900-1		24.12.2013	23:41	43° 46.81' N	31° 17.91' E	1673.8	Seismic reflection profile
MSM34/900-1	Profile-25	24.12.2013	23:53	43° 45.95' N	31° 18.16' E	1705	Seismic reflection profile
MSM34/900-1		25.12.2013	02:44	43° 33.14' N	31° 16.59' E	1639.6	Seismic reflection profile
MSM34/900-1	Profile-26	25.12.2013	02:56	43° 32.42' N	31° 15.89' E	1661.7	Seismic reflection profile
MSM34/900-1		25.12.2013	11:38	43° 8.94' N	30° 33.08' E	1893.6	Seismic reflection profile
MSM34/900-1	Profile-27	25.12.2013	12:36	43° 7.16' N	30° 35.65' E	1936.2	Seismic reflection profile
MSM34/900-1		25.12.2013	21:11	43° 30.37' N	31° 17.70' E	1685.1	Seismic reflection profile
MSM34/900-1	Profile-28	25.12.2013	21:31	43° 31.71' N	31° 18.11' E	1665.3	Seismic reflection profile
MSM34/900-1		26.12.2013	05:59	44° 2.01' N	30° 47.08' E	448.2	Seismic reflection profile
MSM34/901-1		26.12.2013	08:47	44° 1.09' N	31° 2.15' E	784.6	MB und ParaSound Start
MSM34/901-1		26.12.2013	20:00	43°41.18' N	30° 10.73 E	522.2	MB und ParaSound End

7.2 Stationsliste MSM34-2

Station No.	Date	Time [UTC]	Position Lat	Position Lon	Depth [m]	Gear
MSM34/001-1	30.12.13	00:40	43° 5.87' N	29° 58.26' E	1648.3	Multibeam und ParaSound
MSM34/001-1	30.12.13	00:56	43° 6.51' N	29° 59.43' E	1626.3	Multibeam und ParaSound
MSM34/001-2	30.12.13	01:16	43° 6.59' N	29° 58.58' E	1622.6	Multibeam und ParaSound
MSM34/001-2	30.12.13	01:31	43° 5.89' N	29° 59.57' E	1643.9	Multibeam und ParaSound
MSM34/002-1	30.12.13	05:59	43° 51.91' N	30° 31.15' E	700.1	Multibeam und ParaSound
MSM34/002-1	30.12.13	07:52	43° 45.07' N	30° 18.79' E	393.3	Multibeam und ParaSound
MSM34/003-1	30.12.13	09:33	43° 48.35' N	30° 24.79' E	425.5	Heat Flow
MSM34/003-2	30.12.13	10:29	43° 48.35' N	30° 24.78' E	417	Multi corer
MSM34/003-3	30.12.13	11:17	43° 48.35' N	30° 24.78' E	419.2	Gravity corer
MSM34/003-3	30.12.13	11:19	43° 48.35' N	30° 24.79' E	419.4	Gravity corer
MSM34/004-1	30.12.13	15:14	43° 20.80' N	30° 32.99' E	1735	Schallprofilsonde
MSM34/004-2	30.12.13	17:07	43° 20.80' N	30° 32.99' E	1745.2	Heat Flow
MSM34/005-1	30.12.13	19:07	43° 29.18' N	30° 24.31' E	1424.8	Ocean Bottom Seismometer

Station No.	Date	Time [UTC]	Position Lat	Position Lon	Depth [m]	Gear
MSM34/006-1	30.12.13	19:31	43° 28.74' N	30° 24.75' E	1443	Ocean Bottom Seismometer
MSM34/007-1	30.12.13	19:48	43° 28.31' N	30° 25.20' E	1459.4	Ocean Bottom Seismometer
MSM34/008-1	30.12.13	20:02	43° 27.88' N	30° 25.64' E	1465	Ocean Bottom Seismometer
MSM34/009-1	30.12.13	20:16	43° 27.45' N	30° 26.09' E	1494	Ocean Bottom Seismometer
MSM34/010-1	30.12.13	20:38	43° 27.13' N	30° 25.50' E	1497.1	Ocean Bottom Seismometer
MSM34/011-1	30.12.13	20:57	43° 27.57' N	30° 25.06' E	1474.8	Ocean Bottom Seismometer
MSM34/012-1	30.12.13	21:14	43° 28.00' N	30° 24.62' E	1443.3	Ocean Bottom Seismometer
MSM34/013-1	30.12.13	21:29	43° 28.43' N	30° 24.16' E	1466.8	Ocean Bottom Seismometer
MSM34/014-1	30.12.13	21:44	43° 28.86' N	30° 23.72' E	1453.1	Ocean Bottom Seismometer
MSM34/015-1	30.12.13	22:02	43° 28.53' N	30° 23.13' E	1449.6	Ocean Bottom Seismometer
MSM34/016-1	30.12.13	22:27	43° 28.10' N	30° 23.58' E	1470.2	Ocean Bottom Seismometer
MSM34/017-1	30.12.13	22:44	43° 27.67' N	30° 24.02' E	1480.8	Ocean Bottom Seismometer
MSM34/018-1	30.12.13	23:01	43° 27.24' N	30° 24.47' E	1501.2	Ocean Bottom Seismometer
MSM34/019-1	30.12.13	23:27	43° 26.82' N	30° 24.91' E	1514.7	Ocean Bottom Seismometer
MSM34/020-1	31.12.13	02:09	43° 43.16' N	30° 18.86' E	527.8	Multibeam und ParaSound
MSM34/020-1	31.12.13	02:47	43° 45.80' N	30° 22.55' E	443.1	Multibeam und ParaSound
MSM34/020-1	31.12.13	04:13	43° 51.01' N	30° 31.98' E	683.4	Multibeam und ParaSound
MSM34/021-1	31.12.13	05:25	43° 45.73' N	30° 17.98' E	365.8	Multibeam und ParaSound
MSM34/021-1	31.12.13	07:19	43° 52.63' N	30° 30.40' E	739.9	Multibeam und ParaSound
MSM34/022-1	31.12.13	10:32	43° 25.68' N	30° 26.05' E	1551.2	Gravity corer
MSM34/024-1	31.12.13	17:41	43° 25.40' N	30° 28.16' E	1549.9	Seismic reflection profile
MSM34/024-1	31.12.13	19:28	43° 31.07' N	30° 22.34' E	1348.4	Seismic reflection profile
MSM34/024-1	31.12.13	22:17	43° 24.98' N	30° 27.71' E	1617.1	Seismic reflection profile
MSM34/024-1	01.01.14	01:46	43° 27.03' N	30° 20.33' E	1429.9	Seismic reflection profile
MSM34/024-1	01.01.14	03:14	43° 30.57' N	30° 26.83' E	1244.5	Seismic reflection profile
MSM34/024-1	01.01.14	05:23	43° 26.62' N	30° 20.89' E	1466.2	Seismic reflection profile
MSM34/024-1	01.01.14	07:26	43° 29.90' N	30° 27.97' E	1257.8	Seismic reflection profile

Station No.	Date	Time [UTC]	Position Lat	Position Lon	Depth [m]	Gear
MSM34/024-1	01.01.14	09:20	43° 25.81' N	30° 21.89' E	1490.3	Seismic reflection profile
MSM34/024-1	01.01.14	11:16	43° 28.88' N	30° 28.75' E	1315.5	Seismic reflection profile
MSM34/025-1	01.01.14	18:55	43° 25.81' N	30° 25.00' E	1463.4	Seismic reflection profile
MSM34/025-1	01.01.14	20:16	43° 29.14' N	30° 21.54' E	1406.6	Seismic reflection profile
MSM34/025-1	01.01.14	22:11	43° 26.10' N	30° 26.49' E	1537.1	Seismic reflection profile
MSM34/025-1	02.01.14	00:11	43° 29.40' N	30° 21.34' E	1405.9	Seismic reflection profile
MSM34/025-1	02.01.14	02:09	43° 26.43' N	30° 26.25' E	1522.3	Seismic reflection profile
MSM34/025-1	02.01.14	03:58	43° 29.14' N	30° 21.67' E	1407.1	Seismic reflection profile
MSM34/025-1	02.01.14	05:45	43° 26.63' N	30° 26.10' E	1523.6	Seismic reflection profile
MSM34/025-1	02.01.14	07:39	43° 29.15' N	30° 21.73' E	1409.8	Seismic reflection profile
MSM34/025-1	02.01.14	09:32	43° 26.35' N	30° 26.44' E	1529.5	Seismic reflection profile
MSM34/025-1	02.01.14	11:31	43° 29.40' N	30° 21.54' E	1410.5	Seismic reflection profile
MSM34/025-1	02.01.14	13:26	43° 26.44' N	30° 26.43' E	1551.2	Seismic reflection profile
MSM34/025-1	02.01.14	15:26	43° 29.29' N	30° 21.70' E	1413.9	Seismic reflection profile
MSM34/025-1	02.01.14	17:13	43° 26.61' N	30° 26.31' E	1521	Seismic reflection profile
MSM34/025-1	02.01.14	19:05	43° 29.28' N	30° 21.79' E	1417.6	Seismic reflection profile
MSM34/025-1	02.01.14	21:00	43° 26.50' N	30° 26.49' E	1529	Seismic reflection profile
MSM34/025-1	02.01.14	22:58	43° 29.44' N	30° 21.68' E	1411.6	Seismic reflection profile
MSM34/025-1	03.01.14	00:57	43° 26.36' N	30° 26.70' E	1535.8	Seismic reflection profile
MSM34/025-1	03.01.14	02:56	43° 29.33' N	30° 21.86' E	1415.6	Seismic reflection profile
MSM34/025-1	03.01.14	04:44	43° 26.65' N	30° 26.46' E	1524.4	Seismic reflection profile
MSM34/025-1	03.01.14	06:39	43° 29.38' N	30° 21.88' E	1424.5	Seismic reflection profile
MSM34/025-1	03.01.14	08:32	43° 26.56' N	30° 26.62' E	1527.5	Seismic reflection profile
MSM34/025-1	03.01.14	10:33	43° 29.58' N	30° 21.73' E	1405.6	Seismic reflection profile
MSM34/025-1	03.01.14	12:27	43° 26.74' N	30° 26.50' E	1529.2	Seismic reflection profile
MSM34/025-1	03.01.14	14:32	43° 29.37' N	30° 22.02' E	1426.3	Seismic reflection profile
MSM34/025-1	03.01.14	16:29	43° 26.70' N	30° 26.59' E	1530.1	Seismic reflection profile

Station No.	Date	Time [UTC]	Position Lat	Position Lon	Depth [m]	Gear
MSM34/025-1	03.01.14	18:26	43° 29.51' N	30° 21.94' E	1410.3	Seismic reflection profile
MSM34/025-1	03.01.14	20:23	43° 26.52' N	30° 26.89' E	1536.3	Seismic reflection profile
MSM34/025-1	03.01.14	22:26	43° 29.69' N	30° 21.83' E	1399.4	Seismic reflection profile
MSM34/025-1	04.01.14	00:30	43° 26.43' N	30° 27.01' E	1535.5	Seismic reflection profile
MSM34/025-1	04.01.14	02:30	43° 29.48' N	30° 22.10' E	1417.9	Seismic reflection profile
MSM34/025-1	04.01.14	04:19	43° 26.72' N	30° 26.78' E	1526.1	Seismic reflection profile
MSM34/025-1	04.01.14	06:12	43° 29.59' N	30° 22.05' E	1416.4	Seismic reflection profile
MSM34/025-1	04.01.14	08:04	43° 26.63' N	30° 26.95' E	1535.8	Seismic reflection profile
MSM34/025-1	04.01.14	10:01	43° 29.67' N	30° 22.05' E	1402.7	Seismic reflection profile
MSM34/025-1	04.01.14	11:06	43° 28.76' N	30° 24.79' E	1427.4	Seismic reflection profile
MSM34/025-1	04.01.14	11:09	43° 28.64' N	30° 24.91' E	1429.6	Seismic reflection profile
MSM34/026-1	04.01.14	13:48	43° 27.23' N	30° 24.47' E	1498.4	Multi corer
MSM34/027-1	04.01.14	15:20	43° 28.10' N	30° 26.04' E	1465.8	Multi corer
MSM34/028-1	04.01.14	16:57	43° 28.22' N	30° 26.25' E	1438.4	Heat Flow
MSM34/029-1	04.01.14	17:52	43° 28.09' N	30° 26.03' E	1458.2	Heat Flow
MSM34/030-1	04.01.14	18:38	43° 27.95' N	30° 25.79' E	1471.1	Heat Flow
MSM34/031-1	04.01.14	19:19	43° 27.86' N	30° 25.62' E	1471	Heat Flow
MSM34/032-1	04.01.14	19:52	43° 27.75' N	30° 25.44' E	1485.4	Heat Flow
MSM34/033-1	04.01.14	20:24	43° 27.67' N	30° 25.26' E	1473	Heat Flow
MSM34/034-1	04.01.14	20:54	43° 27.55' N	30° 25.05' E	1473.5	Heat Flow
MSM34/035-1	04.01.14	21:21	43° 27.47' N	30° 24.91' E	1506.1	Heat Flow
MSM34/036-1	04.01.14	21:49	43° 27.37' N	30° 24.73' E	1501.8	Heat Flow
MSM34/037-1	04.01.14	22:22	43° 27.27' N	30° 24.56' E	1504.3	Heat Flow
MSM34/038-1	04.01.14	22:53	43° 27.18' N	30° 24.37' E	1499.3	Heat Flow
MSM34/018-1	04.01.14	23:56	43° 27.23' N	30° 24.20' E	0	Ocean Bottom Seismometer
MSM34/017-1	05.01.14	00:41	43° 27.55' N	30° 23.90' E	0	Ocean Bottom Seismometer
MSM34/016-1	05.01.14	01:16	43° 27.99' N	30° 23.44' E	0	Ocean Bottom Seismometer
MSM34/015-1	05.01.14	01:51	43° 28.39' N	30° 23.00' E	0	Ocean Bottom Seismometer
MSM34/014-1	05.01.14	02:19	43° 28.76' N	30° 23.65' E	0	Ocean Bottom Seismometer
MSM34/013-1	05.01.14	02:51	43° 28.30' N	30° 24.00' E	0	Ocean Bottom Seismometer

Station No.	Date	Time [UTC]	Position Lat	Position Lon	Depth [m]	Gear
MSM34/012-1	05.01.14	03:22	43° 27.82' N	30° 24.50' E	0	Ocean Bottom Seismometer
MSM34/011-1	05.01.14	03:48	43° 27.40' N	30° 24.94' E	0	Ocean Bottom Seismometer
MSM34/010-1	05.01.14	04:16	43° 27.04' N	30° 25.41' E	0	Ocean Bottom Seismometer
MSM34/019-1	05.01.14	04:46	43° 26.72' N	30° 24.81' E	0	Ocean Bottom Seismometer
MSM34/009-1	05.01.14	05:14	43° 27.40' N	30° 25.96' E	0	Ocean Bottom Seismometer
MSM34/008-1	05.01.14	05:42	43° 27.85' N	30° 25.48' E	0	Ocean Bottom Seismometer
MSM34/007-1	05.01.14	06:13	43° 28.30' N	30° 24.90' E	0	Ocean Bottom Seismometer
MSM34/006-1	05.01.14	06:40	43° 28.73' N	30° 24.51' E	0	Ocean Bottom Seismometer
MSM34/005-1	05.01.14	07:11	43° 29.17' N	30° 24.06' E	0	Ocean Bottom Seismometer
MSM34/039-1	05.01.14	08:45	43° 27.25' N	30° 24.48' E	1498.8	Gravity corer
MSM34/040-1	05.01.14	10:43	43° 28.10' N	30° 26.04' E	1462.3	Gravity corer
MSM34/041-1	05.01.14	14:39	43° 30.12' N	30° 23.47' E	1381.3	Seismic reflection profile
MSM34/041-1	05.01.14	16:03	43° 26.66' N	30° 27.05' E	1533.9	Seismic reflection profile
MSM34/041-1	05.01.14	17:57	43° 29.65' N	30° 22.12' E	1401.5	Seismic reflection profile
MSM34/041-1	05.01.14	19:51	43° 26.70' N	30° 27.07' E	1528.1	Seismic reflection profile
MSM34/041-1	05.01.14	21:47	43° 29.65' N	30° 22.19' E	1404.9	Seismic reflection profile
MSM34/041-1	05.01.14	23:45	43° 26.65' N	30° 27.13' E	1528.6	Seismic reflection profile
MSM34/041-1	06.01.14	01:50	43° 29.80' N	30° 22.04' E	1350.8	Seismic reflection profile
MSM34/041-1	06.01.14	03:45	43° 26.74' N	30° 27.11' E	1526.4	Seismic reflection profile
MSM34/041-1	06.01.14	05:40	43° 29.68' N	30° 22.24' E	1381.8	Seismic reflection profile
MSM34/041-1	06.01.14	07:35	43° 26.69' N	30° 27.19' E	1531	Seismic reflection profile
MSM34/042-1	06.01.14	16:20	43° 25.68' N	30° 26.07' E	1549.7	Multi corer
MSM34/041-1	06.01.14	21:10	43° 28.19' N	30° 23.84' E	1462.2	Seismic reflection profile
MSM34/041-1	06.01.14	21:47	43° 29.67' N	30° 22.31' E	1377.6	Seismic reflection profile
MSM34/041-1	06.01.14	23:54	43° 26.30' N	30° 27.55' E	1533.4	Seismic reflection profile
MSM34/041-1	07.01.14	01:58	43° 29.82' N	30° 22.16' E	1351.7	Seismic reflection profile
MSM34/041-1	07.01.14	03:52	43° 26.79' N	30° 27.16' E	1508.4	Seismic reflection profile
MSM34/041-1	07.01.14	05:52	43° 29.77' N	30° 22.26' E	1375.2	Seismic reflection profile
MSM34/041-1	07.01.14	07:51	43° 26.73' N	30° 27.29' E	1517.3	Seismic reflection profile
MSM34/041-1	07.01.14	09:48	43° 29.80' N	30° 22.33' E	1368.2	Seismic reflection profile
MSM34/041-1	07.01.14	11:43	43° 26.76' N	30° 27.30' E	1518.3	Seismic reflection profile
MSM34/041-1	07.01.14	13:47	43° 29.87' N	30° 22.28' E	1353.5	Seismic reflection profile

Station No.	Date	Time [UTC]	Position Lat	Position Lon	Depth [m]	Gear
MSM34/041-1	07.01.14	15:39	43° 26.93' N	30° 27.19' E	1502.1	Seismic reflection profile
MSM34/041-1	07.01.14	17:35	43° 29.73' N	30° 22.49' E	1373.5	Seismic reflection profile
MSM34/041-1	07.01.14	19:31	43° 26.80' N	30° 27.37' E	1506.5	Seismic reflection profile
MSM34/041-1	07.01.14	21:28	43° 29.79' N	30° 22.50' E	1363.2	Seismic reflection profile
MSM34/041-1	07.01.14	23:26	43° 26.83' N	30° 27.42' E	1509.3	Seismic reflection profile
MSM34/041-1	08.01.14	01:29	43° 29.95' N	30° 22.38' E	1361.7	Seismic reflection profile
MSM34/041-1	08.01.14	03:25	43° 26.95' N	30° 27.36' E	1494.5	Seismic reflection profile
MSM34/041-1	08.01.14	05:18	43° 29.74' N	30° 22.64' E	1370.3	Seismic reflection profile
MSM34/041-1	08.01.14	07:28	43° 26.65' N	30° 27.01' E	1529.8	Seismic reflection profile
MSM34/041-1	08.01.14	09:24	43° 29.68' N	30° 22.04' E	1380.5	Seismic reflection profile
MSM34/041-1	08.01.14	11:23	43° 26.57' N	30° 27.04' E	1531.1	Seismic reflection profile
MSM34/041-1	08.01.14	11:46	43° 25.36' N	30° 26.60' E	1563.9	Seismic reflection profile
MSM34/041-1	08.01.14	12:54	43° 27.73' N	30° 23.27' E	1390.6	Seismic reflection profile
MSM34/041-1	08.01.14	13:11	43° 28.39' N	30° 22.60' E	1380.7	Seismic reflection profile
MSM34/041-1	08.01.14	13:18	43° 28.68' N	30° 22.35' E	1367.9	Seismic reflection profile
MSM34/041-1	08.01.14	13:32	43° 29.25' N	30° 21.76' E	1411.4	Seismic reflection profile
MSM34/041-1	08.01.14	15:42	43° 26.49' N	30° 26.04' E	1516.7	Seismic reflection profile
MSM34/041-1	08.01.14	17:18	43° 28.19' N	30° 23.12' E	1418.5	Seismic reflection profile
MSM34/041-1	08.01.14	17:24	43° 28.42' N	30° 22.82' E	1395.1	Seismic reflection profile
MSM34/041-1	08.01.14	17:49	43° 29.47' N	30° 21.72' E	1409.5	Seismic reflection profile
MSM34/041-1	08.01.14	19:41	43° 26.58' N	30° 26.55' E	1527.7	Seismic reflection profile
MSM34/041-1	08.01.14	21:47	43° 29.67' N	30° 21.84' E	1391	Seismic reflection profile
MSM34/041-1	08.01.14	23:49	43° 26.41' N	30° 27.03' E	1533.8	Seismic reflection profile
MSM34/041-1	09.01.14	01:53	43° 29.52' N	30° 22.01' E	1413.7	Seismic reflection profile
MSM34/041-1	09.01.14	03:19	43° 28.35' N	30° 24.13' E	1467.6	Seismic reflection profile
MSM34/041-1	09.01.14	03:26	43° 28.09' N	30° 24.46' E	1471	Seismic reflection profile
MSM34/041-1	09.01.14	04:09	43° 26.29' N	30° 26.33' E	1524.7	Seismic reflection profile
MSM34/041-1	09.01.14	05:03	43° 26.95' N	30° 24.09' E	1406.8	Seismic reflection profile
MSM34/041-1	09.01.14	05:32	43° 28.23' N	30° 23.07' E	1408.8	Seismic reflection profile
MSM34/041-1	09.01.14	05:57	43° 29.26' N	30° 22.01' E	1421.7	Seismic reflection profile
MSM34/043-1	09.01.14	11:21	43° 57.43' N	30° 46.50' E	681	Gravity corer
MSM34/043-2	09.01.14	12:19	43° 57.44' N	30° 46.50' E	671.2	Multi corer

Station No.	Date	Time [UTC]	Position Lat	Position Lon	Depth [m]	Gear
MSM34/044-1	09.01.14	13:16	43° 57.05' N	30° 46.90' E	751.6	Heat Flow
MSM34/045-1	09.01.14	14:05	43° 57.18' N	30° 46.76' E	722.9	Heat Flow
MSM34/046-1	09.01.14	14:29	43° 57.31' N	30° 46.63' E	695.3	Heat Flow
MSM34/047-1	09.01.14	14:57	43° 57.44' N	30° 46.50' E	674	Heat Flow
MSM34/048-1	09.01.14	15:21	43° 57.56' N	30° 46.37' E	680.1	Heat Flow
MSM34/049-1	09.01.14	15:46	43° 57.68' N	30° 46.23' E	655.8	Heat Flow
MSM34/050-1	09.01.14	16:12	43° 57.81' N	30° 46.10' E	636.3	Heat Flow
MSM34/051-1	09.01.14	17:42	43° 57.17' N	30° 46.76' E	723.1	Gravity corer
MSM34/051-1	09.01.14	18:09	43° 57.17' N	30° 46.76' E	730.5	Gravity corer
MSM34/052-1	09.01.14	18:44	43° 57.49' N	30° 45.41' E	654.3	Ocean Bottom Seismometer
MSM34/053-1	09.01.14	18:57	43° 57.17' N	30° 45.73' E	680.8	Ocean Bottom Seismometer
MSM34/054-1	09.01.14	19:08	43° 56.84' N	30° 46.08' E	704.2	Ocean Bottom Seismometer
MSM34/055-1	09.01.14	19:20	43° 56.52' N	30° 46.44' E	704.5	Ocean Bottom Seismometer
MSM34/056-1	09.01.14	19:35	43° 56.92' N	30° 47.15' E	792.2	Ocean Bottom Seismometer
MSM34/057-1	09.01.14	19:48	43° 57.23' N	30° 46.82' E	708.8	Ocean Bottom Seismometer
MSM34/058-1	09.01.14	19:58	43° 57.56' N	30° 46.49' E	656.4	Ocean Bottom Seismometer
MSM34/059-1	09.01.14	20:10	43° 57.86' N	30° 46.14' E	602.1	Ocean Bottom Seismometer
MSM34/060-1	09.01.14	20:32	43° 58.28' N	30° 46.83' E	594.6	Ocean Bottom Seismometer
MSM34/061-1	09.01.14	20:43	43° 57.96' N	30° 47.17' E	702	Ocean Bottom Seismometer
MSM34/062-1	09.01.14	20:53	43° 57.65' N	30° 47.51' E	806.3	Ocean Bottom Seismometer
MSM34/063-1	09.01.14	21:05	43° 57.32' N	30° 47.86' E	846.8	Ocean Bottom Seismometer
MSM34/064-1	09.01.14	23:32	43° 55.90' N	30° 47.11' E	712.7	Seismic reflection profile
MSM34/064-1	10.01.14	00:25	43° 58.35' N	30° 44.49' E	522.4	Seismic reflection profile
MSM34/064-1	10.01.14	01:51	43° 56.56' N	30° 48.66' E	830.3	Seismic reflection profile
MSM34/064-1	10.01.14	03:27	43° 57.74' N	30° 43.85' E	527	Seismic reflection profile
MSM34/064-1	10.01.14	04:48	43° 56.14' N	30° 47.99' E	892.8	Seismic reflection profile
MSM34/064-1	10.01.14	06:10	43° 57.81' N	30° 43.90' E	544.1	Seismic reflection profile
MSM34/064-1	10.01.14	07:35	43° 56.14' N	30° 48.11' E	902.3	Seismic reflection profile
MSM34/064-1	10.01.14	09:03	43° 58.02' N	30° 43.83' E	555.3	Seismic reflection profile
MSM34/064-1	10.01.14	10:30	43° 56.06' N	30° 48.32' E	908.9	Seismic reflection profile
MSM34/064-1	10.01.14	11:50	43° 58.19' N	30° 44.30' E	546.7	Seismic reflection profile
MSM34/064-1	10.01.14	13:14	43° 56.04' N	30° 48.40' E	913.2	Seismic reflection profile

Station No.	Date	Time [UTC]	Position Lat	Position Lon	Depth [m]	Gear
MSM34/064-1	10.01.14	14:30	43° 58.25' N	30° 44.27' E	536.5	Seismic reflection profile
MSM34/064-1	10.01.14	15:50	43° 56.23' N	30° 48.29' E	902.8	Seismic reflection profile
MSM34/064-1	10.01.14	17:05	43° 58.19' N	30° 44.43' E	538	Seismic reflection profile
MSM34/064-1	10.01.14	18:23	43° 56.29' N	30° 48.32' E	912.5	Seismic reflection profile
MSM34/064-1	10.01.14	19:38	43° 58.20' N	30° 44.48' E	539.7	Seismic reflection profile
MSM34/064-1	10.01.14	20:53	43° 56.24' N	30° 48.40' E	912.7	Seismic reflection profile
MSM34/064-1	10.01.14	22:10	43° 58.24' N	30° 44.48' E	529.2	Seismic reflection profile
MSM34/064-1	10.01.14	23:28	43° 56.25' N	30° 48.44' E	906	Seismic reflection profile
MSM34/064-1	11.01.14	00:54	43° 58.37' N	30° 44.44' E	517.5	Seismic reflection profile
MSM34/064-1	11.01.14	02:05	43° 56.71' N	30° 48.10' E	869.3	Seismic reflection profile
MSM34/064-1	11.01.14	03:31	43° 58.21' N	30° 44.72' E	532.3	Seismic reflection profile
MSM34/064-1	11.01.14	04:53	43° 56.42' N	30° 48.48' E	865	Seismic reflection profile
MSM34/064-1	11.01.14	06:15	43° 58.30' N	30° 44.69' E	518.8	Seismic reflection profile
MSM34/064-1	11.01.14	07:35	43° 56.44' N	30° 48.52' E	850.7	Seismic reflection profile
MSM34/064-1	11.01.14	08:55	43° 58.32' N	30° 44.75' E	524.1	Seismic reflection profile
MSM34/064-1	11.01.14	10:14	43° 56.26' N	30° 48.75' E	858.8	Seismic reflection profile
MSM34/064-1	11.01.14	11:34	43° 58.44' N	30° 44.68' E	504.9	Seismic reflection profile
MSM34/064-1	11.01.14	12:55	43° 56.33' N	30° 48.75' E	856.6	Seismic reflection profile
MSM34/064-1	11.01.14	14:14	43° 58.32' N	30° 44.86' E	517.3	Seismic reflection profile
MSM34/064-1	11.01.14	15:27	43° 56.55' N	30° 48.59' E	831.2	Seismic reflection profile
MSM34/064-1	11.01.14	16:44	43° 58.26' N	30° 45.00' E	530.9	Seismic reflection profile
MSM34/064-1	11.01.14	18:03	43° 56.58' N	30° 48.71' E	830.2	Seismic reflection profile
MSM34/064-1	11.01.14	19:21	43° 58.38' N	30° 44.94' E	531.6	Seismic reflection profile
MSM34/064-1	11.01.14	20:34	43° 56.59' N	30° 48.76' E	825.9	Seismic reflection profile
MSM34/064-1	11.01.14	21:49	43° 58.40' N	30° 44.97' E	531.3	Seismic reflection profile
MSM34/064-1	11.01.14	23:09	43° 56.46' N	30° 48.93' E	844	Seismic reflection profile
MSM34/064-1	12.01.14	00:27	43° 58.51' N	30° 44.94' E	519.8	Seismic reflection profile
MSM34/064-1	12.01.14	01:47	43° 56.56' N	30° 48.87' E	838.5	Seismic reflection profile
MSM34/064-1	12.01.14	03:05	43° 58.50' N	30° 45.00' E	523.1	Seismic reflection profile
MSM34/064-1	12.01.14	04:24	43° 56.63' N	30° 48.91' E	831.9	Seismic reflection profile
MSM34/064-1	12.01.14	05:40	43° 58.51' N	30° 45.07' E	522.2	Seismic reflection profile
MSM34/064-1	12.01.14	06:59	43° 56.71' N	30° 48.90' E	839.8	Seismic reflection profile

Station No.	Date	Time [UTC]	Position Lat	Position Lon	Depth [m]	Gear
MSM34/064-1	12.01.14	08:06	43° 58.06' N	30° 45.61' E	562.4	Seismic reflection profile
MSM34/064-1	12.01.14	09:37	43° 56.60' N	30° 49.08' E	836.3	Seismic reflection profile
MSM34/064-1	12.01.14	10:57	43° 58.63' N	30° 45.07' E	519.1	Seismic reflection profile
MSM34/064-1	12.01.14	12:14	43° 56.64' N	30° 49.11' E	845.9	Seismic reflection profile
MSM34/064-1	12.01.14	13:31	43° 58.70' N	30° 45.06' E	513	Seismic reflection profile
MSM34/064-1	12.01.14	14:47	43° 56.68' N	30° 49.12' E	823.8	Seismic reflection profile
MSM34/064-1	12.01.14	16:00	43° 58.62' N	30° 45.20' E	520.2	Seismic reflection profile
MSM34/064-1	12.01.14	17:18	43° 56.66' N	30° 49.23' E	841.9	Seismic reflection profile
MSM34/064-1	12.01.14	18:40	43° 58.65' N	30° 45.26' E	520.4	Seismic reflection profile
MSM34/064-1	12.01.14	19:12	43° 57.52' N	30° 45.10' E	631.8	Seismic reflection profile
MSM34/064-1	12.01.14	19:51	43° 55.59' N	30° 47.10' E	690.5	Seismic reflection profile
MSM34/064-1	12.01.14	21:09	43° 58.70' N	30° 45.32' E	514.2	Seismic reflection profile
MSM34/064-1	12.01.14	22:29	43° 56.67' N	30° 49.26' E	848.8	Seismic reflection profile
MSM34/064-1	12.01.14	23:50	43° 58.82' N	30° 45.44' E	495.4	Seismic reflection profile
MSM34/064-1	13.01.14	00:34	43° 57.44' N	30° 45.55' E	673.7	Seismic reflection profile
MSM34/064-1	13.01.14	00:40	43° 57.11' N	30° 45.80' E	690.2	Seismic reflection profile
MSM34/064-1	13.01.14	01:09	43° 55.68' N	30° 47.29' E	727.1	Seismic reflection profile
MSM34/064-1	13.01.14	02:24	43° 58.84' N	30° 45.75' E	494.4	Seismic reflection profile
MSM34/064-1	13.01.14	03:40	43° 56.75' N	30° 49.25' E	834.1	Seismic reflection profile
MSM34/064-1	13.01.14	04:16	43° 56.70' N	30° 47.64' E	859.5	Seismic reflection profile
MSM34/064-1	13.01.14	04:25	43° 57.15' N	30° 47.20' E	758.4	Seismic reflection profile
MSM34/064-1	13.01.14	04:29	43° 57.35' N	30° 46.99' E	664.1	Seismic reflection profile
MSM34/064-1	13.01.14	04:37	43° 57.77' N	30° 46.61' E	605.1	Seismic reflection profile
MSM34/064-1	13.01.14	04:42	43° 58.02' N	30° 46.34' E	580.5	Seismic reflection profile
MSM34/064-1	13.01.14	04:47	43° 58.31' N	30° 46.16' E	555.2	Seismic reflection profile
MSM34/064-1	13.01.14	04:52	43° 58.58' N	30° 45.91' E	510.3	Seismic reflection profile
MSM34/064-1	13.01.14	05:45	43° 58.33' N	30° 45.75' E	543.2	Seismic reflection profile
MSM34/064-1	13.01.14	05:52	43° 57.97' N	30° 46.13' E	583.5	Seismic reflection profile
MSM34/064-1	13.01.14	06:02	43° 57.45' N	30° 46.67' E	673.9	Seismic reflection profile
MSM34/064-1	13.01.14	06:04	43° 57.34' N	30° 46.78' E	686	Seismic reflection profile
MSM34/064-1	13.01.14	06:22	43° 56.42' N	30° 47.76' E	876.8	Seismic reflection profile
MSM34/064-1	13.01.14	07:23	43° 56.33' N	30° 47.99' E	886.3	Seismic reflection profile

Station No.	Date	Time [UTC]	Position Lat	Position Lon	Depth [m]	Gear
MSM34/064-1	13.01.14	07:30	43° 56.66' N	30° 47.65' E	863.3	Seismic reflection profile
MSM34/064-1	13.01.14	07:41	43° 57.16' N	30° 47.11' E	711.6	Seismic reflection profile
MSM34/064-1	13.01.14	08:13	43° 58.69' N	30° 45.51' E	495.7	Seismic reflection profile
MSM34/065-1	13.01.14	12:41	43° 57.17' N	30° 46.77' E	720.5	Multi corer
MSM34/066-1	13.01.14	13:44	43° 57.62' N	30° 46.53' E	638	Multi corer
MSM34/066-2	13.01.14	14:38	43° 57.62' N	30° 46.53' E	633.3	Gravity corer
MSM34/067-1	13.01.14	15:56	43° 57.22' N	30° 46.72' E	713.5	Heat Flow
MSM34/068-1	13.01.14	16:25	43° 57.27' N	30° 46.67' E	707.1	Heat Flow
MSM34/069-1	13.01.14	16:54	43° 57.31' N	30° 46.49' E	697.4	Heat Flow
MSM34/070-1	13.01.14	17:29	43° 57.36' N	30° 46.58' E	680.8	Heat Flow
MSM34/071-1	13.01.14	18:00	43° 57.40' N	30° 46.68' E	676.7	Heat Flow
MSM34/072-1	13.01.14	18:32	43° 57.40' N	30° 46.54' E	686	Heat Flow
MSM34/073-1	13.01.14	19:06	43° 57.48' N	30° 46.44' E	674.2	Heat Flow
MSM34/073-1	13.01.14	19:12	43° 57.48' N	30° 46.45' E	678	Heat Flow
MSM34/072-2	13.01.14	19:44	43° 57.40' N	30° 46.53' E	688.2	Heat Flow
MSM34/074-1	13.01.14	22:22	43° 57.44' N	30° 46.50' E	678.4	Multi corer
MSM34/074-2	13.01.14	23:07	43° 57.44' N	30° 46.50' E	671.9	Gravity corer
MSM34/075-1	14.01.14	01:28	43° 58.00' N	30° 44.01' E	558.4	Seismic reflection profile
MSM34/075-1	14.01.14	03:27	43° 53.09' N	30° 49.14' E	950.4	Seismic reflection profile
MSM34/075-1	14.01.14	06:08	43° 58.42' N	30° 44.46' E	508.1	Seismic reflection profile
MSM34/075-1	14.01.14	08:47	43° 53.74' N	30° 50.47' E	1092.8	Seismic reflection profile
MSM34/075-1	14.01.14	11:20	43° 58.81' N	30° 46.26' E	529.6	Seismic reflection profile
MSM34/075-1	14.01.14	11:40	43° 59.63' N	30° 45.37' E	456.7	Seismic reflection profile
MSM34/075-1	14.01.14	12:05	44° 0.58' N	30° 44.30' E	296.5	Seismic reflection profile
MSM34/075-1	14.01.14	13:02	43° 59.65' N	30° 47.12' E	499.3	Seismic reflection profile
MSM34/075-1	14.01.14	14:59	43° 54.83' N	30° 52.14' E	953.8	Seismic reflection profile
MSM34/075-1	14.01.14	16:57	43° 53.87' N	30° 47.76' E	845.3	Seismic reflection profile
MSM34/075-1	14.01.14	17:50	43° 55.79' N	30° 44.39' E	647.3	Seismic reflection profile
MSM34/075-1	14.01.14	18:58	43° 58.70' N	30° 48.58' E	609.4	Seismic reflection profile
MSM34/052-1	14.01.14	21:24	43° 57.47' N	30° 45.19' E	661.5	Ocean Bottom Seismometer
MSM34/053-1	14.01.14	21:48	43° 57.17' N	30° 45.58' E	686.5	Ocean Bottom Seismometer
MSM34/054-1	14.01.14	22:10	43° 56.84' N	30° 45.88' E	698.5	Ocean Bottom Seismometer

Station No.	Date	Time [UTC]	Position Lat	Position Lon	Depth [m]	Gear
MSM34/055-1	14.01.14	22:36	43° 56.52' N	30° 46.29' E	691.3	Ocean Bottom Seismometer
MSM34/056-1	14.01.14	22:57	43° 56.92' N	30° 46.99' E	799.7	Ocean Bottom Seismometer
MSM34/057-1	14.01.14	23:14	43° 57.21' N	30° 46.62' E	721.4	Ocean Bottom Seismometer
MSM34/058-1	14.01.14	23:33	43° 57.54' N	30° 46.41' E	681.7	Ocean Bottom Seismometer
MSM34/059-1	14.01.14	23:47	43° 57.88' N	30° 46.04' E	604	Ocean Bottom Seismometer
MSM34/060-1	15.01.14	00:08	43° 58.22' N	30° 46.72' E	607.6	Ocean Bottom Seismometer
MSM34/061-1	15.01.14	00:22	43° 57.91' N	30° 47.06' E	697.3	Ocean Bottom Seismometer
MSM34/062-1	15.01.14	00:42	43° 57.60' N	30° 47.41' E	794.3	Ocean Bottom Seismometer
MSM34/063-1	15.01.14	01:00	43° 57.32' N	30° 47.80' E	858.6	Ocean Bottom Seismometer
MSM34/076-1	15.01.14	01:51	43° 57.03' N	30° 46.02' E	698.2	Heat Flow
MSM34/077-1	15.01.14	02:35	43° 57.21' N	30° 46.31' E	706.6	Heat Flow
MSM34/078-1	15.01.14	03:23	43° 57.57' N	30° 46.51' E	641.4	Heat Flow
MSM34/079-1	15.01.14	03:49	43° 57.63' N	30° 46.54' E	615.1	Heat Flow
MSM34/080-1	15.01.14	04:28	43° 57.51' N	30° 46.88' E	626.8	Heat Flow
MSM34/081-1	15.01.14	05:15	43° 57.60' N	30° 47.30' E	752.9	Heat Flow
MSM34/082-1	15.01.14	06:01	43° 57.69' N	30° 47.76' E	827.1	Heat Flow
MSM34/083-1	15.01.14	06:26	43° 57.69' N	30° 47.75' E	819.4	Heat Flow
MSM34/084-1	15.01.14	06:54	43° 57.69' N	30° 47.54' E	816.5	Heat Flow
MSM34/085-1	15.01.14	07:42	43° 57.83' N	30° 47.74' E	827.6	Heat Flow
MSM34/086-1	15.01.14	08:22	43° 57.60' N	30° 47.74' E	819.1	Heat Flow
MSM34/086-1	15.01.14	08:48	43° 57.60' N	30° 47.74' E	834.4	Heat Flow
MSM34/087-1	15.01.14	09:13	43° 57.40' N	30° 47.75' E	845.5	Heat Flow
MSM34/088-1	15.01.14	10:03	43° 57.69' N	30° 47.94' E	794.8	Heat Flow
MSM34/089-1	15.01.14	11:33	43° 57.69' N	30° 47.76' E	818.1	Gravity corer
MSM34/090-1	15.01.14	15:24	43° 37.72' N	30° 38.61' E	1072.5	Seismic reflection profile
MSM34/090-1	15.01.14	16:42	43° 34.63' N	30° 32.94' E	1196.8	Seismic reflection profile
MSM34/090-1	15.01.14	18:00	43° 38.34' N	30° 28.39' E	1042.8	Seismic reflection profile
MSM34/090-1	15.01.14	19:31	43° 42.22' N	30° 34.06' E	967.3	Seismic reflection profile
MSM34/090-1	15.01.14	21:08	43° 47.55' N	30° 29.74' E	612	Seismic reflection profile
MSM34/090-1	15.01.14	22:43	43° 44.45' N	30° 22.74' E	525	Seismic reflection profile
MSM34/090-1	16.01.14	00:06	43° 49.40' N	30° 22.50' E	1064.3	Seismic reflection profile
MSM34/090-1	16.01.14	04:58	43° 35.01' N	30° 38.82' E	1188.5	Seismic reflection profile

Station No.	Date	Time [UTC]	Position Lat	Position Lon	Depth [m]	Gear
MSM34/090-1	16.01.14	05:25	43° 33.79' N	30° 37.19' E	1226.3	Seismic reflection profile
MSM34/090-1	16.01.14	06:15	43° 36.10' N	30° 34.19' E	1172.3	Seismic reflection profile
MSM34/091-1	16.01.14	09:18	43° 13.72' N	30° 10.93' E	1604.5	Multibeam und ParaSound
MSM34/091-1	16.01.14	11:06	43° 4.51' N	29° 55.80' E	1731.8	Multibeam und ParaSound
MSM34/091-1	16.01.14	11:24	43° 6.09' N	29° 53.49' E	1669.2	Multibeam und ParaSound
MSM34/091-1	16.01.14	12:17	43° 10.68' N	30° 0.51' E	1604.2	Multibeam und ParaSound
MSM34/091-1	16.01.14	12:36	43° 12.69' N	29° 58.84' E	1525.9	Multibeam und ParaSound
MSM34/091-1	16.01.14	13:22	43° 9.20' N	29° 52.17' E	1611	Multibeam und ParaSound
MSM34/091-1	16.01.14	13:49	43° 10.47' N	29° 49.23' E	1597.8	Multibeam und ParaSound
MSM34/091-1	16.01.14	14:10	43° 12.57' N	29° 51.76' E	1560.3	Multibeam und ParaSound
MSM34/091-1	16.01.14	15:50	43° 20.97' N	30° 5.93' E	1415.6	Multibeam und ParaSound
MSM34/091-1	16.01.14	16:11	43° 23.20' N	30° 4.38' E	1281.5	Multibeam und ParaSound
MSM34/091-1	16.01.14	17:47	43° 15.29' N	29° 50.60' E	1512.1	Multibeam und ParaSound
MSM34/091-1	16.01.14	18:08	43° 16.99' N	29° 48.05' E	1476.6	Multibeam und ParaSound
MSM34/091-1	16.01.14	19:46	43° 25.04' N	30° 2.09' E	1175.8	Multibeam und ParaSound
MSM34/091-1	16.01.14	20:06	43° 27.18' N	30° 0.39' E	1079.9	Multibeam und ParaSound
MSM34/091-1	16.01.14	21:43	43° 19.84' N	29° 46.61' E	1407.7	Multibeam und ParaSound
MSM34/091-1	16.01.14	22:00	43° 21.19' N	29° 44.47' E	1314.7	Multibeam und ParaSound

8 Data and Sample Storage and Availability

The Kiel Data Management Team (KDMT) provides an information and data archival system where metadata of the onboard DSHIP-System is collected and publicly available.

This Ocean Science Information System (OSIS-Kiel) is accessible for all project participants and can be used to share and edit field information and to provide scientific data, as they become available. The central system OSIS is providing information on granted ship time with information on the scientific program and the general details down to the availability of data files from already concluded cruises. The transparency on the research activities is regarded as an invitation to external scientists to start communication on collaboration on behalf of the newly available data.

The KDMT will take care as data curators to fulfill the here proposed data publication of the data in a World Data Center (e.g. PANGAEA) which will then provide long-term archival and access to the data. The data publication process will be based on the available files in OSIS and is therefore transparent to all reviewers and scientists. This cooperation with a world data center will make the data globally searchable, and links to the data owners will provide points of contact to project-external scientists. The seismic, bathymetric and hydroacoustic raw data as well as processed seismic data will be archived on a dedicated server at GEOMAR, which is daily backed up and which holds all data since the founding days of GEOMAR. OSIS provides contact information for these large data files.

Availability of metadata in OSIS-Kiel (portal.geomar.de/osis): March 2014
Availability of data in OSIS-Kiel (portal.geomar.de/osis): July 2014
Availability of data in a WDC/PANGAEA (www.pangaea.de): January 2017

Table 8.1 provides an overview of contact persons for the different data sets.

Table 8.1 Contact persons for the different data sets

Data	Contact Person	Present Affiliation	Email
Regional 2D seismic	Prof. Gunay Cifci & Dr. Jörg Bialas	IMST-.Seislab GEOMAR	gunay.cifci@deu.edu.tr jbialas@geomar.de
High resolution 2D & 3D seismic	Dr. Jörg Bialas	GEOMAR	jbialas@geomar.de
Heatflow	Dr. Jörg Bialas	GEOMAR	jbialas@geomar.de
Coring samples	Dr. Matthias Haeckel	GEOMAR	mhaeckel@geomar.de
Geochemistry data	Dr. Matthias Haeckel	GEOMAR	mhaeckel@geomar.de
Gas analysis	Dr. Thomas Pape	MARUM	tpape@marum.de

9 Acknowledgements

The cruise MSM34 SUGAR Site Leg 1 and 2 was supported by the German Federal Ministry for Education and Research (Bundesministerium für Bildung und Forschung, BMBF) under project No. 03G0819A (SUGAR-II A) and by the European Union Seventh Framework Programme (FP7/2007-2013) under the MIDAS project, grant agreement n° 603418.

The authors wish to express their gratitude to all the colleagues who have supported the work before, during and after the cruise. Much of the work done during the cruise was only made possible by the scientists', technicians' and the crews' experience.

Particular thanks are directed to the masters (Björn Maaß and Ralf Schmidt) and their entire crew of R/V MARIA S. MERIAN for the excellent support throughout the cruise.

10 References

Bahr A, Lamy F, Arz HW, Major C, Kwiecien O, Wefer G (2008) Abrupt changes of temperature and water chemistry in the late Pleistocene and early Holocene Black Sea. Geochemistry Geophysics Geosystems 9, doi:10.1029/2007GC00 1683.

Baristeas, N. (2006), Seismische Fazies, Tektonik und Gashydratvorkommen im nordwestlichen Schwarzen Meer, Diploma thesis, 110 pp, Hamburg, Hamburg.

Degens ET, Ross DA (1974) The Black Sea - Geology, Chemistry, and Biology. The American Association of Petroleum Geologists, Tulsa, USA.

Grasshoff K, Ehrhardt M, Kremling K (1999) Methods of Seawater Analysis. Wiley-VCH, Weinheim.

Jones GA, Gagnon AR (1994) Radiocarbon chronology of Black Sea sediments. Deep-Sea Research 41, 531–557.

Lamy F, Arz HW, Bond G, Bahr A, Pätzold J (2006) Multicentennial-scale hydrological changes in the Black Sea and northern Red Sea during the Holocene and the Arctic/North Atlantic Oscillation, Paleoceanography 2, PA1008.

Lericolais, G., C. Bulois, H. Gillet, and F. Guichard (2009), High frequency sea level flu Леин Леин Леин ctuations recorded in the Black Sea since the LGM, Global Planet Change, 66(1-2), 65-75.

Limonov AF, Woodside JM, Ivanov MK (1994) Mud volcanism in the Mediterranean and Black seas and shallow structure of the Eratosthenes Seamount. UNESCO reports in marine science 64, 173 pp.

Manheim FT, Schug DM (1978) Interstitial waters of Black Sea cores. In: Ross DA, Neprochnov YP (Eds.), Initial Reports of the Deep-Sea Drilling Project. U.S. Government Printing Office, Washington.

Major CO, Goldstein SL, Ryan WBF, Lericolais G, Piotrowski AM, Hajdas I (2006) The coevolution of Black Sea level and composition through the last deglaciation and its paleoclimatic significance. Quaternary Science Reviews 25, 2031-2047.

Neretin LN, Böttcher ME, Jørgensen BB, Volkov II, Lüschen H, Hilgenfeld K (2004) Pyritization processes and greigite formation in the advancing sulfidization front in the Upper Pleistocene sediments of the Black Sea. Geochimica et Cosmochimica Acta 68(9), 2081-2093.

Popescu, I., G. Lericolais, N. Panin, M. De Batist, and H. Gillet (2007), Seismic expression of gas and gas hydrates across the western Black Sea, Geo-Marine Letters, 27(2), 173-183.

Popescu I., M. Debatist, G. Lericolais, H. Nouzé, J. Poort, N. Panin, W. Versteeg, H. Gillet Multiple bottom-simulating reflections in the Black Sea, Potential proxies of past climate conditions. Mar. Geol., 2006, doi:10.1016/j.margeo.2005.12.006.

Soulet G, Delaygue G, Vallet-Coulomb C, Böttcher ME, Sonzogni C, Lericolais G, Bard E (2010) Glacial hydrologic conditions in the Black Sea reconstructed using geochemical pore water profiles. Earth and Planetary Science Letters 296, 57-66.

11 Appendix

11.1 Core descriptions

11.1.1.1 Site IFREMER Piezometer (in shallow water)

3-2 MIC1

0-49.5 cm

3-3 GC1

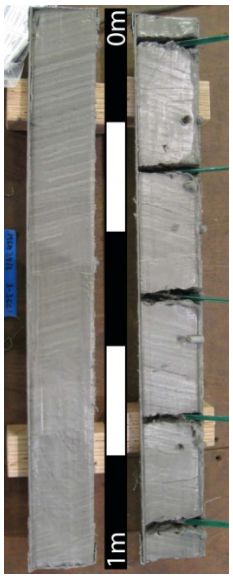

0-100 cm

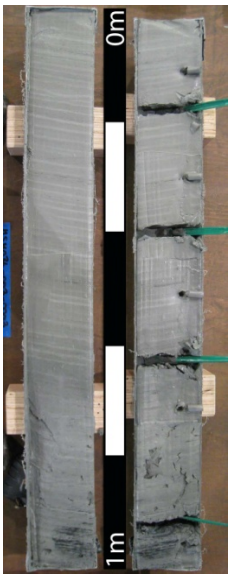

100-200 cm

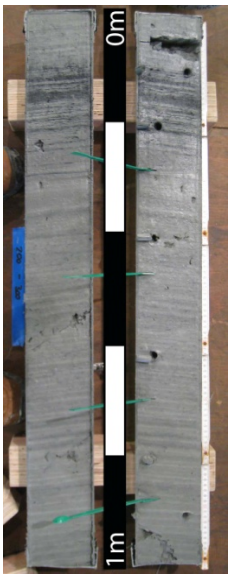

200-300 cm

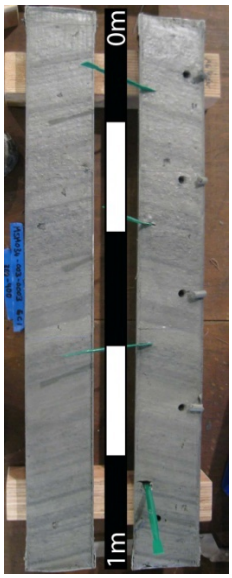

300-400 cm

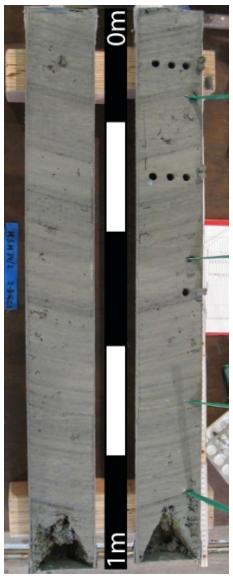

400-500 cm

11.1.1.2 Site SW channel-levee with multiple BSR (on seismic line 8b)

42-1 MIC4

0-42 cm

22-1 GC2

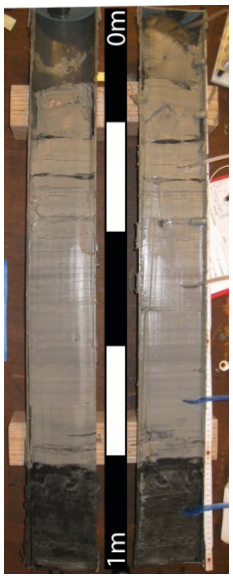

0-100 cm

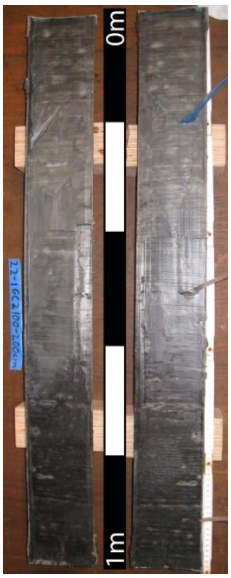

100-200 cm

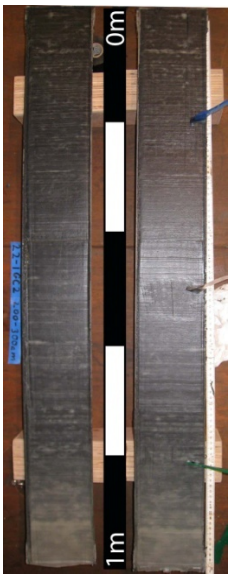

200-300 cm

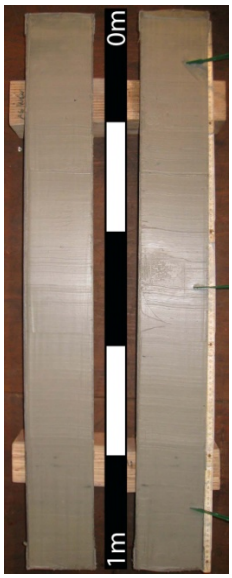

300-400 cm

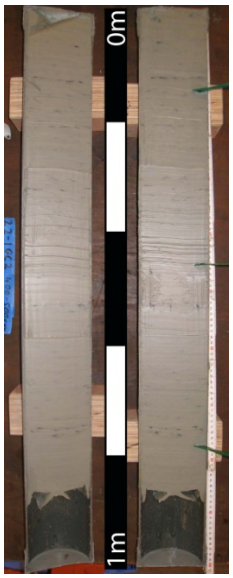

400-500 cm

11.1.1.3 Site SW channel-levee with multiple BSR (channel)

26-1 MIC2

0-51 cm

39-1 GC3

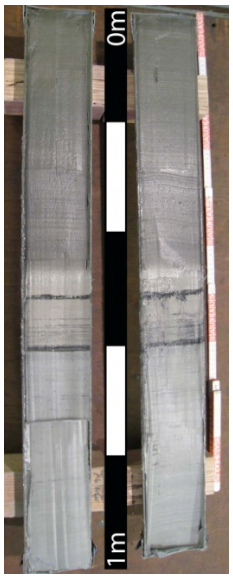

0-100 cm

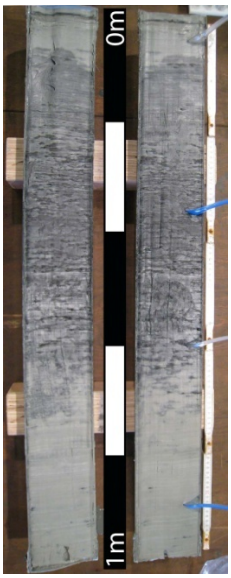

100-200 cm

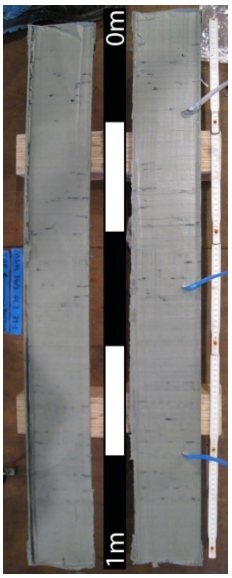

200-300 cm

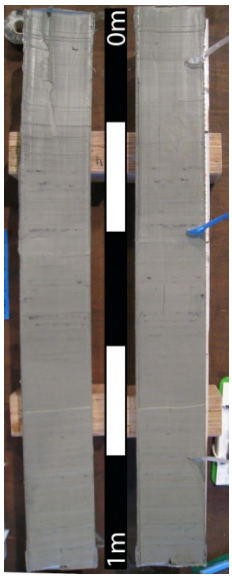

300-400 cm

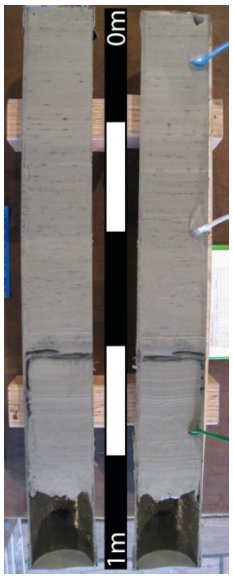

400-500 cm

11.1.1.4 Site SW channel-levee with multiple BSR (levee)

27-1 MIC3

0-40 cm

40-1 GC4

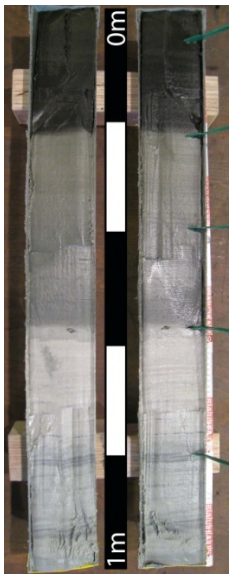

0-100 cm

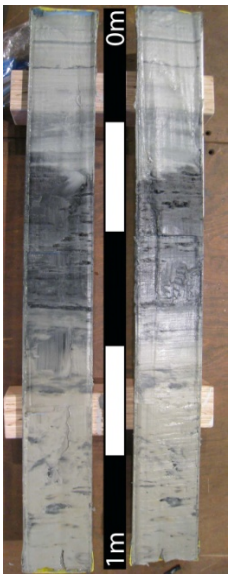

100-200 cm

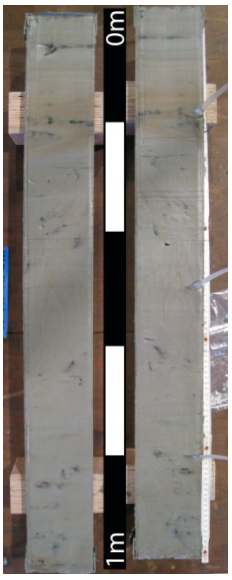

200-300 cm

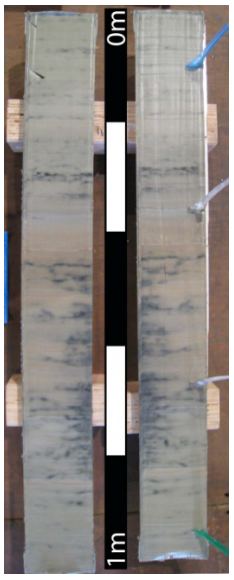

300-400 cm

400-500 cm

11.1.1.5 Site NE channel-levee with upward bending BSR (slump area)

43-2 MIC5

0-38 cm

43-1 GC5

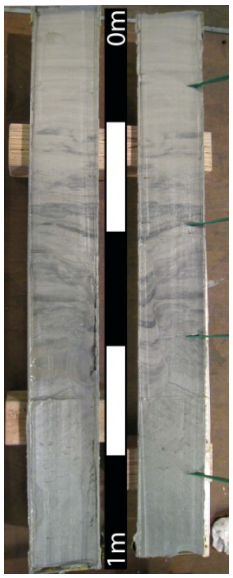

0-100 cm

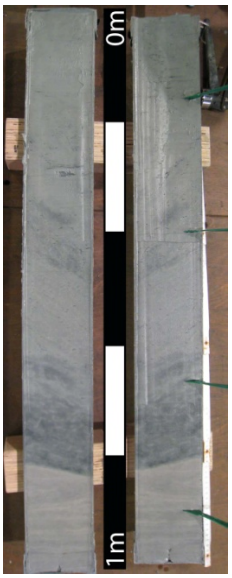

100-200 cm

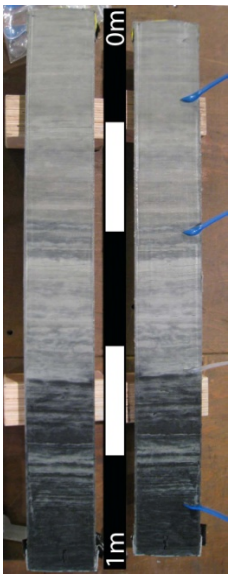

200-300 cm

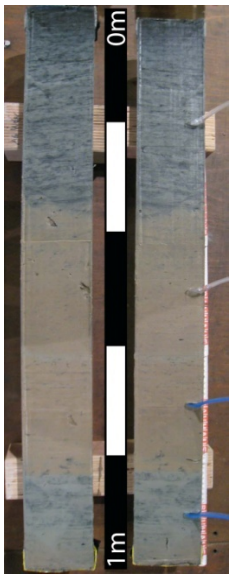

300-400 cm

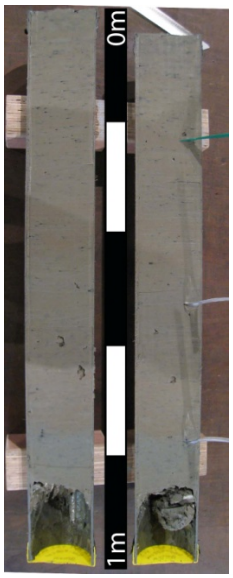

400-500 cm

11.1.1.6 Site NE channel-levee with upward bending BSR (slump area)

65-1 MIC6

0-41 cm

51-1 GC6

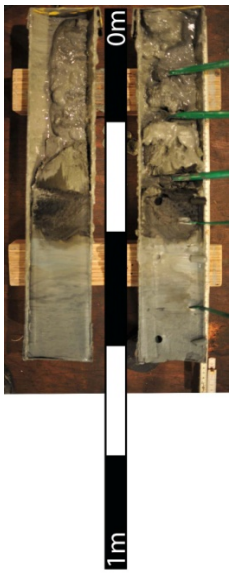

0-63 cm

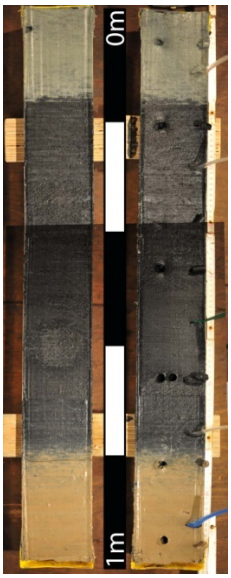

63-163 cm

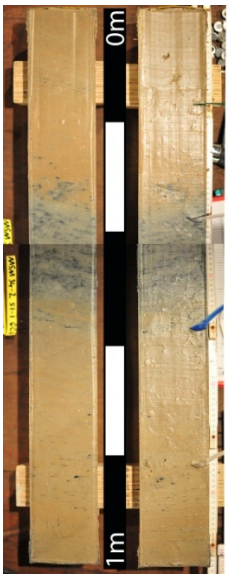

163-263 cm

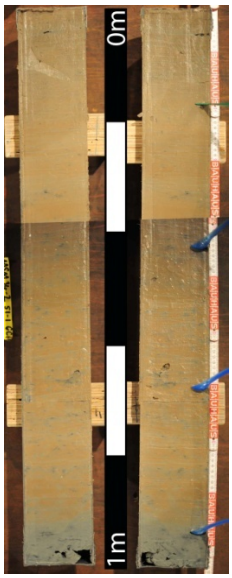

263-363 cm

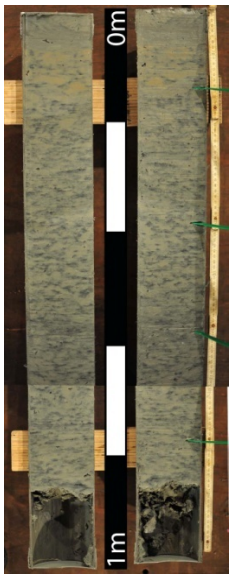

363-463 cm

11.1.1.7 Site NE channel-levee with upward bending BSR (gas seep at slump head wall)

66-1 MIC7

0-44 cm

66-2 GC7

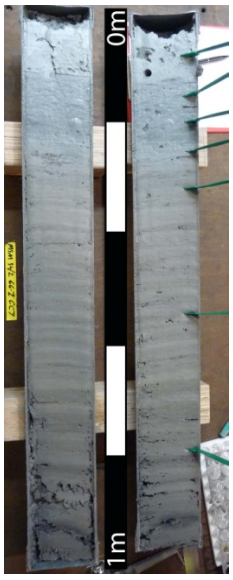

0-100 cm

Corrupted Photo

100-200 cm

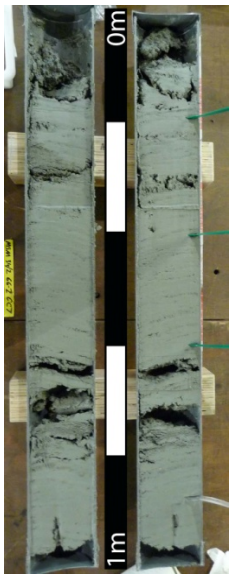

200-300 cm

300-400 cm

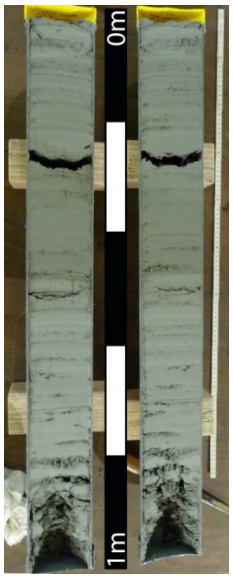

400-500 cm

11.1.1.8 Site NE channel-levee with upward bending BSR (slump area)

74-1 MIC8

0-42 cm

74-2 GC8

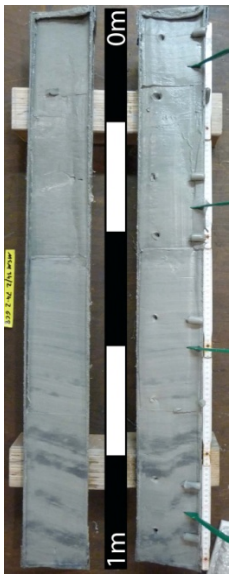

0-100 cm

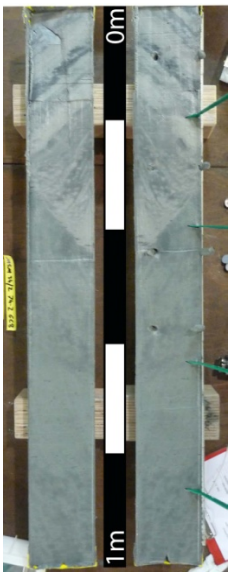

100-200 cm

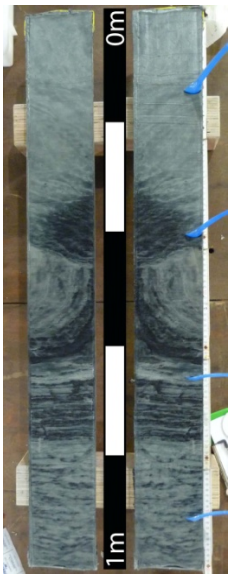

200-300 cm

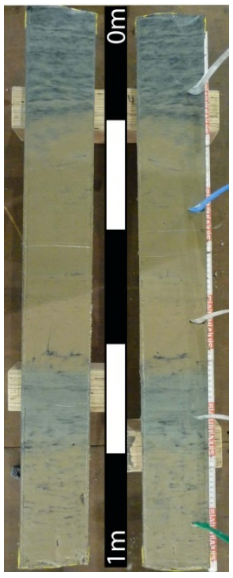

300-400 cm

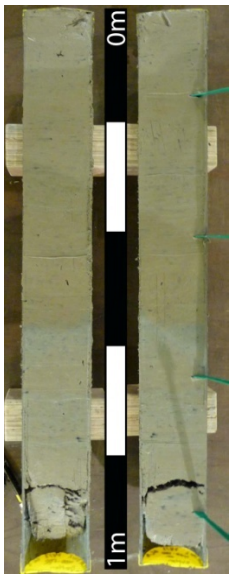

400-500 cm

11.1.1.9 Site NE channel-levee with upward bending BSR (channel)

89-1 GC9

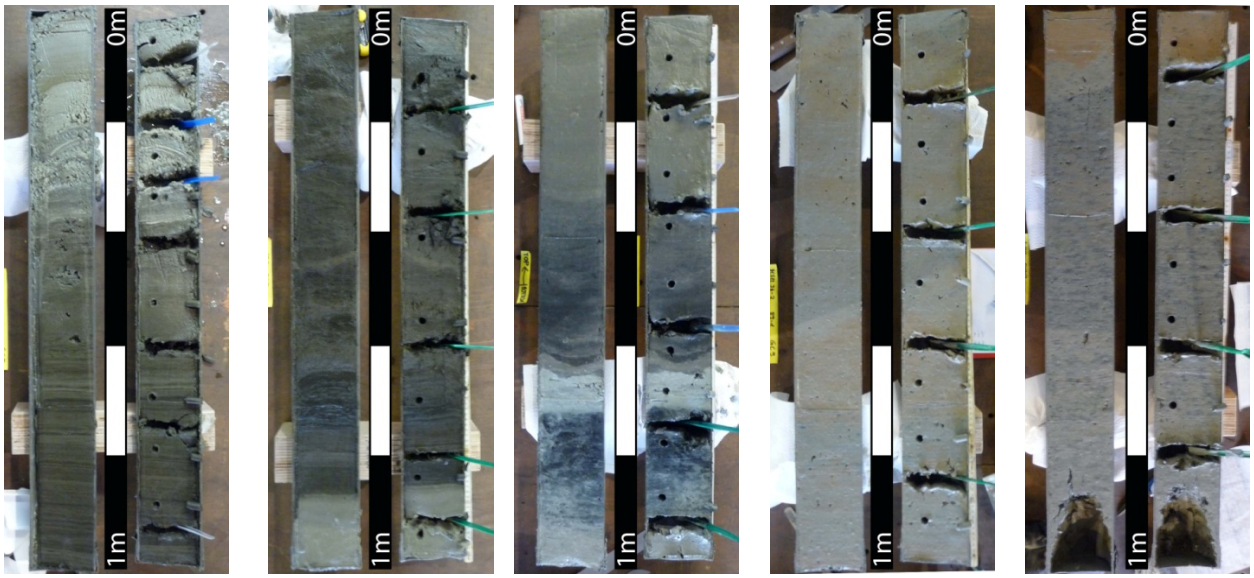

0-100 cm 100-200 cm 200-300 cm 300-400 cm 400-500 cm